Thrust and weight estimation for Doc. 29 noise models

Using ACMS data to more accurately predict noise levels at Amsterdam Airport Schiphol

Master Thesis

Eric van Pijlen

TU Delft

Thrust and weight estimation for Doc. 29 noise models

Using ACMS data to more accurately predict noise levels at Amsterdam Airport Schiphol

Masters Thesis

by

Eric van Pijlen

to obtain the degree of Master of Science
at the Delft University of Technology
to be defended publicly on January 28, 2026 at 10:00

Thesis committee:

Chair:	Ir. J.A. Melkert
Supervisors:	Prof. Dr. Ir. M. Snellen
	Ir. R.C. van der Grift
External examiner:	Dr. Ir. A. Amiri-Simkooei
	Dr. Ir. J. Sun
Place:	Faculty of Aerospace Engineering, Delft
Project Duration:	February, 2025 - January, 2026
Student number:	4783549

An electronic version of this thesis is available at `http://repository.tudelft.nl/`.

Faculty of Aerospace Engineering · Delft University of Technology

Preface

This is it then, my final deliverable of my academic journey through the world of aerospace engineering to obtain my Masters degree. At the start of this journey, I had no idea where it would take me. Just started following the courses that interested me the most. My internship at Luchtverkeersleiding Nederland (LVNL) introduced me to the Document 29 noise model methodology, sparking my interest for the topic of aircraft noise after the introductory course the year before. Therefore, I started the conversation whether I could continue with this topic for my Masters thesis.

I am very grateful that I got the opportunity to do my Masters thesis on behalf of the Knowledge & Development Center (KDC) in the field of aircraft noise. First and foremost, I would like to thank my supervisors, Rebekka van der Grift, Mirjam Snellen and Alireza Amiri-Simkooei for all their feedback and guidance throughout these 11 months. Every monday I had a short meeting with Rebekka to discuss my progress of last week, think about new methodologies I thought of, go through new results, or discuss things I struggled with. Every two to three weeks I had a progress meeting including Mirjam and Alireza as well. These progress meetings allowed me to keep track of the bigger picture and help me make important decisions along the way. Without these three people, the path and result of this thesis would very differnt than it currently is.

Furthermore, I would like to thank everyone that supported me in my work throughout my entire thesis time. During the countless hours I spent both in the iLabs office, Schiphol Hoofdgebouw, and the Echo building, the people who surrounded me created a very pleasant and fun working atmosphere. All of the enjoyable conversations, short (or sometimes longer) coffee breaks, and support during difficult times made the task of writing this thesis much more bearable. I can truly say that I enjoyed the time I spent writing and working on my thesis thanks to these people.

Eric van Pijlen
Delft, January 2026

Nomenclature

Contents

Part I

Scientific Article

1

Scientific Article

This paper investigates whether aircraft noise modeling can be improved by more accurately predicting the aircraft weight and thrust compared to the current methodology European Civil Aviation Conference (ECAC) described in Document 29 (Doc. 29) . Using Aircraft Condition & Monitoring System (ACMS) data from multiple aircraft types, two new weight estimation methods are proposed for departures: a climb slope and distance based approach, and a specific-energy method. The Mean Absolute Percentage Error (MAPE) of the current stage length approach is compared to the newly proposed methods. For thrust estimation, departures during the initial take-off roll and climb out are modeled using weight-dependent interpolations of the Fixed-Point Profile (FPP)s. For the other parts of the departure process, median FPPs, for which boundaries are determined by a flight segmentation model, are used. Arrival thrust values are predicted using a random forest regression model trained on flight path angle, calibrated airspeed, and corrected net thrust. This random forest model accurately captures thrust peak magnitudes and locations for most flights. Noise contour plots are generated for an original Doc. 29 model, an ACMS Doc. 29 and a new weight and thrust Doc. 29 model. For the ACMS Doc. 29 model, the ACMS thrust and weight data is directly used as input data for the noise model. The new weight and thrust estimates reveal closer agreement with ACMS Doc. 29 contours than with the original Doc. 29 method. This result indicates the rigidity of the FPPs and outdated Aircraft Noise & Performance (ANP) database entries contribute to current modeling inaccuracies. The results demonstrate that the incorporation of performance relationships can significantly improve the theoretical Doc. 29 model.

1.1. Introduction

Aircraft noise has a significant impact on the health of communities located in the vicinity of airports. People living in these areas suffer from sleep disturbances and have an increased risk of cardiovascular diseases [1]. Furthermore, long term noise exposure can be associated with a poorer psychological health condition, although the effect is not as strong as the previously named health outcomes [2]. As these negative effects of aircraft noise cannot be ignored, it is crucial that the aviation industry makes efforts to minimize noise pollution.

To gain insight into the amount of noise pollution around airports, aircraft noise can be measured and monitored with measuring equipment. By recording flyover events, the instantaneous sound levels at the time of the flyover can be determined. However, capturing every flight with measuring equipment around an airport as large as Amsterdam Airport Schiphol is infeasible due to both technical and budget constraints. Real life noise measurements always contain background noise in varying levels, impacting the quality of measurements. The routing options, combined with the variability of the weather conditions, make it impossible to get a sound measurement of every flight. In addition, the impact of noise reduction measurements prior to implementation, such as new flight routes, cannot be determined with measurements alone and requires a model capable of accurately predicting aircraft noise emissions.

To limit noise exposure in the surroundings of airports, several Noise Abatement Procedures (NAP) are already being used for both departures and arrivals. For departures, two different Noise Abatement Departure Procedures (NADP) have been designed by International Civil Aviation Organization (ICAO). The NADP1 procedure minimizes noise directly underneath the flight path of the aircraft, while the NADP2 procedure

minimizes noise in areas located relatively further away from the airport [3]. For Schiphol airport, densely populated areas are located relatively further away and are often not located directly underneath the flight path. Therefore, the NADP2 procedure is the preferred departure procedure at Schiphol Airport [4]. For arrivals, no default arrival procedure is in place at Amsterdam Airport Schiphol during the day, as aircraft are guided to the airport by Luchtverkeersleiding Nederland (LVNL). During night time runway usage is limited to minimize noise effects. For Doc. 29 best-practice noise models, altitude and thrust are modeled with a set of arrival profiles. The real altitude trajectory of every flight is compared to all altitude trajectories in the database and assigned to the best matching one. The noise load for this flight is then computed based on this matched trajectory [5]. The current existing profiles and procedure do not allow for much variability between flights. This paper aims to introduce a more dynamic way of modeling these procedures to reduce model errors.

The most commonly used calculation method in Europe for aircraft noise modeling is the Doc. 29 best-practice noise model. This model is described in three volumes, giving comprehensive guidance in the way noise contours have to be calculated [6]. The model requires input parameters such as altitude, latitude, longitude, and airspeed [7]. Furthermore, weight and thrust values are required as input parameters, but data for these two parameters is usually not publicly available, as they are proprietory to airlines. Therefore, in the original Doc. 29 methodology, both of these parameters are estimated depending on the trip length and flight procedures. An accurate prediction of the weight and the thrust of the aircraft is required, as errors in the estimation of these input parameters propagate all the way to the final outcome of the model. Research by Sun et al. showed that estimating aircraft weight is possible based on the take-off run [8]. The runway recursive estimator showed more promising results than the lift-off moment estimator. Ayzit et al. suggested a deep learning method to determine the weight of the aircraft. This method concluded that the flight performance parameters are indicative for the aircraft weight, but differ per flight phase [9]. For predicting thrust, Schwab and Zellman showed that derated climb segments can be categorized [10]. However, this categorization of derated climb modes is dependent on the type of aircraft. These methods show that flight performance parameters can be used to get more accurate estimates for thrust and weight.

This thesis proposes a new method to estimate the weight and thrust input parameters for the Doc. 29 noise model for Airbus A330-303, Boeing 777-300ER, Airbus A321neo and Boeing 737-800 aircraft. The goal of this paper is to improve the weight and thrust estimation method of the current Doc. 29 method, resulting in a more accurate prediction of the noise contours around the airport. To assess performance, the noise contour plots of the original Doc. 29 model, the new thrust and weight Doc. 29 model, and an ACMS Doc. 29 are compared with each other. The ACMS data is regarded as 'gold standard' operational data [6], meaning more accurate data is not available at all. Therefore, using the ACMS data as direct input for the Doc. 29 noise model, the theoretical best Doc. 29 baseline model is obtained. Furthermore, the ACMS data can be used for verification and validation of the estimated parameters, allowing the development and evaluation of these new methods. For radar track data, weight and thrust data are unavailable. Therefore, in this paper, the aim will be to estimate the weight and thrust of nominal flights using the other available aircraft performance parameters. In conclusion, the results in this paper can be linked to the following research question; What effect does improving the weight and thrust estimation using ACMS data have on the noise contour plots around Amsterdam Airport Schiphol?

Section 1.2 explains the data used in this paper, Section 1.3 the original Doc. 29 methodology, and Section 1.4 the newly proposed methodologies for estimating both weight and thrust. In Section 1.6, the results of the weight estimation are presented, and the impact on the noise load is evaluated. Finally, in Section 1.7, conclusions and recommendations are discussed.

1.2. Description of the data

For this research, flight data to and from Schiphol Airport originating from the ACMS of aircraft is provided by an airline for Airbus A330-300, Boeing 777-300ER, Airbus A321neo and Boeing 737-800 aircraft. As this ACMS data is obtained directly from the systems onboard the aircraft itself, it is a highly reliable data source [6]. The methodology presented in this research was developed with data for the Airbus A330-300 aircraft and was later applied and adapted to the other evaluated aircraft types. For this reason, the methodology presented in this paper will be based on Airbus A330-300 data. Similar plots for other aircraft types, following

the same methodology, are given in the Appendix A.

The data is sampled at intervals of 5 seconds and contains different aircraft performance parameters, such as airspeed, altitude, thrust, and weight. Although thrust is provided in this dataset, it is not measured directly by the aircraft itself. Based on the N1% values recorded in flight, thrust values are calculated post-flight by a General Electric (GE) engine model. This engine model is used by airlines to gain insight into achieved thrust values and is therefore deemed very reliable. In the rest of this paper, new thrust estimation methods will be compared to the output of this GE engine model. All flight data in the dataset is anonymized, meaning it is impossible to retrieve exact aircraft tail-numbers, flight times, or exact weather data. Although aircraft might be of the same type, aircraft can still have significant differences in performance specifications, such as different Maximum Take-Off Weight (MTOW)s. In the current Doc. 29 noise model these performance specifications are extracted from a database based on the aircraft tail-number, which is in this case unavailable due to anonymization. Therefore, some background information on aircraft in the airliner fleet is required to perform a proper analysis of the flight data.

Currently, the airline operates A330-303 aircraft, all having GE CF6-80E1A3 engines. The MTOW and Maximum Gross Landing Weight (MGLW) are 233,000 kilograms and 187,000 kilograms, respectively. Differences within the fleet appear when evaluating the noise record numbers. Two of the five aircraft in the fleet have slight modifications to the acoustic linings in the engines, meaning that they show different acoustic behavior and are assigned and certified for a different noise record number. The noise record numbers mainly impact the correction factors that need to be applied to values obtained from the Noise Power Distance (NPD)-tables. This can cause a difference of 0.8 dB for departures and a difference of 0.5 dB for arrivals, as can be seen in Table 1.1. For creating noise contour plots for the A330-303 aircraft, the record number is assumed to be A5625. As the data was anonymized, it is impossible to determine the actual noise record number of every flight. Therefore, this assumption is necessary to make. The A5625 record number is linked to the A330-301 ANP-proxy.

Table 1.1: Overview of the A330 fleet.

Model	MTOW [kg]	MGLW [kg]	Noise Record	△ Dep [dBA]	△ Arr [dBA]
A330-303	233,000	187,000	A5625	1.4	0.3
A330-303	233,000	187,000	A18091	0.6	0.8

The airline also owns several Boeing 737-800 aircraft, for which 6 slightly different variants can be identified. The main differences between these variants are the winglet configurations. Three variants have a MTOW of 72,000 kilograms and the other three variants 69,000 kilograms. This difference in certified MTOW can be an important factor in estimating the MTOW. The MGLW of all variants is 66,360 kilograms. An overview of all different variants is presented in Table 1.2. To every of the 6 variants, a different aircraft noise record number has been assigned. The correction factors for the A122278 are shown in italics, because no exact match with correction factors was found in the database. As the values of the A120089 proxy showed the most similarity with other data of the A122278 proxy, the data of the A120089 proxy was used as substitution data. Due to the correction factors, the noise contour plots can differ up to 0.5 dB for the Boeing 737-800. The assumed record number in this paper is A120105, as most aircraft in the fleet are of this type. This noise record number is linked to the 737800 ANP-proxy.

Table 1.2: Overview of the B738 fleet.

Model	MTOW [kg]	MGLW [kg]	Noise Record	△ Dep [dBA]	△ Arr [dBA]
737-800	72,000	66,360	A120089	-1.8	-0.1
737-800	72,000	66,360	A120092	-1.8	-0.1
737-800	72,000	66,360	A122278	*-1.8*	*-0.1*
737-800	69,000	66,360	A120105	-2.1	-0.2
737-800	69,000	66,360	A120109	-2.3	-0.1
737-800	69,000	66,360	A120113	-2.3	-0.1

All Airbus A321neo aircraft from this airline are rated with the same specifications, which means that all aircraft are equipped with LEAP-1A30 engines. For the A321neo's, the MTOW and MGLW are 89,000 and 72,900 kilograms, respectively, and the noise data in the ANP-database can be found with the record number A73260. However, this record number does not currently exist in the database, meaning that a proxy from an already existing aircraft should be copied [7]. For this, the A72917 entry of another Airbus A321neo type was used, since this entry had equal values for the lateral, flyover and arrival EPNdB levels. This entry uses the A321-232 ANP-proxy.

All Boeing 777-300ER aircraft in the fleet are also certified equally. These aircraft have a MTOW of 351,534 kilograms and a MGLW of 251,290 kilograms. The correction factors for these aircraft can be found with the noise record number A5609, resulting in an ANP-proxy of 7773ER. Both the data of the Airbus A321neo and Boeing 777-300ER can be found in Table 1.3

Table 1.3: Overview of the B77W and A21N fleet.

Model	MTOW [kg]	MGLW [kg]	Noise Record	△ Dep [dBA]	△ Arr [dBA]
A321-252N	89,000	72,900	A73260	-5.2	-1.5
777-300ER	351,534	251,290	A5609	0.0	0.0

For both the Boeing 777-300ER and the Boeing 737-800, no FPPs are available for the corresponding ANP-proxies. Therefore, only to model thrust behavior, these proxies are replaced with the 737700 and 777300 ANP-proxies. This is done according to Doc. 29 substitution guidelines, which state that in case no profiles are available, the best matching entry should be selected [7].

For all aircraft types, the airline flies a NADP2 800 feet procedure, so all flights in this analysis are assumed to follow this type of NADP. This procedure performs the thrust cutback at an altitude of 800 feet and retracts the flap at this same altitude, given that the zero-flap speed has been reached. In case the zero-flap airspeed has not been reached at 800 feet, the flaps are retracted as soon as this speed is reached.

1.3. Current Doc. 29 modeling implementation

In the Doc. 29 methodology, the weight of the aircraft for departures is estimated based on stage lengths. The stage length category depends on the distance between the departure airport and the destination airport, also referred to as trip length. Table 1.4 summarizes the categorization from trip length to stage length. Based on the stage length, for every aircraft type a weight is assigned using the ANP database. For arrivals, it is assumed that the weight of every aircraft is equal to 90% of the MGLW [7].

Table 1.4: Definition of the stage lengths as presented in Doc. 29 as function of Nautical Miles (NM). [7]

Stage Length	1	2	3	4	5	6	7	8	9
Trip Length (NM · 1000)	<0.5	0.5 - 1	1 - 1.5	1.5 - 2.5	2.5 - 3.5	3.5 - 4.5	4.5 - 5.5	5.5 - 6.5	>6.5

The Doc. 29 best-practice noise model estimates thrust values using FPPs. FPPs are constructed by several data points, giving information on altitude, true airspeed, and thrust values at different distances from the Start Of Roll (SOR). As the parameters of speed, thrust, altitude and distance differ per aircraft type, weight category, and type of procedure, a separate FPP is constructed for every possible combination of these factors. In Figure 1.1a and Figure 1.1b, the corrected net thrust and altitude of several FPPs are plotted against the distance from the SOR. Figure 1.1a shows the dependence of thrust behavior on the type of procedure used and the weight of the aircraft, while Figure 1.1b shows that altitude trajectories are mainly affected by the type of NADP flown. The FPPs used for the analysis in this paper are not the standard profiles provided in the ANP database, but are an adjusted version to better suit the actual operations at Schiphol Airport. Part of the adjusted version is the implementation of derated engine settings for departures. Therefore, no additional correction for derating during initial take-off and climb has to be applied, as it is already accounted for in the FPPs.

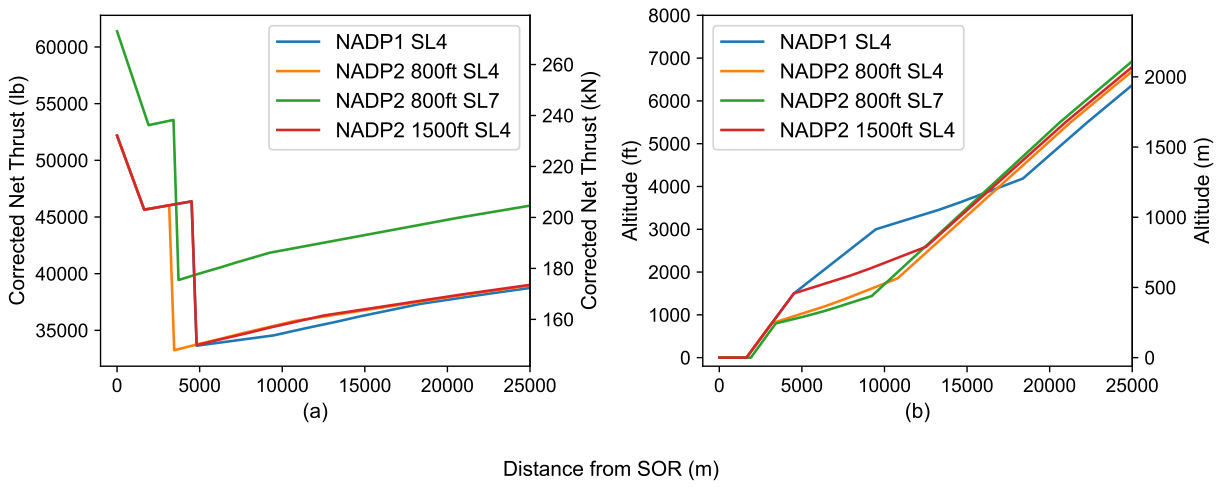

Figure 1.1: (a) Thrust values and (b) altitude trajectories of varying NADP and TOW plotted against the distance from the SOR.

Thrust values are required for the noise calculation as these values can be converted to sound exposure levels by using NPD-tables. These NPD-tables are valid for sea-level pressure conditions and a reference speed of 160 knots. To achieve correct sound exposure for every speed, additional correction factors are applied [7]. It is important to remember that Doc. 29 uses corrected net thrust values to model aircraft noise, thus correcting thrust values at altitude with the ambient pressure ratio at sea level [7].

To reduce the complexity and computational cost of the model, assumptions and simplifications are made in the Doc. 29 modeling methodology. Many of these assumptions are related to how flight procedures have to be implemented in the model for both departures and arrivals, and are therefore directly linked to the implementation of these FPPs. By simplifying the model, errors are simultaneously introduced into the model. To properly understand the functioning and limitations of the Doc. 29 model, these assumptions should be carefully evaluated.

Firstly, in the Doc. 29 methodology, real altitude trajectories of a flight are never used to compute the noise calculation. Instead, the altitude trajectory is always replaced by the altitude of the corresponding FPP. For departures, the NADP considered, for which the FPPs are selected accordingly, is determined based on historical data. The historical dataset contains information about which NADP have been used for every combination of airliner and aircraft type [11]. For arrivals, the method for assigning a procedure, and thus FPPs, to flights is more extensive. The altitude trajectories of the real flight data (z_{real}) are compared with the altitude trajectories of all available FPPs ($z_{profile}$) by computing a least squares error ϵ between an interval of 12 and 50 kilometers to the landing threshold, as described in Equation 1.1. The FPP with the lowest least squares error is finally assigned to the flight. The corresponding thrust values for this FPP are used for further calculations in the noise analysis [5].

$$\epsilon = \sum_{n} \left(\frac{z_{profile} - z_{real}}{z_{real}} \right)^2 \tag{1.1}$$

Secondly, for departures, aircraft behavior between an FL100 and FL200, corresponding to altitude values between 3 and 6 kilometers, is heavily simplified in the FPPs. The climb rate is assumed to be constant and extrapolated from the two preceding data points, while the thrust and the airspeed are assumed to be constant for this part of the flight [5]. Here, a Flight Level (FL) is the standardized altitude, which means the altitude is calculated with respect to the standard sea level conditions of 101325 pascals, per 100 feet. In Figure 1.5a and Figure 1.5b, it can be seen that the flight performance of real flights is no longer accurately predicted due to this simplification in the modeling between FL100 and FL200. Although this segment of the flight is less relevant noise modeling due the relatively higher altitude values, it can still have a significant

impact on the final outcome of the noise model.

Third, for both departures and arrivals, a headwind of 8 knots is assumed at all times to model flight performance parameters. For calculating the sound propagation through the air, no wind conditions are considered. Inconsistent with the assumption of the headwind, the FPPs for departures start at a true airspeed of 0 knots, meaning the aircraft would be moving backwards relative to the ground. In this paper, this error will not influence the outcome of the noise model. However, this error should be taken into account when generating aircraft noise forecasts for flights that have not yet occurred.

Also, the weight of the aircraft changes constantly throughout a flight. For best-practice noise modeling, only a small part of the total flight is considered. Therefore, to simplify the model, the weight of the aircraft is assumed to be constant during the entire part of the flight considered for noise modeling. For departures, the weight at the SOR is considered to be the Take-Off Weight (TOW), while for arrivals the landing weight is set to the weight at the landing threshold. For both departures and arrivals, these weights are obtained from the ACMS.

Overall, the current Doc. 29 calculation method can be summarized for departures and arrivals by the flow charts in Figure 1.2 and Figure 1.3.

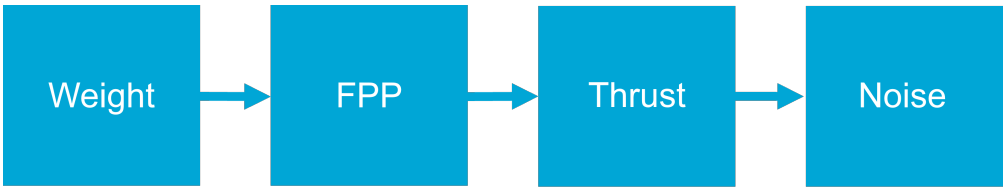

Figure 1.2: Flow chart summarizing the current Doc. 29 modeling methodology for departures.

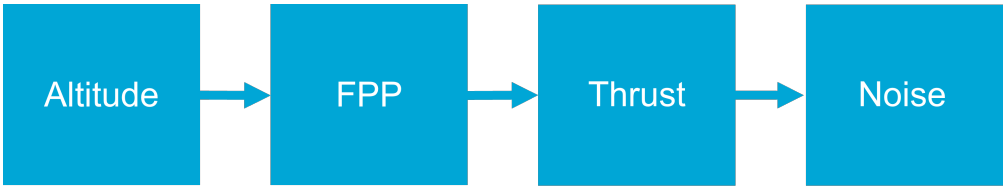

Figure 1.3: Flow chart summarizing the current Doc. 29 modeling methodology for arrivals.

1.4. Proposed methodology departures

With the current methodology of Doc. 29 explained, changes to the weight and thrust estimation methods are introduced in this section. This paper aims to improve the estimation methods with publicly available flight performance parameters, such as altitude, true airspeed, calibrated airspeed, and ground speed. The rotational speed of the low pressure compressor (N1%) and thrust values, present in the ACMS dataset, are only used as validation or training data. The flow chart for departures in Section 1.3 can be adapted for the changes introduced in this paper, resulting in the flow chart in Figure 1.4. The methodology proposed in the paper can be performed with open source data and is valid for nominal flights only. Therefore, as a first step, anomalous flights are filtered from the dataset before evaluation. The criteria the flights are filtered on are as follows:

- Flights with a thrust cutback during the climb phase are removed
- Flights failing to be identified as a NADP2 procedure are removed
- Flights accelerating past a calibrated airspeed of 250 knots before FL95 within the Terminal Maneuvering Area (TMA) boundaries are removed

The filtered altitude trajectories of the A333 departures are plotted against distance from the SOR in Figure 1.5a. This plot shows that lighter aircraft generally climb with a steeper climb gradient compared to

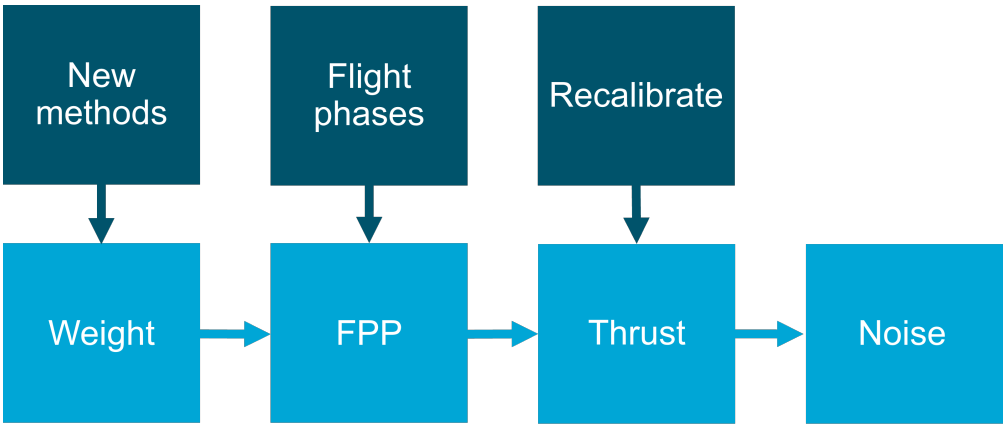

Figure 1.4: Flow chart summarizing the proposed Doc. 29 modeling methodology for departures.

heavier aircraft, thus requiring less distance from the SOR to achieve a specified height. Especially, between an altitude of 2500 and 10,000, feet the trajectories in the plot fan out. Similar behavior is visible from 11,000 feet onward.

The altitude data of the flights in the dataset, can be immediately compared against the FPPs. Here, the upper black line in Figure 1.5a corresponds to the lowest stage length category (1), and the lower black line corresponds to the highest available one (7). The operational range of the Airbus A330 is insufficient to reach the trip lengths associated with stage lengths 8 and 9. For the altitude trajectories, it can be seen that the bandwidth of the FPPs is too small compared to the flight data. Therefore, altitude behavior is not accurately modeled by the FPPs for this aircraft type.

In Figure 1.5b, the True Airspeed (TAS) trajectories of A333 flights are visualized. All TAS trajectories follow the same trend and no dependence on the TOW is visible. The TAS indicates the actual velocity of air over the wings. As this speed can be directly compared to the stall speed of the aircraft to check whether sufficient lift is generated by the wings to stay in the air, it makes sense that the Flight Management System (FMS) of aircraft controls this speed. All TAS trajectories follow the same trend, as the stall speed dictates a minimum speed to be flown. The original FPPs, suitable for operations at Schiphol Airport, aim to predict the mean trend of all flights. Up to 30 kilometers from the SOR, these speed trajectories match with the actual flight data. After passing this distance, the trajectories start to deviate as linear interpolation of performance is assumed between FL100 and FL200. [5].

In Figure 1.5c and Figure 1.5d, the N1 and thrust values of all departures are visualized. The N1% values for all Airbus aircraft are corrected with the square root of the total temperature ratio with the reference value set to the sea level condition. For Boeing aircraft, applying this correction factor decreased the correlation between N1% at the SOR and take-off weight. Therefore, it assumed that the ACMS of Boeing aircraft automatically corrects with this correction factor. For corrected net thrust, the initial thrust values were corrected with the air pressure ratio, again with the reference value set to the sea level condition. During the initial take-off roll on the ground, the N1% setting is seen to depend on the TOW of the aircraft. However, during the later stages of the flight, this dependency is no longer present.

Contrary to the altitude trajectories, the bandwidth for thrust in the FPPs is too large. This time, the upper black line in Figure 1.5d corresponds to the largest stage length and the lower black line corresponds to the lowest stage length. However, in the flight data an opposite effect is visible. Less heavy aircraft seem to climb at a higher net corrected thrust value. This can be explained by the fact that the net corrected thrust is corrected with the air pressure ratio between the air pressure at altitude and the air pressure at sea level. As lighter aircraft climb faster, the air pressure at an equal distance from the SOR is smaller, therefore the correction factor is larger resulting in a larger net corrected thrust value.

From Figure 1.5a and Figure 1.5d, it can be concluded that the current method of modeling the FPPs does not match the flight data. Instead of increasing engine power for heavier flights, the power is kept constant.

As a result, the climb performance of aircraft degrades with increasing TOW. The effect of the difference between the assumed and real flight performance on noise contour plots is hard to predict, since this will be a balance between a decreasing distance to the observer and a decreasing amount of engine power. Both effects counteract each other, and noise contours should show which effect of the two is dominant in the end.

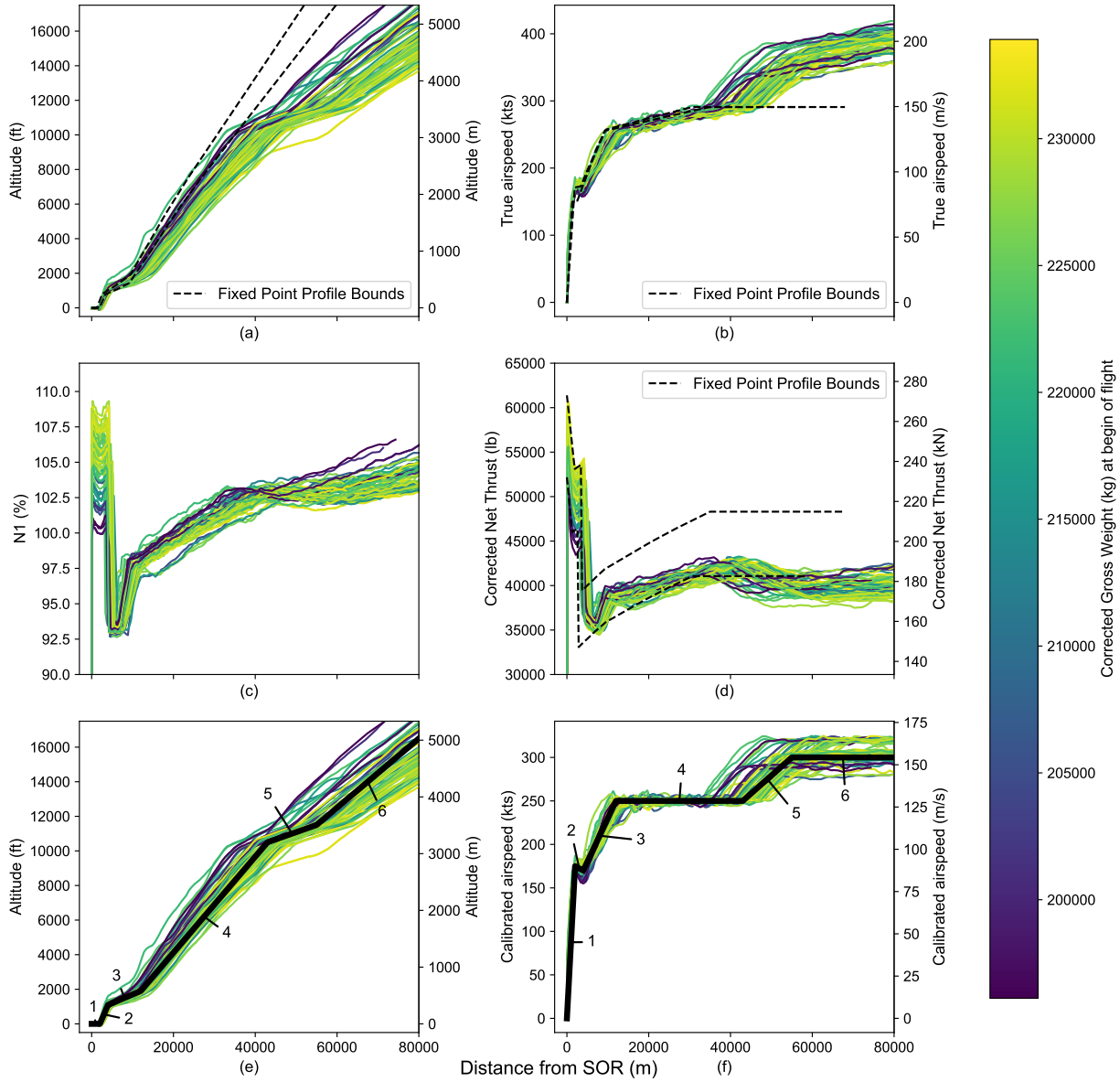

Figure 1.5: (a) Filtered altitude trajectories compared to the FPPs, (b) filtered true airspeed values compared to the FPPs, (c) N1 values, (d) thrust values compared to the FPPs, (e) altitude trajectories showing 6 separate flight phases, and (f) filtered CAS values showing 6 separate flight phases of A333 departures with varying TOW obtained from the ACMS data.

In the ACMS data, a clear departure pattern can be identified consisting of six phases. For clarity, these six phases are highlighted with a black line in the altitude trajectory plot in Figure 1.5e and Figure 1.5f. From 1 to 6, these flight phases can be identified as: initial take-off roll, initial climb phase, second acceleration phase, second climb phase, third acceleration phase, and the third climb phase. The start and end points of these flight segments can vary significantly between flights, and thrust settings often change between these

flight phases. Identifying the boundary points of these flight phases for every single flight is needed to fit the FPPs accordingly. Computational efforts should be minimized to allow application to larger datasets as well. As Calibrated Airspeed (CAS) is corrected for both compressibility and density, this airspeed can be seen as a normalized version of the TAS. This CAS is a representation of the dynamic loading on the aircraft, ensuring equal handling for different altitudes and temperatures at similar CAS values. Within 30 km of the SOR, all aircraft are required to stay below 250 kts CAS, since this is speed restriction within the TMA of Schiphol [12]. After leaving the TMA, this speed restriction is lifted and aircraft are allowed to accelerate further towards their cruising speed.

As the Doc. 29 methodology always replaces the real altitude values of a flight with the altitude values of a FPP, an error is introduced in the model. However, real altitude values are publicly available and can be used for noise modeling purposes. Therefore, both the ACMS Doc. 29 and the new thrust and weight Doc. 29 models will use real altitude values.

Furthermore, for departures, the interpolation of aircraft performance from FL100 towards FL200 is invalid and does not match with real flight data. This result is expected since several important airspace restrictions are lifted after FL95, the altitude which corresponds to the upper limit of the TMA [12].

1.4.1. Flight Phase Identification

From Figure 1.5e and Figure 1.5f, it can be seen that during acceleration phases the altitude trajectory tends to flatten. Contrary, the CAS trajectories flatten during the climb phases. This means that, for departures, engine power is converted to either potential energy (altitude) or kinetic energy (speed). Because the CAS is corrected for both the compressibility and the density effect, the speed remains constant during climb sections. For this reason, CAS is preferred over TAS and ground speed to identify the boundaries of every flight phase.

Furthermore, to identify the flight phases, the derivatives of both altitude and calibrated airspeed are taken with respect to time. The derivatives of the flight performance parameters represent the instantaneous rate of change of that parameter. Both derivatives for altitude and calibrated airspeed are expected to show smooth behavior when the derivatives are evaluated. However, when examining the derivative data, noisy patterns were observed. Therefore, both parameters were smoothed with a moving average filter of a window size of 3 to limit the noisiness of the data.

To ensure that the two parameters are comparable, they are normalized prior to analysis. For this case, the min-max normalization technique was selected, as this method works well for bounded parameters and preserves the original distribution of the data. The formula applied for min-max normalization is given in Equation 1.2. For every single flight, this min-max normalization is applied separately, meaning the reference conditions vary between flights.

$$x' = \frac{x - \min(x)}{\max(x) - \min(x)} \tag{1.2}$$

To determine the exact boundaries of every flight phase, a linearly penalized segmentation method is used in the form of a Pruning Exact Linear Time (PELT) algorithm. This method is implemented using the ruptures library in Python [13]. In this PELT algorithm, a global cost function is minimized to find the exact change points in the data with Equation 1.3. This global cost function contains an error term determined by the lack of fit of every segment, called C_i, and a penalty term scaled by the number of change points. The model to determine the lack of fit between the model and the data is selected to be an absolute deviation (L1) model. This model is more robust against outliers as the cost function grows linearly with deviations, instead of quadratically.

$$\text{cost} = \sum_{seg} C_i + \text{penalty} \cdot \text{number of change points} \tag{1.3}$$

As this method is an optimization function, it can also generate change points in nonlogical locations due to the noisiness of the data or sudden deviations. Therefore, to guide this function, some constraints are

specified to which the model should adhere. This ensures that the result of the segmentation model is meaningful and matches the reality. However, these conditions should be constructed with care not to over-constrain the model. For example, in the case of a thrust cutback, the model should still identify this part of the flight as a separate segment. Therefore, the conditions are mainly constraining the early flight phases. The conditions imposed on the model are as follows:

- The initial take-off roll should be finished within the first 75 seconds of the flight
- The initial climb phase should be finished within the first 150 seconds of the flight
- The minimal duration of every flight phase is set to 20 seconds
- The flight should have at least six flight phases

At initialization, the constraint for the number of flight phases is set to six. The penalty of the PELT-function is adjusted accordingly to aim towards a converging segmentation with six flight phases, while satisfying all other constraints. In case convergence cannot be reached, the number of flight phases is increased with one and the program is reinitialized. This continues until finally the program converges and all constraints are satisfied.

A result of the flight phase identification process for a nominal flight is depicted in Figure 1.6. Six clear flight phases are visible in this graph, determined by the change in CAS and altitude of the aircraft. During the second climb phase, variations in the CAS and vertical velocity are clearly visible, but their are not significant enough to be separated into different flight phases.

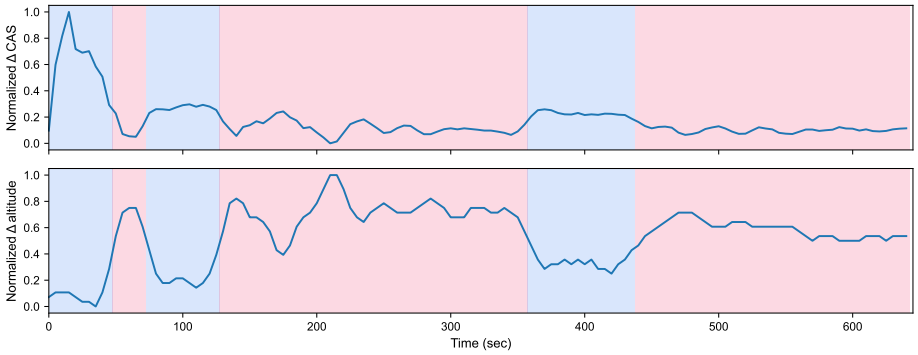

Figure 1.6: Result of the flight segmentation model for flight 0 of an A333 aircraft showing 6 segments.

In Figure 1.7, the result of an anomalous flight is visualized. In this figure, eight flight phases are identified due to a thrust cutback during the second climb phase. The decrease in the vertical velocity of the aircraft is in this case significant enough to cause the second climb phase to split. For further analysis, flights with thrust cutbacks are filtered out.

Unfortunately, the model is not perfect and sometimes misidentifies flight phases. In Figure 1.8 seven flight phases are identified, which is one more than expected. However, due to the TMA restrictions, the correct boundary points can still be identified because the third acceleration phase may not start before FL95 [12]. The altitude values are not indicated in the flight phase segmentation plots, but usually this altitude is reached around 400 seconds into the flight. If more than 3 change points are identified below FL95, only the first 3 of this set are taken. If more than 2 change points above the TMA boundary altitude are observed, the two change points closest to FL95 are selected. Therefore, a complete set of boundary conditions can still be obtained for flights with 7 identified flight phases.

1.4.2. New weight estimation methods

The second climb phase, the third acceleration phase, and third climb phase show dependencies on the weight of the aircraft for different aircraft performance parameters. Therefore, these flight phases are investigated in more detail to be used for a weight estimation method based on flight performance parameters.

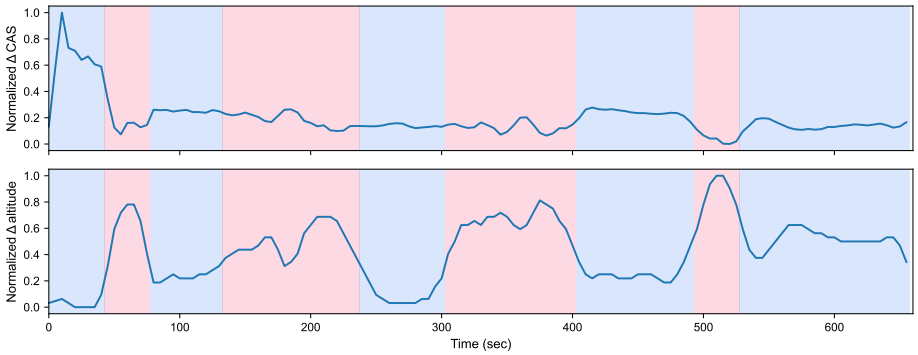

Figure 1.7: Result of the flight segmentation model for flight 24 of an A333 aircraft showing 8 segments.

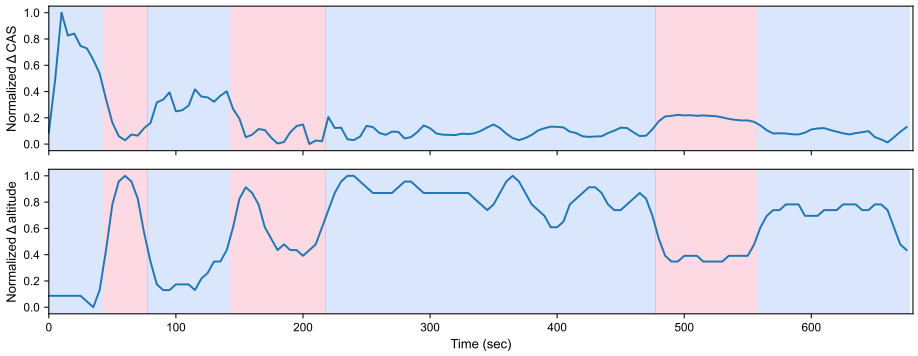

Figure 1.8: Result of the flight segmentation model for flight 17 of an A333 aircraft showing 7 segments.

Two different weight estimation methodologies will be developed in this paper, trained and validated with the ACMS data;

- A climb slope and distance based method between 3000 and 9000 feet (roughly 0.9 and 2.7 kilometers) altitude
- A specific energy method between 12,500 and 17,500 feet altitude (roughly between 3.8 and 5.3 kilometers)

For the A333 climb slope and distance based method, the evaluated distance is the distance from the SOR to the aircraft reaching a ground speed of 325 knots.

The inverse of the average climb slope between 3000 feet and 9000 feet altitude for every flight is plotted against the TOW in Figure 1.9a. It is visible that the division of weights in the dataset is not equally distributed. Relatively, there are more heavy flights in the dataset than lighter ones. Furthermore, it can be seen that the heavier flights show quite a large spread in the inverse climb slope compared to lighter flights. Although not very clear, still a linear trend is visible.

In Figure 1.9b, the distance from the SOR to the aircraft passing a ground speed of 325 knots is visualized. For this weight estimation, the ground speed parameter has been chosen above other speeds. The ground speed parameter is the only speed parameter that captures changes in drag due to wind effects. A clear linear relationship is visible in the plot. Four outliers are still present in the right half of the graph.

To fairly compare the inverse climb slope and the distance to reach a ground speed of 325 knots with each other, the parameters should be normalized. As was visible in Figure 1.9b, outliers are still present in the dataset. A min-max normalization technique, as was used in the flight identification process, is sensitive to these outliers and is therefore not suited for this application. As a z-score normalization method directly

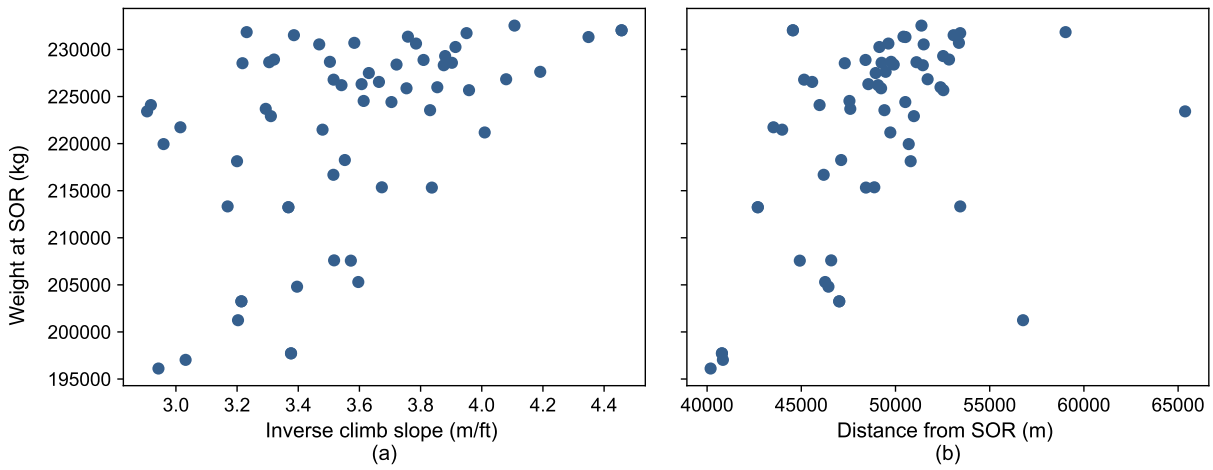

Figure 1.9: Weight plotted against (a) the inverse climb slope and (b) the distance from the SOR at which a ground speed of 325 knots is reached for A333 departures.

gives information on how many standard deviations data points are located away from the mean, this method is selected. This makes anomaly detection and statistical analysis easier at a later stage. Therefore, the method of z-score normalization is selected. The formula to calculate the z-score is given in Equation 1.4. To combine both of the z-score values, the average of the inverse climb z-score and the distance to 325 knots z-score are taken, as described in Equation 1.5.

$$z_i = \frac{x_i - \mu}{\sigma} \tag{1.4}$$

$$\bar{z_i} = \frac{z_{climb} + z_{dist}}{2} \tag{1.5}$$

Due to the normalization, all z-scores can now be compared with each other. To remove the outliers from the dataset, a confidence interval of 95% is selected. This means that all average z-scores with an absolute value greater than two are removed from the dataset. However, removing these outliers changes both the mean and the standard deviation of the dataset. This requires all z-scores to be recomputed in an iterative process until the absolute values of the average z-scores are below two. The remaining data points are visualized in Figure 1.10a. Through these remaining data points, an Ordinary Least Squared (OLS) solution is fitted to extract a linear relationship. However, by fitting a OLS solution, the solution is biased towards the heavier flights because the weights in the dataset are not equally distributed. Therefore, it would be more logical to fit a Weighted Least Squared (WLS) based on the distribution of TOWs. To apply the WLS method, the data is divided into 6 bins, all covering an equally distributed weight range for every aircraft type. This method therefore assigns relatively greater weight to bins containing fewer observations than bins with many observations. In practice, this means that a relatively larger weight is applied to flights with a lower TOW.

The second method is a more direct one, immediately computing the specific energy per meter based on the increase in potential and kinetic energy. The advantage of this method is that the computation of z-scores is no longer necessary, meaning the calculation can be performed without having the statistical relationship of this dataset. The specific energy between a two altitudes can be computed with Equation 1.6. Here, g is the gravitational constant in m/s, Δh the difference in altitude in meters, v the ground speed in m/s and Δv the difference in ground speed between the altitude boundaries in m/s. Finally, this specific energy is divided by the distance of the segment to equally compare flights with each other.

$$\frac{E}{m} = \frac{g\Delta h + \frac{1}{2}(v + \Delta v)^2}{\Delta d} \tag{1.6}$$

The plot of the specific energy per meter against the weight of the aircraft for A333 flights is presented in Figure 1.10b. In this plot, a clear linear trend is visible, showing that lighter aircraft usually have a higher specific energy per meter. The benefit of analyzing the specific energy instead of the separate climb slope is that increments in velocity between the altitude boundaries are also taken into account.

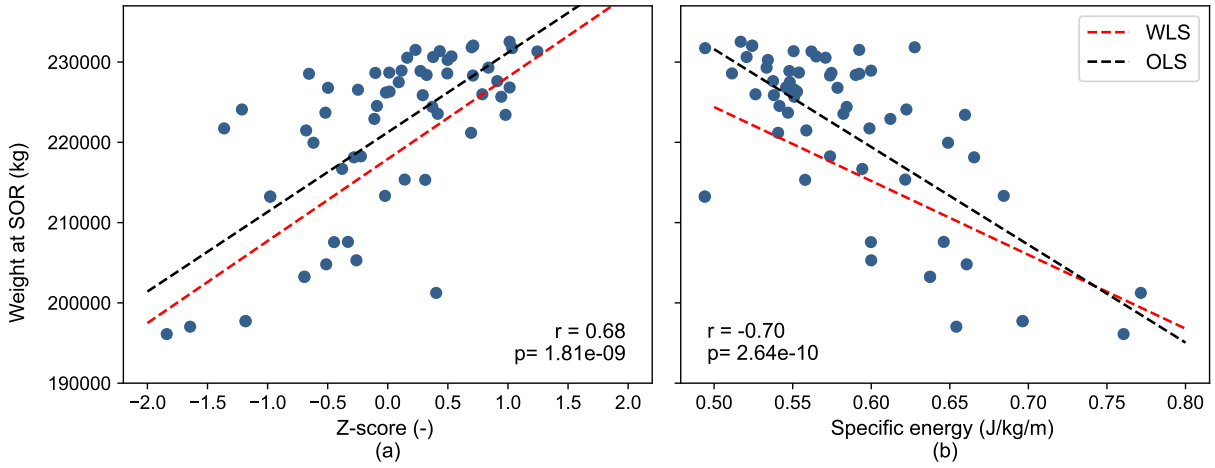

Figure 1.10: Aircraft weight plotted against (a) the combined z-scores and (b) specific energy per meter fitted with an OLS and a WLS trend line for A333 departures.

Taking into account velocity increments is necessary for aircraft types with multiple climb modes during climb. This can best be illustrated by Figure 1.11a. Here, during climb, between 5,000 and 40,000 meters from the SOR, three different climb modes can be clearly observed. In addition, a dependency based on TOW seems to exist. As a result of these climb modes, the performance of climb slope and distance based method decreases significantly. The linear relationship (r-value) even becomes insignificant, as can be seen in Figure 1.11b. The p-value of the relationship is still significant, indicating that the datasets are sufficiently large. Therefore, it is expected that the specific energy weight estimation method will outperform the climb slope and distance based weight estimation method.

To compare the results of the weight estimation fairly with each other, a metric should be selected. For this, the MAPE is selected, as this parameter allows comparisons between different datasets. The formula used to calculate the MAPE is presented in Equation 1.7.

$$\text{MAPE} = 100\% \cdot \frac{1}{n} \sum_{t=1}^{n} \frac{|W_{real} - W_{pred}|}{W_{real}} \tag{1.7}$$

Because the dataset is anonymized, the destination airport of every flight remains unknown. Therefore, it is not possible to determine the distance between the destination airport and the departure airport, as is the standard for the original Doc. 29 model. However, the actual departure weight found in the ACMS can be linked to the closest weight entry of the stage length categories in the ANP database, thus creating a best possible estimate. For this estimate, the MAPE can be determined and immediately gives the optimal weight estimation that can be achieved by the stage length method. In reality, the error of the stage length method will always be larger than presented in this paper. For aircraft types other than the A333, the same methodology for estimating the weight will be used and similar plots as presented in this section are visible in Appendix A.

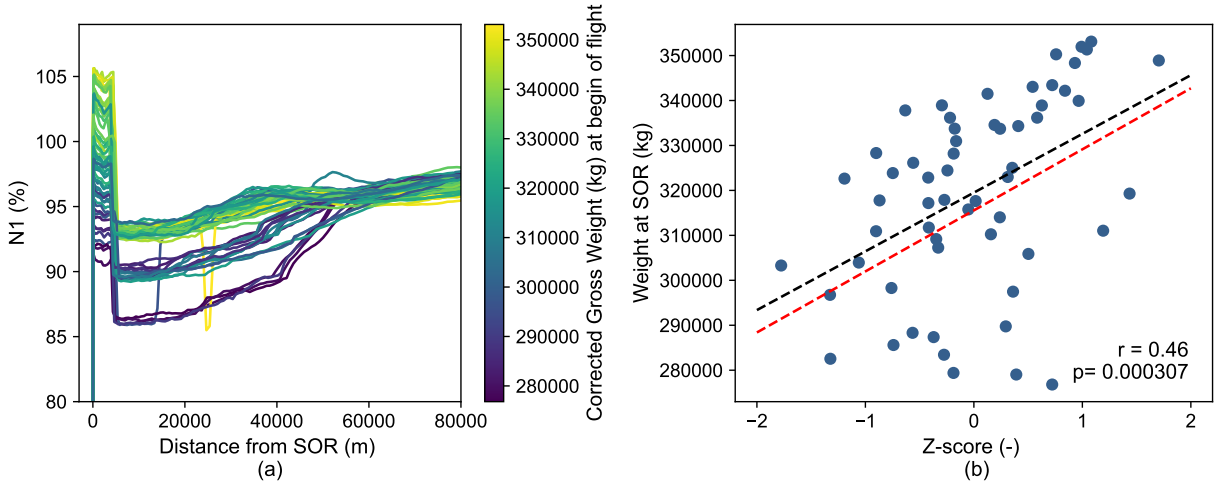

Figure 1.11: (a) Filtered N1% settings of B77W flights with varying TOW and (b) aircraft TOW plotted against the combined z-scores fitted with an OLS and a WLS method for B77W departures.

1.4.3. Thrust estimation

Current FPPs do not allow for any variability in the thrust modeling based on observed behavior of specific flights. To add variability to the FPPs, the boundaries of the identified flight phases in Subsection 1.4.1 can be used. For example, the thrust cutback for an NADP2 procedure at Schiphol Airport is usually performed at an altitude of 800 feet, which coincides with the start of the second acceleration segment. Therefore, the distance flown from the SOR to this point of thrust cutback is already identified and can be used to set the new thrust values in the FPPs.

During the initial take-off roll and initial climb out, the net corrected thrust of the aircraft depends on the weight of the aircraft, as can be seen in Figure 1.5d. Maximum thrust values are achieved for the heaviest aircraft. Therefore, the thrust values in these stages of the flight will be interpolated linearly between the thrust values observed for the heaviest and lightest flights, depending on the estimated weight.

As no correlation with weight was observed for the A333 after the point of thrust cutback, a median thrust level is assigned to every flight. This means that the thrust is equal for every flight. The variability then depends on the distance from the SOR at which certain thrust levels are activated. As stated earlier, this distance is dependent on the boundaries of the identified flight phases. Combining both the weight dependent element of the flight with the median value at the identified boundaries, generates the thrust variation along the flight trajectory. The thrust values can then be used in the Doc. 29 model to generate noise contour plots.

1.5. Proposed methodology arrivals

Similarly to departures, the arrival data is plotted against the distance. The arrival data is expected to show more spread compared to the departure data, as traffic towards Schiphol Amsterdam Airport is often vectored. Vectoring means that the path the aircraft needs to follow is fully determined by Air Traffic Control (ATC) to avoid collisions with other aircraft in the airspace. This results in irregular altitude and thrust along the flight trajectory due to ATC restrictions prior to the final approach. In the final approach, the aircraft behavior is expected to be predictable, since all aircraft are following an equal altitude trajectory.

Flight data confirms this hypothesis of irregular behavior, as can be seen in Figure 1.13a and Figure 1.13b. For the altitude, many different altitude trajectories can be distinguished and three FPPs altitude trajectories are plotted as an example. Based on the Doc. 29 methodology, modeling aircraft behavior with a fixed set of profiles, bundling of several flights following a similar procedure is expected. However, such 'bundling' is not visible in the data used for this research. When considering the thrust, as depicted in Figure 1.13b, no clear trends with distance or weight are observed. These two plots indicate that the weight of arriving aircraft has no correlation with altitude and thrust values. This means that accurately predicting the weight

of the aircraft is not required to predict thrust values. Therefore, for arrivals, the focus in this paper will be on finding flight parameters that are indicative of the occurrence of thrust peaks. An overview of the proposed methodology for arrivals is presented in Figure 1.12.

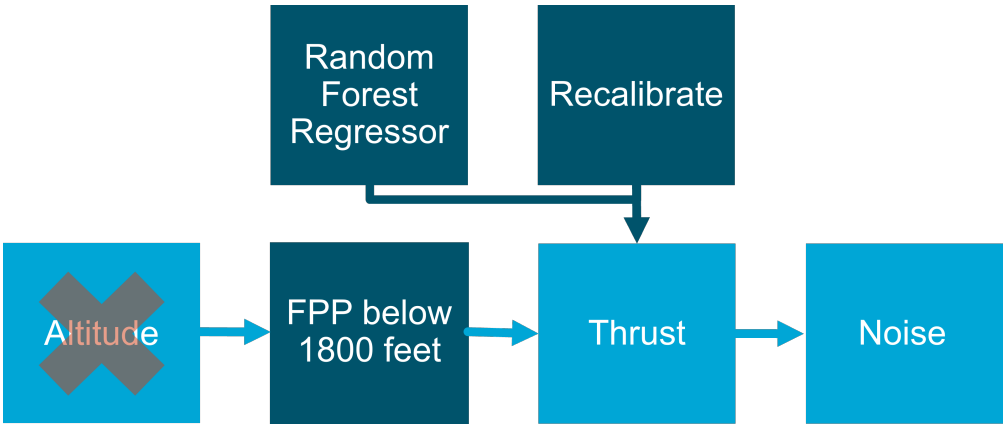

Figure 1.12: Flow chart summarizing the proposed Doc. 29 modeling methodology for arrivals.

An arrival of an aircraft can be simplified to an arbitrary energy system that should come to a standstill at the end of the runway. Both potential energy in the form of altitude and kinetic energy in the form of velocity should be reduced to zero. Furthermore, the aircraft should adhere to all instructions received from ATC. These instructions from ATC can require an aircraft to keep the speed or altitude constant. In case an insufficient amount of energy is available in the system to adhere to these instructions, thrust can be applied as an additional energy input. However, this means that a thrust input should be visible in other flight performance parameters, such as the flight path angle or the change in airspeed. As the CAS is corrected for altitude effects, this airspeed parameter is selected to be used. Evaluating the available data trends for these two parameters, a correlation between flight path angle, differences in CAS and thrust values was detected (not shown in this paper). However, it was difficult to draw clear conclusions from these trends. Therefore, to see if a relationship could be extracted, a random forest regressor model was trained on the flight path angle and calibrated airspeed data to obtain net corrected thrust values. This method will be applied to flight data above an altitude of 1800 feet, as below this altitude the standard 3° glideslope of the Instrument Landing System (ILS) is followed.

To train a random forest regressor model, data pre-processing is essential to get meaningful results. For random forest models, the input data is required to be independent of each other. Randomizing the order of the data points ensures this independence and prevents a bias to be introduced into the model [14]. Additionally, to ensure this independence, the dataset should be split into a training set and a test set. Not splitting the data would again result in a bias in the results, as the test data will contain the exact data points the model is trained on. Therefore, the first 50 flights of every dataset are used for training and the remaining flights are used for testing the model. The training set is randomized with sample command in Python using random state 42 as setting. Because the ACMS data contains measurement noise, a centered moving-average filter is applied to all parameters prior to usage in the model. For the CAS trajectories, the window is set to 8, while for the flight path angle and the net corrected thrust values, a window of 7 is applied. These settings ensured that the best performance of the model was achieved.

The thrust behavior of two flights in the test dataset is visualized in Figure 1.14a and Figure 1.14b. The predicted thrust values in Figure 1.14a closely match the values obtained from the GE-engine model in the ACMS data. Although idle thrust values vary with distance and contain some error, both the location and magnitude of the thrust peak is predicted accurately. The error for idle thrust settings was expected, as slight differences in flight path angle and CAS occur in flight. In Figure 1.14b, one thrust peak is not captured by the random forest regression model, whereas the other thrust peak is accurately predicted. In this particular flight, the thrust value was increased without a corresponding increase in flight path angle or a significant change in the CAS trajectory. Therefore, the thrust peak was missed, showing that this model still contains

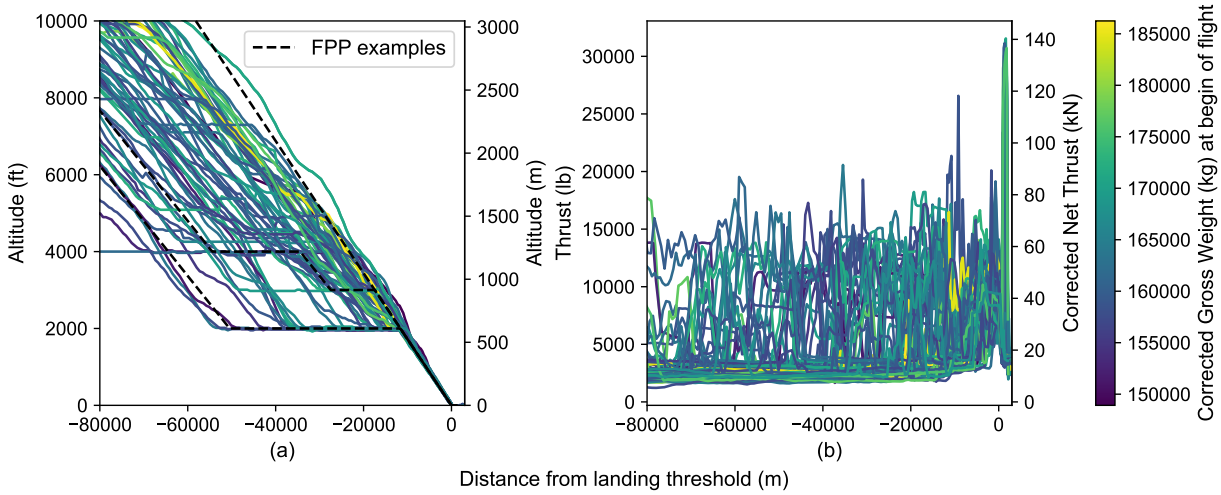

Figure 1.13: (a) Altitude trajectories and (b) thrust values of A333 arrivals with varying TOW.

some errors. Out of the 19 evaluated flights for the A333, this was the only flight with a thrust peak over a thrust value of 6500 pounds that was missed.

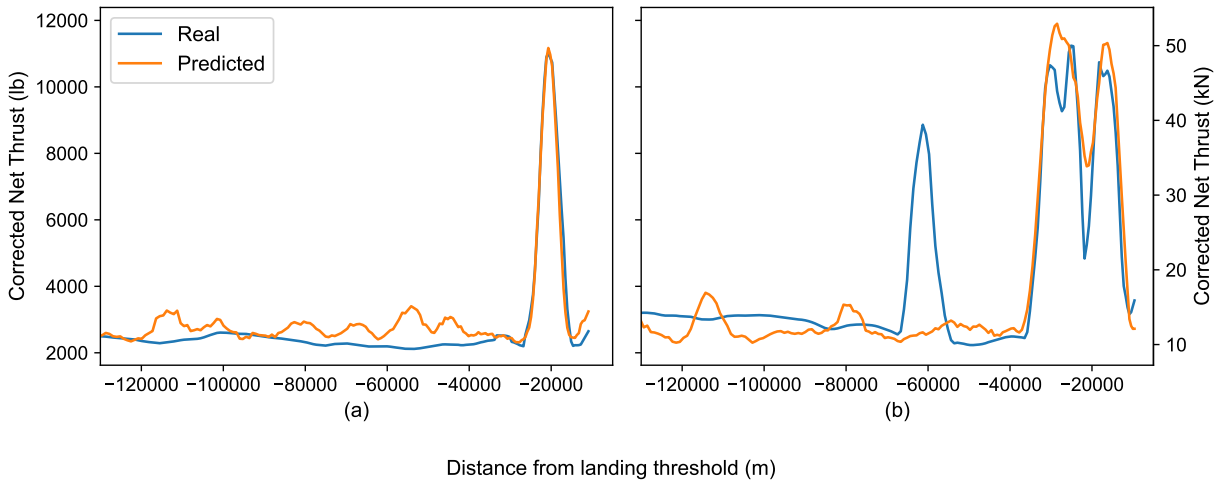

Figure 1.14: Net corrected thrust values (a) for flight 68 and (b) for flight 67 estimated with a random forest regressor model compared to the original thrust values calculated with the GE-engine model.

In this paper, the final approach section of arriving flights is modeled by using FPPs below an altitude of 1800 feet. Since aircraft follow the same altitude trajectory in this part of the flight, thrust is much more predictable and mainly shows a dependency on the flap setting used during landing. If the flap setting at landing is known, the thrust can be accurately modeled by using FPPs due to this predictable behavior. However, estimating the flap setting during landing is outside the scope of this paper and will therefore not be investigated. Flap handle position data is available in the ACMS dataset and therefore the flap setting at landing is known in this paper.

To approximate the thrust values below 1800 feet altitude, the original FPPs are re-calibrated. The re-calibration is performed for every observed flap setting at landing, which are a full flap (flap 4) and a reduced flap (flap 3) setting, by approximating the median thrust behavior of all flights in the dataset. The result of the re-calibration is shown in Figure 1.15. As these re-calibrated FPPs do not start at 1800 feet altitude itself, a linear interpolation is performed for the period between the start of the FPPs and the last predicted thrust value by the random forest generator. This interpolation ensures a smooth transition towards thrust

modeling on the ILS glideslope.

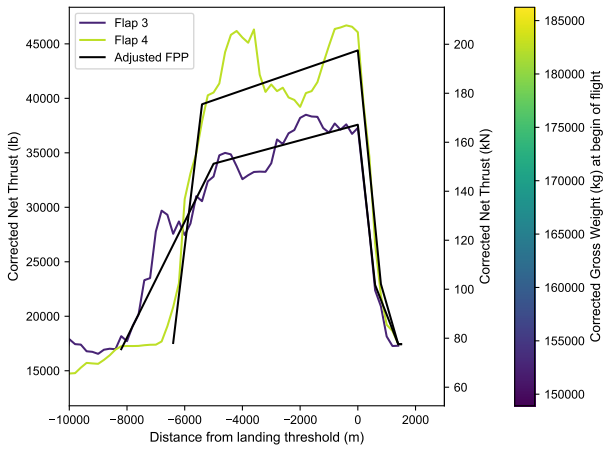

Figure 1.15: Median thrust values for reduced flap settings and full flap settings of A333 flights approximated by FPPs

1.6. Results

In this section, the results of the weight estimation methods will be presented in Subsection 1.6.1. In Subsection 1.6.2, the noise contour plots of the original Doc. 29 model, the ACMS Doc. 29 model, the new thrust and weight Doc. 29 model are compared. Flight data originating from the ACMS of aircraft and the thrust values GE engine model are directly inputted in the ACMS Doc. 29 model. Therefore, this model will give the most accurate results and can be considered the baseline model. The performance of the original Doc. 29 model and the new thrust and weight Doc. 29 model will be compared to this baseline. Both the ACMS Doc. 29 model and the new thrust and weight Doc. 29 model use real altitude trajectories for the noise calculation. An overview of all 3 models is given in Table 1.5.

Table 1.5: Caption

	Original Doc. 29	ACMS Doc. 29	New thrust and weight Doc. 29
Altitude	FPPs	Real altitude	Real altitude
Weight	Stage length	ACMS	Specific energy
Thrust	FPPs	ACMS	Dynamic FPPs + random forest regressor

1.6.1. Weight estimation

For the weight estimation, only nominal flight are considered. This means that for the A333, 65 flights out of 71 remain after filtering. For the B77W, 59 remain out of 71, for the A21N, 64 remain out of 70, and for the B738, 56 remain out of 70. For the climb slope and distance method, flights outside the 95% confidence interval are also filtered out. Therefore, one additional flight is filtered for the A333, B77W, and the A21N only for this method. By assigning a weight from the ANP database closest to the real TOW, the MAPE was calculated to be 3.52% for the original weight estimation method described in Doc. 29 for the A333. The climb slope and distance method resulted in a MAPE of 2.68% and the specific energy method in a MAPE of 2.74% for the A333. Following the same methodology, similar results were obtained for the other aircraft types. These results are summarized in Table 1.6. Overall, the specific energy method outperforms the climb slope and distance method. Therefore, the specific energy method is selected to be used when generating the noise contour plots for the new weight and thrust estimation Doc. 29 model.

The weight estimation methods presented in this paper did not outperform the deep learning methods found in the literature, for which MAPE-values were found from 0.98% to 1.35% [9]. However, the method in this paper showed that it is possible to estimate the TOW with flight performance parameters of later flight segments, as well as improving on the current weight estimation methodology of Doc. 29 for Airbus A330.

Table 1.6: Table with MAPE results of the weight estimation for all aircraft types.

ICAO code	# of flights	Stage Length	Climb slope and distance	Specific energy
A333	65	3.52 %	2.68% (*64 flights*)	2.74%
B77W	59	1.57%	6.23% (*58 flights*)	2.43%
A21N	64	3.03%	4.76% (*63 flights*)	3.24%
B738	56	1.75%	4.67%	4.19%

Values for weights in the ANP database often contain entries of older aircraft models than currently in use. For example, weight data in the ANP database is only available for Airbus A330-301 aircraft, while the airline is operating only Airbus A330-303 aircraft. Also, the results of the stage length method are the optimal results that can be achieved. In reality, the MAPE of this method will be larger.

1.6.2. Noise Contour Plots

Following the Doc. 29 calculation method, noise contour plots can be created to visualize the noise levels in an area. For the three Doc. 29 models considered in this paper, the original Doc. 29 model is only modified for the thrust estimation, weight estimation, and altitude trajectories. All other calculation guidelines are followed as described in Volume 3 of the Doc. 29 methodology. In every figure, the noise levels are visualized in a summed Sound Exposure Level (SEL)-metric, which is an A-weighted noise metric normalized with a reference duration of one second. Usually, SEL-values are used to indicate noise levels of a single aircraft event. For visualizing multiple events, SEL-values can be computed by adding dBA values logarithmically together. The advantage of expressing an aircraft noise event in SEL over LA_{max} is that both the duration and intensity of the event are taken into account [6]. For other noise metrics, such as L_{den}, similar trends as observed in the SEL noise contour and delta plots are expected.

In Figure 1.16 the noise contour plot for Airbus A330 departures is visualized following the original Doc. 29 methodology. The ground tracks of the flights match accurately with the noise contour. Similar noise contour plots can be created using the ACMS model or the new thrust and weight model as input parameters and are shown in Appendix A. To better spot differences between the noise contour plots, delta plots are generated. These delta plots show the absolute differences in dBA between two model.

The delta plot in Figure 1.17 compares the outcome of the original Doc. 29 model with the model that uses ACMS data directly as input for departures. This plot clearly shows that the ACMS input data results in lower noise levels than the original model, as the grid from the original Doc. 29 model is subtracted from the ACMS Doc. 29 model. Therefore, the original Doc. 29 overestimates noise levels for A333 departures. Also, it can be concluded that the effect of the thrust error in the FPPs, weighs greater than the error in altitude trajectories in most areas. Directly underneath the flight tracks, increased noise levels are observed.

Figure 1.18 and Figure 1.19 compare the new thrust and weight Doc. 29 model with the original Doc. 29 model and the ACMS Doc. 29 model. Figure 1.17 and Figure 1.18 generate similar delta plots, indicating that the new thrust and weight model produces outcomes close to the ACMS model. Figure 1.19 confirms this hypothesis, showing only small areas where the noise levels differs slightly. Furthermore, the new thrust model for departures gives a conservative prediction, slightly overestimating the noise levels closer to the airport. As the thrust values at take-off are estimated based on the TOW of the aircraft, errors in the weight estimation likely propagate to the thrust estimating, resulting in the difference between the models. Another cause for the overestimation of the noise levels could be the delay in observing changes in the flight performance parameters. A change in thrust or attitude does not lead to an instantaneous spike in the altitude or CAS trajectory, thus causing this delay. It is expected that the effect of phenomenon on the noise contour plot is small.

In Figure 1.20 the noise contour plot of the original Doc. 29 model for arriving Airbus A330 flights is visualized. The vectoring of incoming flights by ATC causes the a larger spread in the noise emissions compared to departures. Again, the flight tracks match accurately with the noise contour shape. For arrivals, the impact of several individual flights with thrust peaks become significant for the noise contour. The ground tracks in the noise contour plots provide context for explaining deviates observed in the delta plots. Noise contour

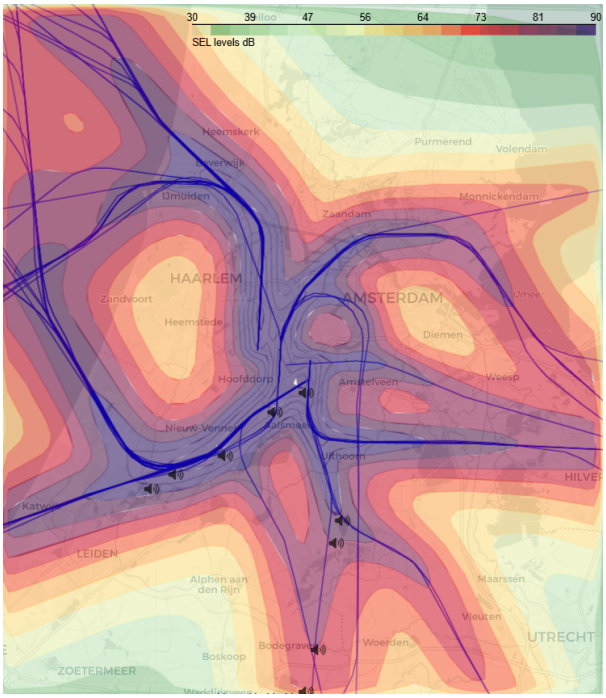

Figure 1.16: Noise contour plot of A333 departures using the original Doc. 29 calculation methodology without any alterations.

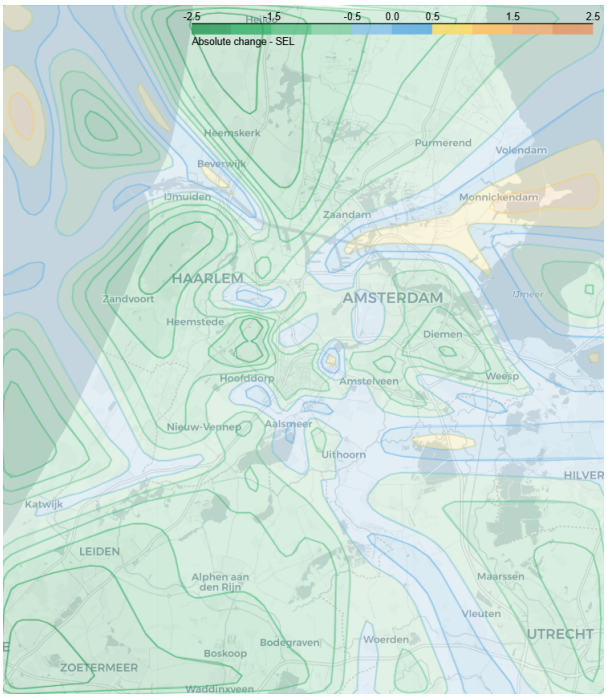

Figure 1.17: Noise contour delta plot of A333 departures comparing the original Doc. 29 model with the ACMS Doc. 29 model.

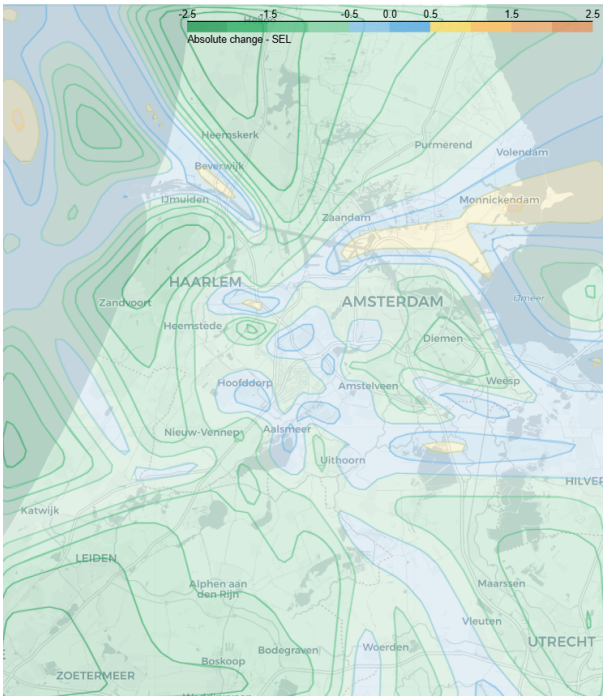

Figure 1.18: Noise contour delta plot of A333 departures comparing the new thrust and weight Doc. 29 model with the original Doc. 29 model.

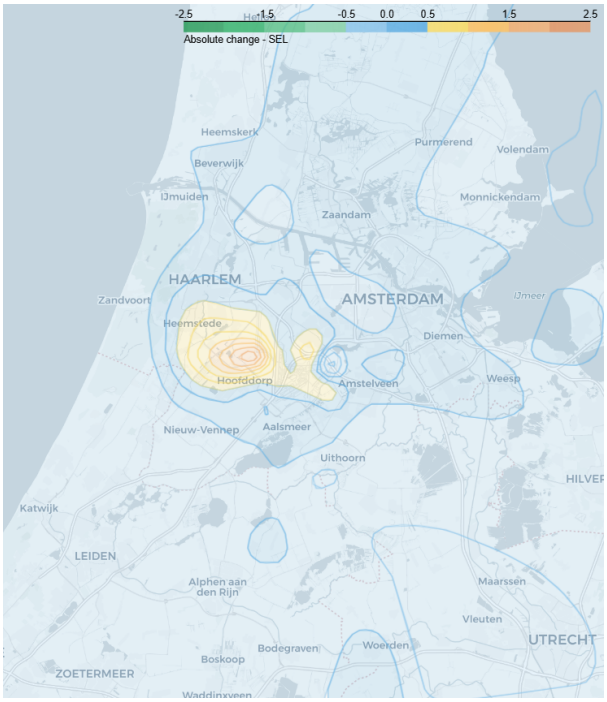

Figure 1.19: Noise contour delta plot of A333 departures comparing the new thurst and weight Doc. 29 model with the ACMS Doc. 29 model.

plots of the other Doc. 29 models can be found in Appendix A.

In Figure 1.21, the ACMS Doc. 29 model is compared to the original Doc. 29 model. Clear differences between the models are visible, especially around the area of Haarlem, Zandvoort, and IJmuiden. These areas are located relatively further away from the airport and are in the region between 12 and 50 kilometers from the landing threshold. For this part of the flight the altitude trajectory is compared to the altitude trajectory of the FPPs. Therefore, differences in altitude trajectories between the real trajectories and the FPPs will be minimal. This implies that the observed differences in noise levels can be attributed to deviations from the FPP thrust values. The current methodology of modeling arrival thrust with a FPP does not accurately capture the thrust peak behavior for arrivals.

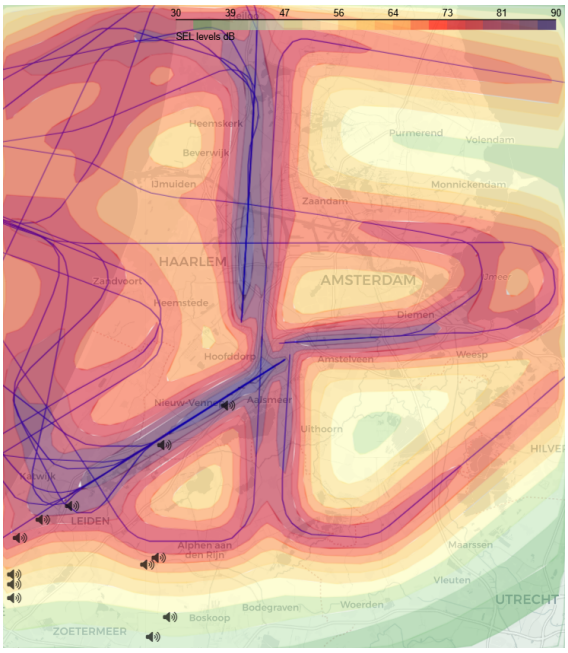

Figure 1.20: Noise contour plot of A333 arrivals using the original Doc. 29 calculation methodology without any alterations.

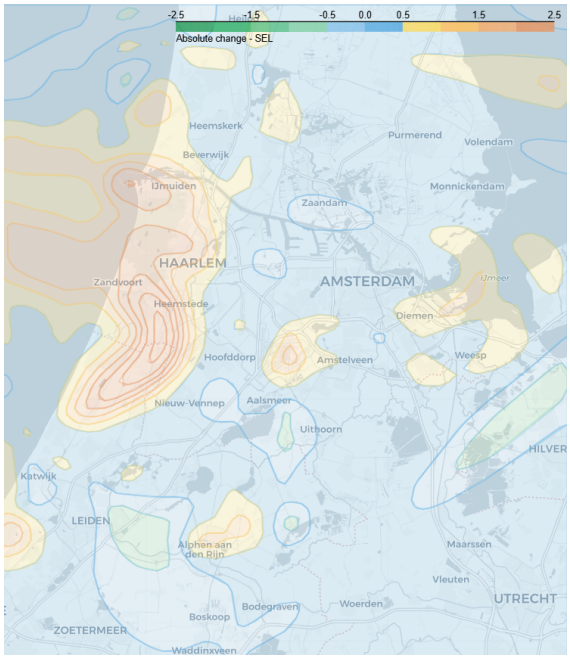

Figure 1.21: Noise contour delta plot of A333 arrivals comparing the original Doc. 29 model with the ACMS Doc. 29 model.

In Figure 1.22, the differences between the new thrust Doc. 29 model and the original Doc. 29 model are visualized. The areas, for which the noise load differs from the original Doc. 29 model, are similar to the areas observed in Figure 1.21.

Differences between the new thrust Doc. 29 model and the ACMS Doc. 29 model are visualized in Figure 1.23. The new model demonstrates that accurate prediction of thrust peaks by the random forest regressor model enables a reliable visualization of the noise contours of arriving flights. Nevertheless, small deviations with the ACMS Doc. 29 model remain, likely due to variations in idle thrust settings.

To understand similar noise contour plots of other aircraft types in Appendix A, some additional context is required, especially regarding the Boeing 777-300ER, the Boeing 737-800. For both of these types, no FPP are available for the corresponding ANP-IDs. Therefore, proxy FPPs should be used in the original Doc. 29 model. The FPPs of the Boeing 777-300 and the Boeing 737-700 were selected as proxy ANP-IDs, respectively. However, the use of these proxies can lead to significant differences in noise contour plots as aircraft specifications of the proxy aircraft differ from the actual aircraft. This directly introduces error in the model. For example, to extend the range of the Boeing 777-300 aircraft, new more powerful engines were fitted on the Boeing 777-300ER. As these two engines produce around 25% more thrust at their maximum setting, using this proxies to model thrust will ultimately lead to large errors in the noise contour plot. The main difference between the 737-800 and the 737-700 is the lenght of the aircraft itself. The 737-800 variant is a lenthened version of the 737-700. In general, equal performance is expected [15].

Although direct FPPs are provided for the Airbus A321neo ANP-ID, errors are still expected for this aircraft

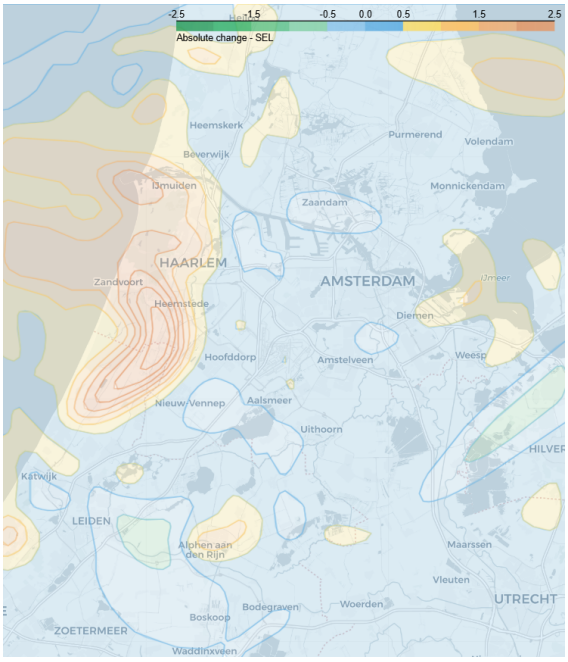

Figure 1.22: Noise contour delta plot of A333 arrivals comparing the new thrust and weight Doc. 29 model with the original Doc. 29 model.

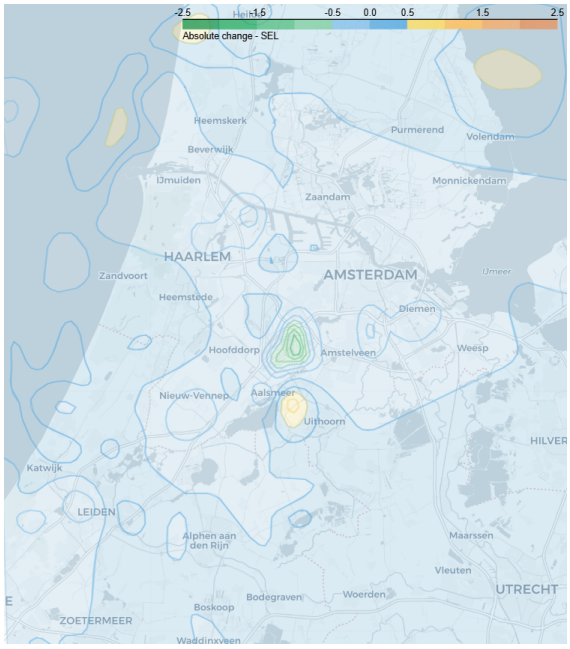

Figure 1.23: Noise contour delta plot of A333 arrivals comparing the new thrust and weight Doc. 29 model with the ACMS Doc. 29 model.

type. The current FPPs are designed for the Airbus A321ceo. The Airbus A321neo received an equal ANP-ID as the ceo variants, which could cause differences in performance.

1.7. Conclusion and Recommendations

The purpose of this paper was to investigate whether the weight and thrust estimation for noise modeling could be improved compared to the original Doc. 29 methodology. Weight estimation was deemed necessary only for departures, as no clear correlation between thrust and weight was found for arrivals. FPPs could be adjusted on a flight to flight basis to more accurately predict departure thrust. The location and magnitude of arrival thrust could be predicted with a random forest regressor trained on flight path angle, changes in CAS and corrected net thrust values.

Using ACMS data directly as input for altitude and thrust parameters showed significant differences with the original way of modeling. Implementing the methodology proposed in this paper, resulted in more accurate noise contour plots, close to the results of the ACMS Doc. 29 model. The differences with the original Doc. 29 model are mainly caused by the rigid and oversimplified implementations of the FPPs in Doc. 29. Altitude trajectories are always replaced by standard procedural trajectories, introducing errors in known input data. Furthermore, entries in the ANP database often link back to older aircraft models than are currently in use. And lastly, some assumptions in the Doc. 29 methodology are too simplified. For example, linear interpolation of FPPs between FL100 and FL200 does not match with real aircraft behavior. The new thrust and weight estimation method improved these factors, resulting in a closer match with reality.

However, it should be noted that this research was performed with ACMS data from a single airline. Other airlines use slightly different procedures, this can result in different aircraft behavior. Therefore, flight data of other airlines should be carefully evaluated before this method is applied. On top of that, methods from literature still outperformed the weight estimation methods introduced in this paper, indicating even better results might be obtained by trying these other methods. Also, the current methodology uses flap setting data to determine the flap position at landing. This data is not commonly available, and therefore it is recommended to develop a method that can detect the flap setting used at landing.

An interesting next step in this research would be the comparison between the new thrust and weight Doc. 29 model and actual measurements of the area around Schiphol Airport. By comparing the results of this paper with the measurements, a conclusion can be drawn about whether this new methodology reduces the gap between aircraft noise modeling and measurements.

Part II

Additional Work

2
Literature Review

This chapter will go into detail about the latest research and developments in the field of thrust modeling and weight estimation for aircraft noise modeling. Gathering information on novel techniques gives an overview of research already done in this scientific field. Based on missing information and recommendations from this literature, the knowledge gap can be determined afterwards. To understand these developments, acoustic noise metrics and the current methodology described by Doc. 29 will be discussed first in Section 2.1 and Section 2.2. In Section 2.3 current profiles for departing and arriving flights will be discussed. With a clear overview of the current situation, novel weight estimation techniques and thrust modeling techniques will be discussed in Section 2.4 and Section 2.5 respectively.

2.1. Noise Metrics

Sound is defined as pressure disturbance that propagates through the air. For humans, sound can be experienced either pleasant or disturbing. If the sound falls into the latter category, it can be classified as noise [6]. To express the emitted noise from aircraft, there are several noise metrics that exist. The sound emitted per unit time corresponds to a measure of power and is therefore called the acoustic power W. The formula for the Power Watt Level (PWL) is presented in Equation 2.1. The values of acoustic power range from an order of magnitude of 10^{-12} to 10^{8} [16].

$$\text{PWL} = 10 \log \left(\frac{W}{W_0} \right) \tag{2.1}$$

The Sound Pressure Level (SPL) is described by Equation 2.2 and can be measured by evaluating the effective pressure p_e of a sound wave. The reference effective pressure is set to be $2 \cdot 10^{-5}$ N/m^2. This way the loudness of the sound is evaluated in relation to time. However, the loudness can also be evaluated in relation to frequency, yielding a pressure band level as described by Equation 2.3. In this equation, the power spectral density is $P(f)$ and the width of the frequency band is Δf. In this frequency domain, the results are often averaged by integrating the spectral density over a set of bandwidth values. For aircraft noise calculations, often a 1/3-octave band is used [16].

$$\text{SPL} = 10 \log \left(\frac{P_e^2}{P_{e0}^2} \right) \tag{2.2}$$

$$\text{PBL} = 10 \log \left(\frac{P(f)\Delta f}{p_{e0}^2} \right) \tag{2.3}$$

As the sensitivity of human hearing depends on the frequency of the sound, a weighting function is applied to fairly compare different frequency bands with each other. For aircraft noise the method of A-weighting is commonly applied [16]. This method is based on an equal loudness contour around 40 phon, see Figure 2.1. The formula to apply the A-weighting method is presented in Equation 2.4. With this correction applied, the Overall A-weighted Sound Pressure Level (OASPL) can be calculated with Equation 2.5. The unit of this sound pressure level is expressed in dBA, indicating A-weighting has been applied [16].

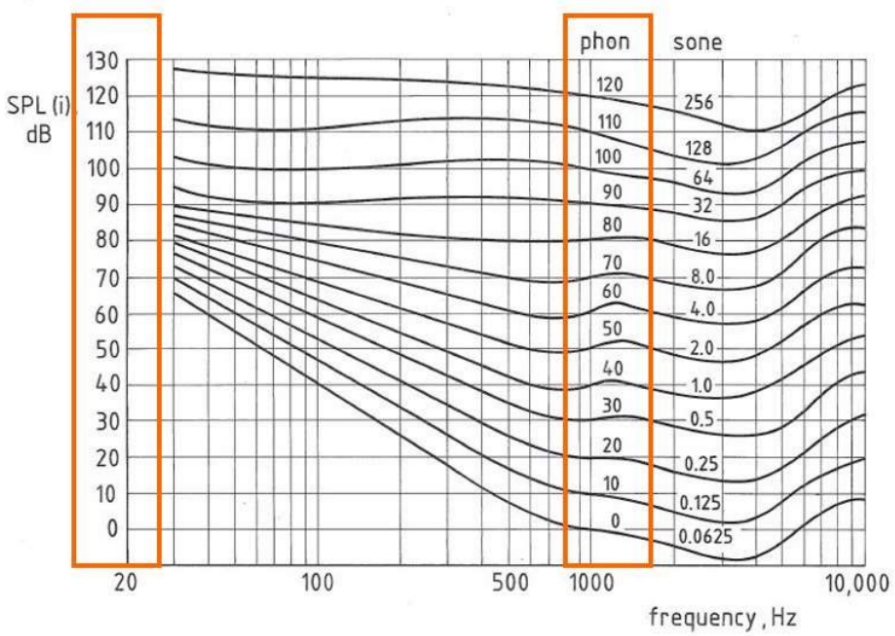

Figure 2.1: Equal loudness contours in terms of frequency and sound pressure level [16]

$$\Delta L_A = -145.528 + 98.262 \cdot \log(f) - 19.509 \cdot \log(f)^2 + 0.975 \cdot \log(f)^3 \tag{2.4}$$

$$L_A = 10 \log \sum_i 10^{\frac{\text{SPL(i)} + \Delta L_A(i)}{10}} \tag{2.5}$$

The A-weighted sound pressure level can accurately capture the noise exposure of stationary objects. However, it is an inaccurate metric for evaluating moving objects, such as aircraft, because the human hearing is also sensitive to the duration of a sound event. Therefore, the sound exposure level of an event can be calculated by applying Equation 2.6, integrating the A-weighted sound pressure level over time. In this equation, the value of T_1 is set to 1 second to remove the dependency on the integration time. The difference between the two metrics can clearly be seen in Figure 2.2 and Figure 2.3 respectively. Two noise events are depicted in these images. Although the peak on the right does not have the highest maximum A-weighted sound pressure level, the SEL value of this event is large due to its longer duration [16].

$$\text{SEL} = 10 \log \left(\frac{1}{T_1} \int_0^T 10^{\frac{L_A(T)}{10}} dt \right) \tag{2.6}$$

To evaluate multiple noise events over a full year, the L_{DEN} noise metric is used. For this metric, a noise penalty for events during the evening and night are applied of 5 and 10 dBA respectively. These penalties aim to limit the amount of sleep disturbance for the surroundings, accepting that aircraft noise is far more disturbing during evening and night hours [6].

$$L_{DEN} = 10 \log \left(\sum_{i=1}^{N_d} 10^{\frac{SEL_i}{10}} + \sum_{j=1}^{N_e} 10^{\frac{SEL_j + 5}{10}} + \sum_{k=1}^{N_n} 10^{\frac{SEL_k + 10}{10}} \right) - 75.0 \tag{2.7}$$

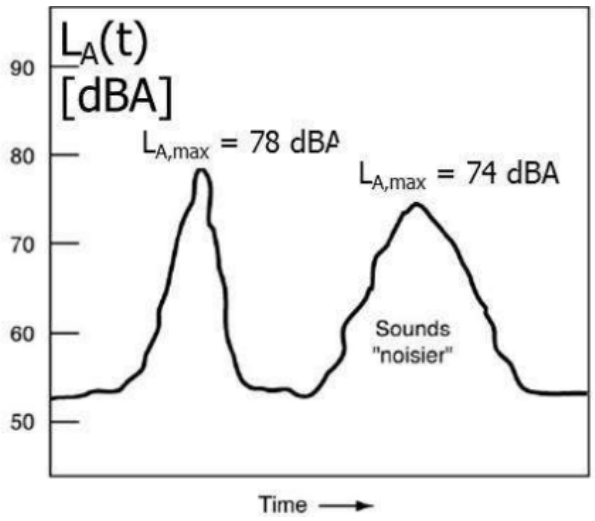

Figure 2.2: Graph with two noise events expressed in L_{Amax} [16].

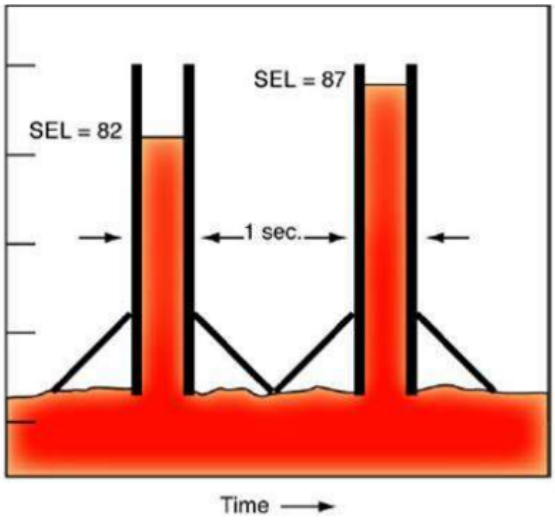

Figure 2.3: Graph with two noise events expressed in SEL [16].

2.2. Doc. 29 methodology

The Doc. 29 noise model published by the ECAC is internationally regarded as the best-practice aircraft noise model. The documentation about this model does not directly provide a code to calculate aircraft noise emissions but rather fully describes the method that can be used in a computer code to calculate the desired results. Therefore, the result of every Doc. 29 noise model will be very slightly different, but overall these differences are negligible. As every flight is split up into multiple straight line segments, the Doc. 29 model is categorized as a segmentation model. For every segment, the fraction of the noise emitted by the finite segment compared to the infinite segment is determined. This fraction is converted to sound levels with NPD data. Important to note is that the thrust values of the flight are directly converted to noise levels. This means that errors in the thrust calculation directly effect the outcome of the Doc. 29 noise model. To this sound level, several correction factors for directionality, impedance, velocity, attenuation, and start of roll are added. Aircraft performance parameters such as weight and thrust have to be fully defined by input parameters and therefore often need to be estimated [6].

To understand the calculation behind modeling aircraft noise, it is of utmost importance to understand the relationship between the weight and the thrust of the aircraft. Both of these parameters are usually unavailable input parameters for the aircraft noise model, as this data belongs to the airliners operating the aircraft. It is not common for airliners to share this data. Therefore, these two input parameters should be estimated. Given input parameters such as speed, altitude, latitude and longitude, the combination of possible thrust and weight values is bounded by the balance of energy [17]. Although being bounded by this balance, a large number of combinations still exist and therefore at least one of the parameters should still be estimated accurately to be able to derive the other.

The estimation of the aircraft weight in Doc. 29 is performed by weight classes. Based on the distance between the destination airport and the departure airport, a stage length is assigned to the flight, which for every flight corresponds to a specific take-off weight. This take-off weight is based on a representative range for every class and is calculated with Equation 2.8. This means that in this methodology the TOW is considered to depend only on the fuel weight. Other factors, such as the passenger load factor or extra freight, are not considered. For destinations close to the boundaries of the stage length classes, significant differences in the TOW can be observed. The division of stage lengths is presented in Table 2.1. For approach procedures, the weight of the aircraft is set to 90% of the MGLW, eliminating all dependence on influential operational parameters [7].

$$\text{Representative Range} = \text{Min. Range} + 0.7 \cdot (\text{Max. Range} - \text{Min. Range}) \tag{2.8}$$

Table 2.1: Definition of the stage lengths as presented in Doc. 29. [7]

Stage Length	1	2	3	4	5	6	7	8	9
Trip Length (nm · 1000)	<0.5	0.5 - 1	1 - 1.5	1.5 - 2.5	2.5 - 3.5	3.5 - 4.5	4.5 - 5.5	5.5 - 6.5	>6.5

The technical guide of Doc. 29 prescribes to estimate the thrust of the aircraft for the noise calculation model by dividing the operational procedure into procedural steps. These procedural steps are represented by straight-line segments, resulting in a series profile points. For the sections between the profile points, the flight performance parameters can be estimated by using aerodynamic and thrust equations summarized in Appendix B of Doc. 29 [7]. The main formula to determine the thrust is presented in Equation 2.9. Based on the value for the net corrected thrust and the distance between the observer and the sound source, the desired sound levels can be interpolated by using NPD tables [7].

$$\frac{F_n}{\delta} = E + F \cdot V_C + G_A \cdot h + G_B \cdot h^2 + H \cdot T \tag{2.9}$$

where:

F_n	is net thrust per engine (lbf)
δ	is the ratio of ambient air pressure at the airplane to the standard air pressure at mean sea level
$\frac{F_n}{\delta}$	is the corrected net thrust (lbf)
V_C	is the calibrated airspeed (kt)
T	is the ambient air temperature in which the airplane is operating (°C)
E, F, G_A, G_B, H	are engine thrust constants or coefficients for temperatures below the engine flat rating temperature at the thrust rating in use

To simplify the implementation of this methodology, the results for different sections of the flight are directly given by default fixed-point profiles. The default fixed-point profiles are presented in the ANP database for multiple aircraft types and an example is shown in Figure 2.4 [18]. However, these default fixed-point profiles result in an extremely simplified representation of the reality, as this method results in a single default profile for every aircraft type and weight class. Not correctly identifying the stage length category leads to assigning a wrong thrust profile, severely altering the noise load of a flight. By identifying a wrong profile, not only the maximum thrust levels used are changed, but also higher thrust levels are usually maintained for a longer period of time, as climb performance degrades with increasing weight. Several important assumptions are necessary to achieve the result described in Doc. 29 and the impact of these assumptions on the output is unknown. Some important assumptions are as follows.

- For every variation of aircraft type and weight class, the thrust profile is fixed
- The derating applied for take-off are scaled by the ratio between the TOW and MTOW.
- When the take-off thrust is reduced, it is recommended to reduce the climb thrust by 10%
- All take-off operations start at the end of the runway
- In case an aircraft type is not in the ANP database, data from a comparable aircraft is taken
- Decelerations during approach are performed at an idle thrust level

These assumptions mean that operational variations in the take-off or approach procedures are not captured. For consistency, procedures are generalized for all airliners and are assumed to cancel out over the number of flights. However, a bias of a main airliner at an airport can therefore cause significant deviations in the noise results. The assumptions regarding the engine derating for take-off and climb are heavily generalized and are not coupled with for example take-off weight. Also, the obtained profiles for departures do not take

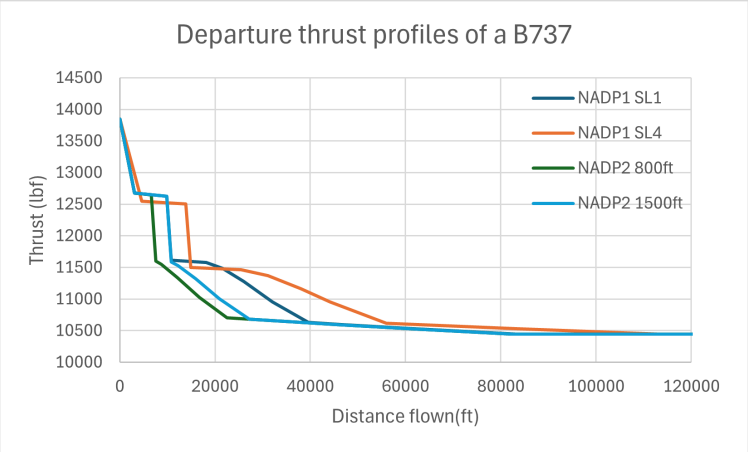

Figure 2.4: Examples of several thrust profiles of a Boeing 737-700.

into account any variations of the NADP, which are the current standard at Amsterdam Airport Schiphol. Furthermore, for approach procedures aircraft often deviate from the specified fixed point profile due to different aircraft configurations and air traffic control instructions.

In order to improve the accuracy of this method, the default fixed point profiles are adapted by the Nederlands Lucht- en Ruimtevaartcentrum (NLR) to match them with the procedures used at Schiphol airport. These adaptations provide multiple default fixed-point profiles, following the same method as described in Doc. 29. For approach procedures, the the optimal profile should be selected, while for departures the profile is selected based on empirical data. Important to note is that these changes are still based on the ANP database and no data from a Flight Data Recorder (FDR) or ACMS is used. [5].

As stated earlier, data containing aircraft weight and indicative thrust values are usually unavailable. However, the ACMS does log information about the weight of the aircraft and the rotational speed of the engine's compressor. Although it is a complicated process, this compressor speed can be used to accurately predict the thrust value of an aircraft engine. Obtaining data from the ACMS therefore allows for an accurate specification of the input parameters for the Doc. 29 noise model.

2.3. Flight procedures for departures and arrivals

To regulate and minimize aircraft noise around the vicinity of an airport, ICAO prescribes specific departure procedures often referred to as NADP. A distinction can be made between two variants of these procedures, namely between the ICAO-A and ICAO-B types. In the literature, these terms are often also categorized as NADP1 and NADP2 procedures respectively. These procedures specify the order and altitude at which the flap retraction and thrust cutback are performed.

For the NADP1, the thrust cutback is performed first around 1500 feet altitude. The flaps remain extended until an altitude of 3000 feet. After this, the aircraft accelerates to a speed of 250 knots, before resuming the climb to cruise altitude. This procedure aims to minimize the noise pollution directly beneath the ground track of the aircraft [4]. For the NADP2, the flaps are retracted at a specified altitude, which is either at 800 feet, 1000 feet, or 1500 feet at Amsterdam Airport Schiphol. The thrust cut-back is performed either simultaneously with the flap retraction or immediately after the flap retraction has been finished. Next, the aircraft accelerates to 250 knots before resuming the climb towards its cruise altitude [4]. The main difference between the two procedures is the altitude at which the aircraft accelerates to 250 knots, preparing for the remaining climb phase. Because this acceleration altitude is lower for the NADP2 profile, less noise is produced in areas located relatively further away from the ground track. For Schiphol airport the departure routes are designed to avoid flying directly over closely populated areas and therefore the NADP2 procedure is preferred. A visualization of the altitude profiles of different NADP is presented in Figure 2.5 [4].

For aircraft with a weigth below the MTOW, often derated engine settings are used during take-off. This

means that the engines are not set at full thrust at take-off and initial climb. Running the aircraft engines at lower settings during take-off reduces maintenance of the engines and is therefore beneficial for the airliner. In the FPP for Schiphol Airport, the use of derated engine settings is implemented. The methodology for applying the derated eninge settings is based on NADP1 procedures. Later in 2016, this method was compared with known NADP2 flights of two Dutch airlines to check for discrepancies [5].

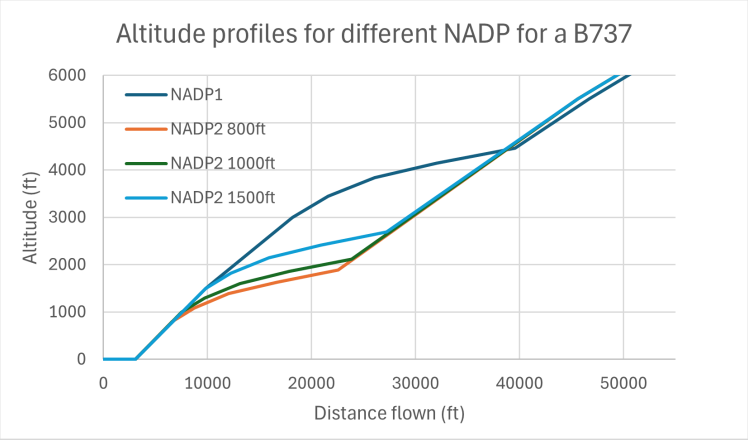

Figure 2.5: Altitude profiles of the different types of NADP for a Boeing 737-700

Every year Schiphol publishes two reports on noise pollution produced by the operation in the surroundings of the airport. One report is a prediction about the noise levels expected for the upcoming year (gebruiksprognose), and the other is an evaluation of this first prediction (evaluatie gebruiksprognose). To predict the expected noise pollution for the upcoming year, the runway usage and tracks are estimated with empirical data from previous years. In addition, the altitude is set to be exactly equal to the NADP corresponding with the airline and aircraft type. In the evaluation the ground track of every flight is updated to exact values recorded by radar technology. However, the altitude of every flight is not updated accordingly in the evaluation. This introduces errors in the overall outcome of the model, as this could be a significant deviation from the reality. Updating the altitude profiles however, would require the re-identification of the flight stages of every flight, including the recalibration of the thrust profiles.

For approach procedures ICAO also provides a single default landing procedure. For Amsterdam Airport Schiphol specific, additional approach profiles have been provided to better suit the current procedures. These procedures include different flap settings and descent profiles.

2.4. Weight estimation techniques

An important novel development for estimating the weight of the aircraft for both departures and landings is the introduction of the Automatic Dependent Surveillance-Contract (ADS-C) down-link. The ADS-C technology is originally being developed to predict the intended flight path of an aircraft to optimize air traffic control operations. To allow for this optimization the ADS-C connection provides a 4D trajectory for the ground air traffic service unit. The ADS-C event can contain up to 128 data points of flight performance parameters and are directly obtained from the FMS. Interestingly, for noise modeling purposes, these signals include information about the current gross mass of the aircraft and the predicted gross mass at the top of descent. In combination with the latitude, longitude, altitude and speed of the aircraft, the exact weight at specific points in flight is known. This allows the aircraft gross mass to be estimated with the help of a fuel mass flow model, allowing weight estimates to be much more accurate than achieved by the method proposed in Doc. 29.

Currently, EUROCONTROL performs tests with the ADS-C technology at the Maastricht Upper Area Control Centre (MUAC) capturing flights approaching / departing from Amsterdam Airport Schiphol. Unfortunately, only relatively new aircraft produced by Airbus are equipped with the ADS-C technology, resulting in data about only a very limited number of aircraft types. At this moment in time, only 130 of the 5500 aircraft

handled by the MUAC are able to send ADS-C signals. In the near future, more aircraft manufacturers will implement this technology in their aircraft since from 31 December 2027 new aircraft will be required to equip their aircraft with this new ADS-C technology [19].

Without information from the systems onboard the aircraft, other available data might be used to get a more accurate prediction of the aircraft mass. A method proposed by Sun et al. is to estimate the take-off weight of the aircraft by analyzing available positional data of the take-off phase itself [8]. The acceleration of the aircraft is closely related to the aircraft weight for comparable atmospheric conditions. In this paper, two methods were tested, one estimating the mass at the take-off moment and one estimating the take-off mass recursively. The method of estimating the take-off mass recursively looks the most promising, as almost all points are between the Operational Empty Weight (OEW) and the MTOW. In Figure 2.6, the result of the estimation of both methods is presented. As this research used Automatic Dependent Surveillance-Broadcast (ADS-B) data in combination with a Base of Aicraft Data (BADA) thrust model, it is suggested that a more accurate thrust model could improve the results obtained. Data from the ACMS of the aircraft definitely satisfies this quality requirement.

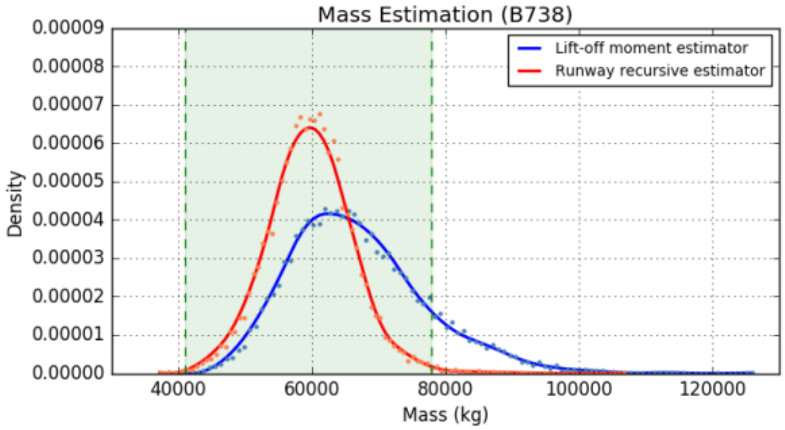

Figure 2.6: Estimation of the TOW of a Boeing 737-800 aircraft. [8]

Another method could be to use a deep learning model to predict the TOW as suggested by Ayzit et al. [9]. First, the flight data is divided into five different phases for this method. For every phase, different parameters are indicative features for the TOW, therefore requiring this split. By performing a Shapeley Additive Explanations (SHAP)-analysis, as can be seen in Figure 2.7, the mean thrust during the climb phase showed the largest correlation with the TOW. In addition, the flight range, cruise time, and mean rate of climb were among the indicative parameters to evaluate. Deep learning models only trained with wide-body aircraft data reached a mean absolute percentage error ranging from 0.98% to 1.35%, for which a simple linear regression model performed best. Training the model with both narrow-body and wide-body aircraft a mean absolute percentage error of 1.48% could be achieved with an extra trees regressor model. Since most of the indicative operational parameters are available through data sources such as ADS-B, this can be a powerful method to get a more accurate estimation of the aircraft TOW.

2.5. Thrust estimation techniques

A study was performed at Hannover Airport to test the Doc. 29 methodology for predicting aircraft noise for single events [20]. For modeling thrust, the ICAO default fixed-point profiles from the ANP-database were used, meaning no specific adjustments for Hannover Airport are applied to these profiles. Doc. 29 is not built to predict aircraft noise levels for these individual events, but analyzing the deviations on a individual flight level could indicate fields for which improvements could be made. When comparing the results of the Doc. 29 calculation and the real measurements, large deviations and outliers were observed. These deviations were mainly attributed to the mismatch between the flight profiles and the fixed-point profiles and further research in this area was suggested.

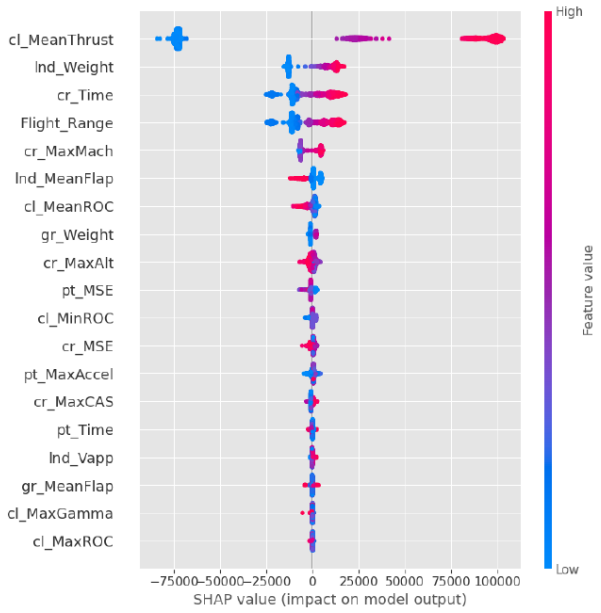

Figure 2.7: SHAP analysis with parameters influencing the TOW of aircraft [9].

The evaluation of the take-off profiles between 2008 and 2017 shows a decrease in the climb gradient. The change in this climb gradient can be attributed to airlines implementing new departure procedures for economic and environmental benefits. However, due to aircraft thrust settings not being publicly available, it is difficult to determine the effects on aircraft noise. The analysis of noise measurements near Narita International Airport in Japan showed a relationship between the thrust setting and the take-off weight for derated departures. For departures without a derated thrust setting, a relationship between the take-off weight and altitude was found. This research therefore indicates that implement derating in the thrust estimation is essential to achieve accurate results [21].

In contrast, Schwab and Zellman concluded that the thrust settings for derated climb segments can be categorized [10]. Depending on the aircraft type, one or more modes are available, as is visible in Figure 2.8 and Figure 2.9. Data for this research was obtained directly from flight data recorders in aircraft from Swiss International AirLines, providing very accurate and reliable data for this study. Furthermore, thrust settings during the initial approach phase of an arrival showed a large variation in thrust settings. Ideally, this phase of the flight is performed with an idle thrust setting. However, due to other air traffic in the vicinity of airports, irregular compressor fan speeds can be observed in this segment, therefore disagreeing with the assumption made in Doc. 29

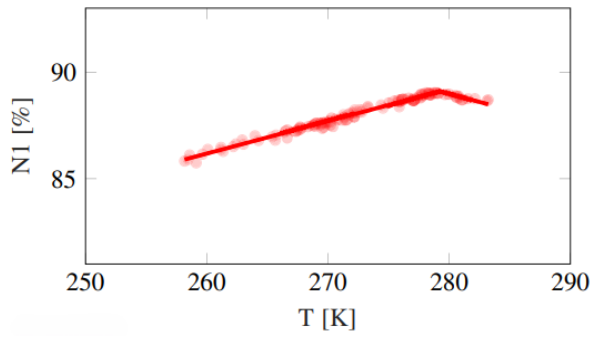

Figure 2.8: Single class derated departure for an Airbus A320 [10].

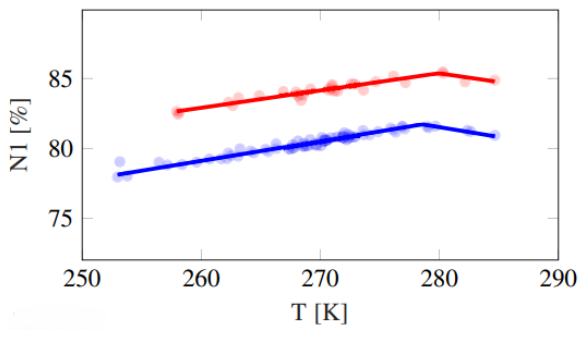

Figure 2.9: Multiple class derated departure for an Airbus A333. [10]

In a research conducted by Merino-Martínez in 2019, a method was suggested to predict thrust levels based on acoustic measurements [22]. Due to the rotational movement of the compressor fan of an aircraft engine, a pattern of the blade passing frequency and its overtones can be recognized in the spectrograms of the audio recordings. Such a spectrogram is vizualized in Figure 2.10. Due to the relative velocity of the aircraft with respect to the observing microphone, the frequencies of the compressor fan blades are Doppler shifted in the spectrogram, thus explaining the variations in frequency over time. Correcting for this shift with the velocity of the aircraft results in a single value of the rotational speed of the compressor fan. This rotational speed can be used as the thrust setting for the aircraft noise event and is converted to the net corrected thrust by using Equation 2.10. This equation is similar to Equation 2.9, but also includes correction terms using the fan rotational speed. For arriving aircraft, the spread of thrust values was found to be much greater than for departing aircraft. This can be explained by the fact that approach operations often require corrections to keep the aircraft on the desired flight path. With the obtained thrust values as an input for the Doc. 29 model, the noise exposure of the event can be calculated. Using the measured fan rotational speed to estimate thrust, an increased correlation between the modeled and recorded noise pollution could be achieved. A major disadvantage of this proposed method is the requirement for spectrogram measurement to determine the N1% of the aircraft. This data is not always available for every flight, making it impossible to calculate accurate L_{den} values.

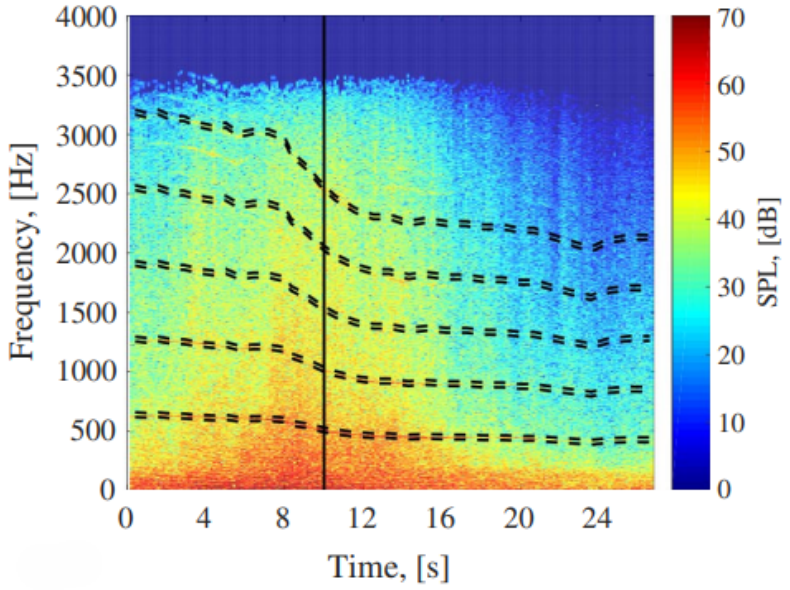

Figure 2.10: Spectrogram of the audio signal of an aircraft flyover with dectected engine tones [22]

$$\frac{F_n}{\delta} = E + F \cdot V_C + G_A \cdot h + G_B \cdot h^2 + H \cdot T + K_3 \left(\frac{N1\%}{\sqrt{\theta_T}}\right) + K_4 \left(\frac{N1\%}{\sqrt{\theta_T}}\right)^2 \tag{2.10}$$

Although Equation 2.10 provides a method to convert the N1% into thrust, this formula should be used carefully. In a recent paper it was found that thrust profiles from the ANP database did not correspond well with thrust profiles from airliner models [23]. In addition, the airliner model was also compared with a Gas Turbine Simulation Program (GSP) and a fuel flow estimation model. The GSP corresponded well, while the fuel flow estimation was inaccurate in predicting the thrust. To improve the correlation between the thrust model from ANP database and the airliner model, new ANP engine coefficient were calculated based on the GSP model with a least squares method. Both a bounded and an unbounded method were evaluated. The unbounded method yielded a physically unfeasible combination of coefficients, while the bounded method yielded accurate results that closely match the airline model. The results are visualized in Figure 2.11.

In addition to discussing the derated take-off modes, Schwab and Zellman propose an estimation method for the fan compressor speed taking into account different flight phases [10]. For departures, the flight is divided

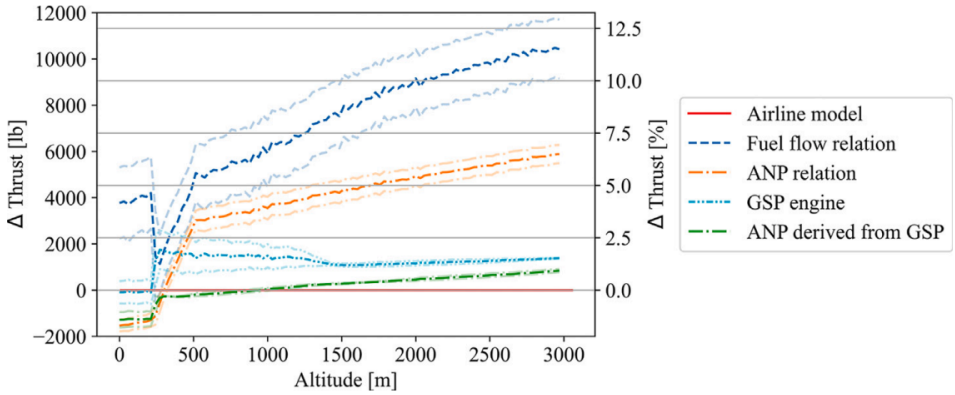

Figure 2.11: Average deviation and standard deviation of thrust estimations compared to the airline model of 7 different take-off weights of the B777-200 [23].

into a take-off phase, a climb phase with extended flaps, and a climb phase with retracted flaps. For arrivals, the flight is divided into an initial approach, a transition segment, and a final approach. The identification of these phases is depicted in Figure 2.12 and Figure 2.13 for departure and approach operations respectively. The identification of these flight phases was only performed for a NADP1 profile and should therefore be adjusted to be applied to NADP2 profiles. With this method, it is possible to accurately estimate N1%-values with only positional data as input. In this positional data, the thrust cutback can be recognized by a dent in the altitude profile.

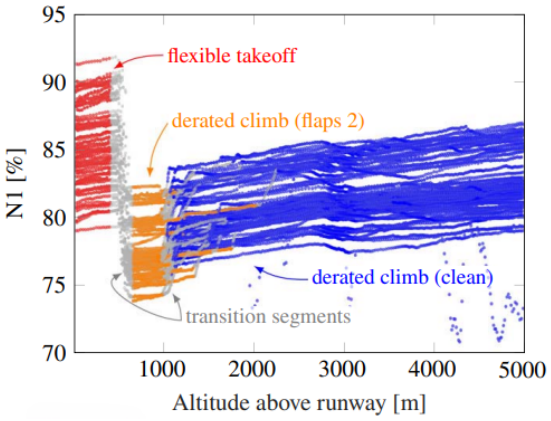

Figure 2.12: Sample of N1% departure profiles of A333 events and arrangement into flight phases [10].

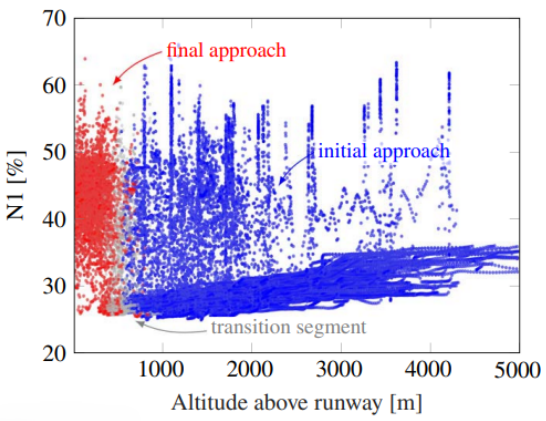

Figure 2.13: Sample of N1% approach profiles of A333 events and arrangement into flight phases [10].

Pretto et al. proposed a method to improve the aircraft noise thrust prediction model based on available ADS-B data [24]. For both approach and departure operations, the thrust profiles are changed with the help of optimization parameters. For departures, these optimization parameters are procedure type, take-off thrust reduction, climb thrust reduction, weight fraction, initial climb height, mid-climb height, and energy share fraction. For arrivals, the initial descent angles, initial descent calibrated airspeed, length of level-flight phase, and height of level-flight phase. For a given ground track and altitude profile, the objective function is minimized. For this function low altitude values are weighted with a factor of 20, middle altitude values are weighted with a factor of 10 and high altitude values are weighted with a factor of one. Therefore, flight parameters for lower altitude are weighted more heavily than at higher altitudes. As the lower altitude phase of the take-off is the noisiest, this part requires the most accuracy. Therefore, this method allows to take into account deviations from the non-standard flight profile in the modeling of aircraft noise. A disadvantage of this research is that it was only based on ADS-B data. Therefore, changes to the thrust setting of the aircraft could not be validated by comparing it with actual engine parameters. To accurately predict the impact of

the thrust this validation is required and can be achieved with data from the ACMS onboard of the aircraft.

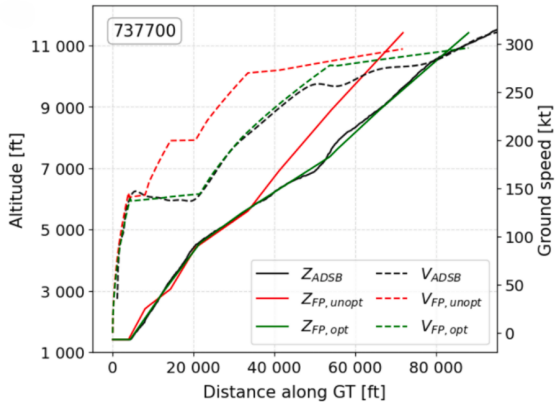

Figure 2.14: Optimized flight profile for a departure at Zurich Airport of a Boeing 737-700 [24].

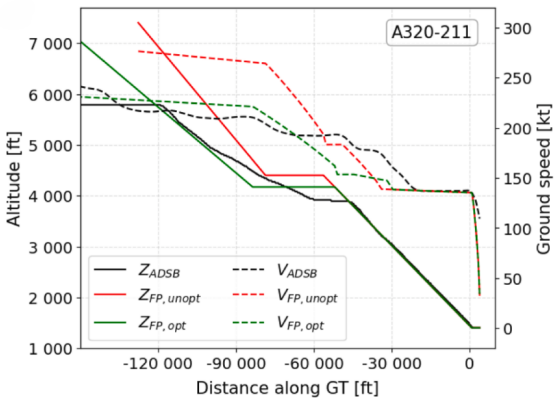

Figure 2.15: Optimized flight profile for a arrival at Zurich Airport of an Airbus A320-211 [24].

3
Research proposal

3.1. Knowledge Gap

The current methodology used to model the weight and thrust of aircraft in Doc. 29 noise models introduce significant uncertainties in the calculated noise levels. For weight, only fuel mass is currently considered as an input variable as the mass is determined based on the distance between the departure and destination airport. This method completely neglects other important weight variables such as the passenger load factor and cargo weight. For thrust, the existing default fixed-point profiles are highly simplified representations of the reality, and it is unsure how much these profiles differ from the procedures used in practice. Noise calculations performed on a single event basis showed large deviations from reality. Although the Doc. 29 method is not intended to be used to evaluate a single noise event, it could indicate errors in the methodology used. It is stated that for the fixed-point profiles for Schiphol a derating setting is taken into account, but the implementation of this remains unsure. Furthermore, it is unknown whether the thrust cutback point within the profiles corresponds with the cutback points used in practice. Any variability of flight segments is removed by the implementation of the thrust profiles, as well as its dependence on atmospheric conditions. All in all, with the amount of uncertainties in the thrust prediction method, the differences between aircraft noise models and measurements remain unexplained.

Regarding the estimation of the aircraft weight, in literature several methods showed promising results to improve the accuracy of the current prediction. Ideally, ADS-C data of every aircraft for both take-off and landing procedures is desired as the ADS-C technology provides data directly from the ACMS onboard of the aircraft. ADS-C data has not yet been used in aircraft noise prediction models, as the technology is still in its testing phase. This technology will become more readily available in the near future as from 2028 onward new aircraft are required to be equipped with this technology. Meanwhile, for aircraft without this technology, other methods for estimating the weight should be sought. Techniques such as deep learning models or recursive take-off mass estimation result in an improved weight prediction.

Efforts have been made to improve the thrust modeling method described in Doc. 29 for aircraft noise purposes. Research showed that it is possible to measure the rotational speed of the compressor fan on the ground to estimate the thrust of an aircraft. However, a significant drawback of this method is the requirement of a spectrogram of the flyover event. Therefore, this method cannot be applied to calculate L_{DEN} values. The method developed by Schwab and Zellman does not require additional measurements and is constructed with FDR data from Swiss International Air Lines. However, this method was developed for NADP1 profiles used at Zurich Airport. Since for Amsterdam Airport Schiphol NADP2 profiles are the preferred take-off procedure, it should be investigated if similar results can be achieved for this NADP2 procedure. Furthermore, the model was unable to capture short increments in thrust for arrivals. As Schiphol does not have fixed arrival routes, this could induce significant errors in the noise calculation model. The method of Pretto et al. uses optimization parameters to accurately adjust the procedural steps to match the flight profile. However, this method is not validated with data from an ACMS of FDR. Therefore, it is unknown whether the modified thrust profile matches the thrust profile used in practice. On top of that, there is no explanation present of the method how the profiles are altered for both approach and departure procedures.

By assessing the impact of the Doc. 29 assumptions regarding thrust and weight estimations, this research

will aim to explain a part of the mismatch between models and measurements. The accessibility to data from the ACMS of the aircraft allows for a fair comparison with the operational procedures.

3.2. Research Questions

This thesis will try to overcome the knowledge gap described in Section 3.1. For this, the focus will not only be on improving the estimation methods, but the improvements will be implemented in a full Doc. 29 model. With this model, it will be possible to visualize contour plots on a map and compare the new methodology with the old one. Therefore, the main research question that will be answered in the thesis is:

What effect does improving the weight and thrust estimation using ACMS data have on the noise contour around Amsterdam Airport Schiphol?

To better answer this main research question, separate questions are created for both the weight estimation and the thrust estimation. These sections are then further split up into sub-questions. At the end of the thesis process, the answers to all of the sub-research questions can be combined to answer the main question.

Weight Estimation

How well does the weight estimation method described in Doc. 29 perform and can the aircraft noise model be improved by implementing another more accurate weight estimation method?

- What is the current method prescribed by Doc. 29 to model the weight of an aircraft?
- How do novel weight estimation techniques, such as ADS-C, deep learning, recursive TOW estimation, compare to the method used is Doc. 29 and how do these weights differ from the values obtained via the ACMS?
- What effect do errors in the weight estimation method have on the calculated noise contours?

Thrust Estimation

How does the thrust estimation method described in Doc. 29 compare to the values obtained by the ACMS, and can the aircraft noise model be improved by implementing another more accurate thrust estimation method?

- What is the current method prescribed by Doc. 29 to model the thrust of an aircraft and what assumptions are made in this method?
- What adaptations have been made to the default fixed-point profiles of the ANP database to adjust them for the current departure procedures of Amsterdam Schiphol Airport?
- What is the difference between the Schiphol fixed-point profiles and the ACMS thrust values and what deviation patterns can be recognized between them?
- To what extent is it possible to adjust the fixed-point profiles by using individual flight data to improve the thrust model?
- What effect do errors in the thrust estimation method have on the calculated noise contours?

Based on existing literature and the knowledge gap defined earlier, it is expected that by improving the weight and thrust estimation methodology for a Doc. 29 noise model will significantly improve the performance of the model. Therefore, it is expected that the difference between the noise model and the measurements will decrease, as the model will be a more accurate representation of reality. It is hard to predict whether the noise exposure in the surroundings will increase or decrease, as this depends mainly on the deviation in weight and thrust values.

The hypothesis for the weight estimation is that deep learning methods are able to highlight relationships in the data which are hard to predict beforehand. This would allow for a more accurate weight estimate than could previously be achieved. Having this more accurate estimation propagates towards increasing the accuracy of the thrust estimation, which will be the most important effect.

For the current thrust profiles for Schiphol adaptations have been performed make them correspond with the procedures. However, this adaptation was performed already 7 years ago. Therefore, it is expected that some of these adaptations are outdated. Furthermore, it is expected that for economic benefits of the airlines the thrust of engines is derated more than currently modeled. An increased derating will result in lower thrust values and thus less noise exposure during take-off. For climb thrust the same methodology can be followed. Based on the position and velocity data of the aircraft, it should be possible to adjust the thrust profiles for every flight. Small deviation will most likely be difficult to predict, but important parameters such as derating setting, thrust cutback, flap retraction and climb continuation should be recognized. In general, a decrease in thrust will likely result in a decrease in emitted noise and vice versa.

3.3. Research Activities

First, the weight estimation techniques should be worked out in detail to investigate which method provides the best estimation. The verification and validation of the methods will be performed using data from the ACMS of the aircraft. The most accurate method will be implemented in the Doc. 29 noise model and changes in the noise contour will be visualized.

For the thrust modeling, the fixed-point profiles will be compared to the ACMS data to quantify the deviations between the literature and operations. Next, the trends in the ACMS data will be captured to allow for adjusting the fixed point profiles. For this it will be necessary to accurately identify different phases of the flights. Again, verification and validation will be performed by comparing the newly developed thrust model with the ACMS data. This can be achieved by splitting the data in a training and validation set. Finally, the total impact of on the noise contour plots will be visualized.

References

[1] *Aviation noise impacts: State of the science*, 2017. DOI: 10.4103/nah.NAH_104_16.

[2] C. Clark, "Aircraft noise effects on health prepared for the airports commission", University of London, Tech. Rep., 2015.

[3] F. Hoyas, "Revisiting noise abatement departure procedures (nadp) application", ICAO, Tech. Rep. [Online]. Available: chrome-extension://efaidnbmnnnibpcajpcglclefindmkaj/https://www.icao.int/sites/default/files/sp-files/environmental-protection/Documents/EnvironmentReport-2010/2025/Envreport2025_94.pdf.

[4] H. W. Veerbeek and M. A. Brouwer, "Noise measurement analysis during a noise abatement departure procedure trial", in *41st International Congress and Exposition on Noise Control Engineering 2012, INTER-NOISE 2012*, vol. 7, 2012.

[5] S. Heblij and J. Derei, "Methodenrapport doc29", Tech. Rep. [Online]. Available: chrome-extension://efaidnbmnnnibpcajpcglclefindmkaj/https://zoek.officielebekendmakingen.nl/blg-931606.pdf.

[6] European Civil Aviation Conference, *Volume 1, applications guide*, https://www.ecac-ceac.org/images/documents/ECAC-Doc_29_4th_edition_Dec_2016_Volume_1.pdf, 4th Edition, 2016.

[7] European Civil Aviation Conference, *Volume 2, technical guide*, https://www.ecac-ceac.org/images/documents/ECAC-Doc_29_4th_edition_Dec_2016_Volume_2.pdf, 4th Edition, 2016.

[8] J. Sun, J. Ellerbroek, and J. Hoekstra, "Modeling and inferring aircraft takeoff mass from runway ads-b data", *7th International Conference on Research in Air Transportation*, 2016. [Online]. Available: https://www.researchgate.net/publication/305403975_Modeling_and_Inferring_Aircraft_Takeoff_Mass_from_Runway_ADS-B_Data.

[9] R. Ayzit, M. S. Cengiz, M. Uzun, *et al.*, "Generalizable aircraft takeoff weight estimation from trajectory data using machine learning", in *AIAA Aviation and Aeronautics Forum and Exposition, AIAA AVIATION Forum 2023*, American Institute of Aeronautics and Astronautics Inc, AIAA, 2023, ISBN: 9781624107047. DOI: 10.2514/6.2023-4108.

[10] O. Schwab and C. Zellmann, "Estimation of flight-phase-specific jet aircraft parameters for noise simulations", *Journal of Aircraft*, vol. 57, 6 2020, ISSN: 15333868. DOI: 10.2514/1.C035779.

[11] Royal Schiphol Group, *Evaluatie gebruiksprognose 2024*, 2024. [Online]. Available: https://assets.ctfassets.net/biom0eqyyi6b/7g1qitLy1UtYxHZiK8rIwv/f14cace981726d980cb87d205bfc89f2/Evaluatie_Gebruikprognose_2024.pdf.

[12] LVNL, *Aeronautical information publication*, Electronic AIP (eAIP) PDF, version 18 SEP 2025, 2025. [Online]. Available: https://www.lvnl.nl/aip.

[13] C. Truong, L. Oudre, and N. Vayatis, *Selective review of offline change point detection methods*, 2020. DOI: 10.1016/j.sigpro.2019.107299.

[14] K. Millard and M. Richardson, "On the importance of training data sample selection in random forest image classification: A case study in peatland ecosystem mapping", *Remote Sensing*, vol. 7, 7 2015, ISSN: 20724292. DOI: 10.3390/rs70708489.

[15] Janes. (2024), [Online]. Available: https://customer.janes.com/ (visited on 12/06/2025).

[16] D. Simons and M. Snellen, "An introduction to general acoustics and aircraft noise", in *Course AE4431-23 Aircraft Noise*, TU Delft, 2023.

[17] E. S. RUTOWSKI, "Energy approach to the general aircraft performance problem", *Journal of the Aeronautical Sciences*, vol. 21, 3 1954. DOI: 10.2514/8.2956.

[18] EASA. "Aircraft noise and performance data". (2024), [Online]. Available: https://www.easa.europa.eu/en/domains/environment/policy-support-and-research/aircraft-noise-and-performance-anp-data (visited on 01/02/2025).

[19] V. Jagasits. "Muac pioneers digital connectivity between ground and air with ads-c". (2024), [Online]. Available: https://www.eurocontrol.int/article/muac-pioneers-digital-connectivity-between-ground-and-air-ads-c (visited on 03/11/2025).

[20] M. L. Lautsch, T. P. Ring, and S. C. Langer, "Validation of the doc 29 best-practice prediction method of aircraft noise on the ground at a single flight level using ads-b data", Tech. Rep. [Online]. Available: chrome-extension://efaidnbmnnnibpcajpcglclefindmkaj/https://pub.dega-akustik.de/DAGA_2024/files/upload/paper/177.pdf.

[21] T. Nakazawa, N. Shinohara, and K. Hanaka, "The effects of aircraft take-off thrust reduction on noise exposure around the airport", in *INTER-NOISE 2019 MADRID - 48th International Congress and Exhibition on Noise Control Engineering*, 2019. [Online]. Available: https://www.sea-acustica.es/INTERNOISE_2019/Fchrs/Proceedings/2085.pdf.

[22] R. Merino-Martínez, S. J. Heblij, D. H. Bergmans, M. Snellen, and D. G. Simons, "Improving aircraft noise predictions considering fan rotational speed", *Journal of Aircraft*, vol. 56, 1 2019, ISSN: 15333868. DOI: 10.2514/1.C034849.

[23] R. C. van der Grift, M. Snellen, and A. Amiri-Simkooei, "The effect of using n1% as input for aircraft noise modelling", *Transportation Research Part D: Transport and Environment*, vol. 142, May 2025, ISSN: 13619209. DOI: 10.1016/j.trd.2025.104710.

[24] M. Pretto, L. Dorbolò, P. Giannattasio, and A. Zanon, "Aircraft operation reconstruction and airport noise prediction from high-resolution flight tracking data", *Transportation Research Part D: Transport and Environment*, vol. 135, p. 104 397, Oct. 2024, ISSN: 1361-9209. DOI: 10.1016/J.TRD.2024.104397.

Appendix A

This appendix contains plots and noise contours, which were not presented in the paper, for the other evaluated aircraft types. All of the figures are obtained following the same methodology described in **??**. This appendix is split into 4 sections, Section A.1 for the Airbus A330-300, Section A.2 for the Boeing 777-300ER, Section A.3 for the Airbus A321neo, and Section A.4 for the Boeing 737-800.

A.1. Airbus A330

For the A330-300, the noise contour plots of the ACMS and the new thrust and weight Doc. 29 models are visualized for both departures and arrivals.

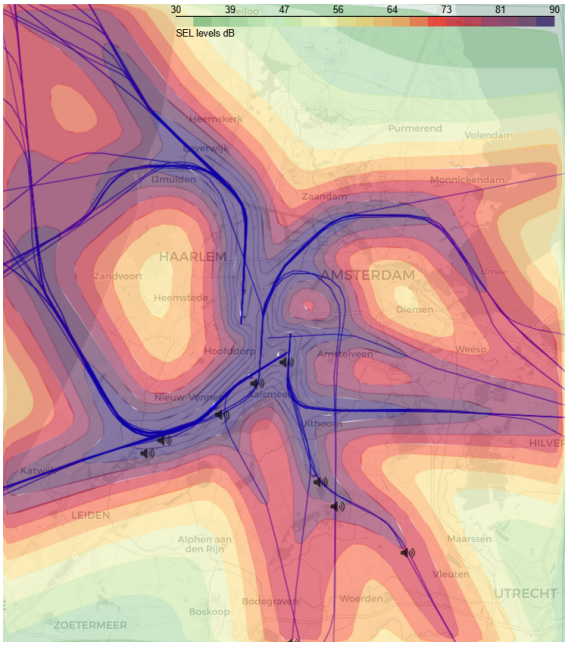

Figure A.1: Noise contour plot of A333 departures using the ACMS Doc. 29 calculation methodology.

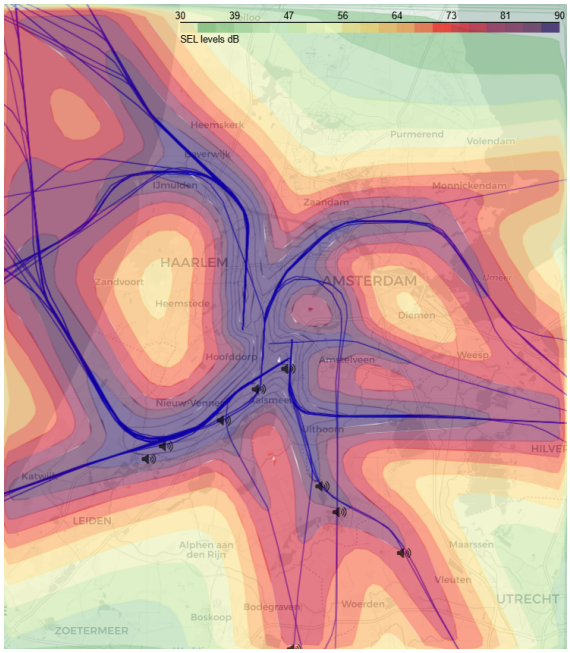

Figure A.2: Noise contour plot of A333 departures using the new thrust and weight Doc. 29 calculation methodology.

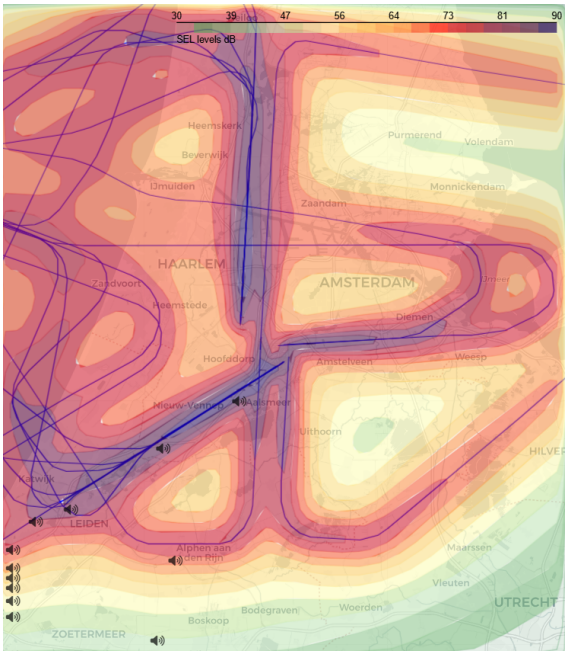

Figure A.3: Noise contour plot of A333 arrivals using the ACMS Doc. 29 calculation methodology.

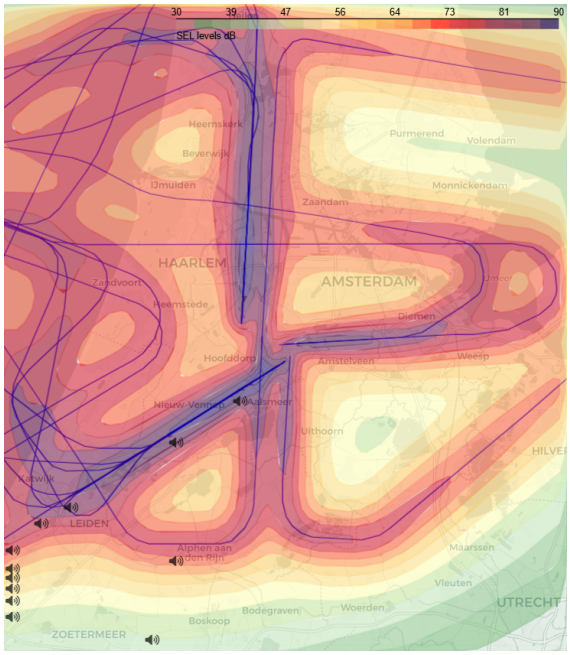

Figure A.4: Noise contour plot of A333 arrivals using the new thrust Doc. 29 calculation methodology.

A.2. Boeing 777-300ER

For the Boeing 777-300ER, it should be first noted that only 37 flights were present in the dataset for both departures and arrivals compared to the 70 of other aircraft types. The altitude and velocity profiles of the FPP match accurately with the flight data. The N1% plot in Figure A.7 shows 3 different climb modes are used during departures. Thrust profiles, as shown in Figure A.8, show large differences between the FPP and the flight data. This result is to be expected since the flight data is compared to the Boeing 777-300 FPP, as no profiles were available for the Boeing 777-300ER. The main difference between these two aircraft types is the engine. The Boeing 777-300ER is fitted with GE90 engines, which are rated for a maximum take-off thrust 25% larger than the Rolce-Royce Trent 800 engines of the Boeing 777-300. The observed differences in thrust indicate the importance of keeping the fixed-point profiles up to date.

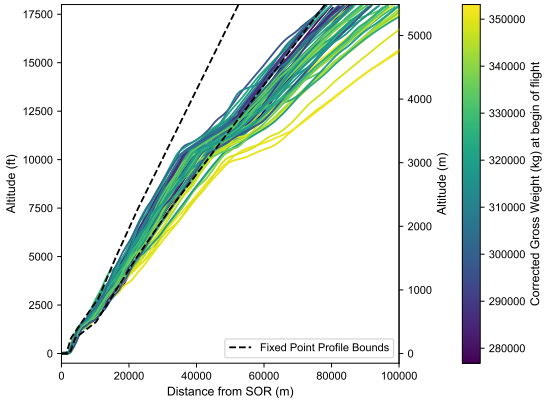

Figure A.5: Filtered altitude profiles of B77W departures with varying TOW compared to the FPP.

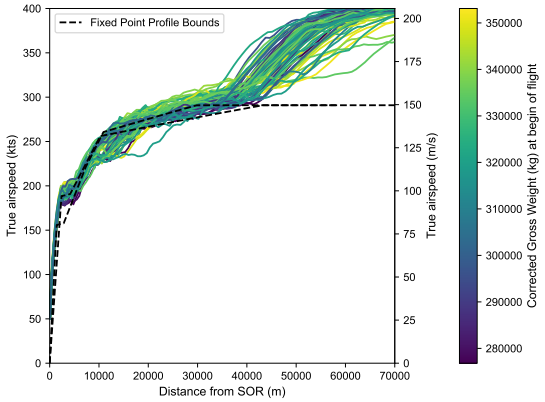

Figure A.6: Filtered TAS profiles of B77W departures with varying TOW compared to the FPP.

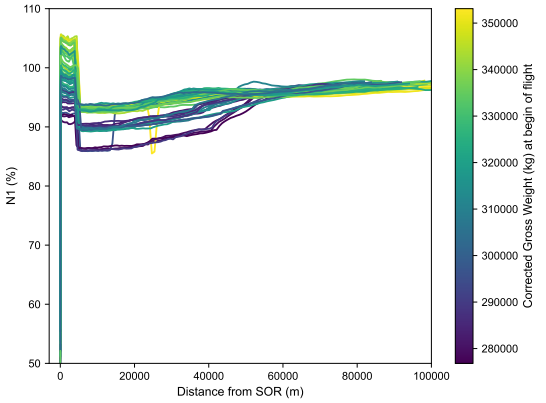

Figure A.7: Filtered N1% profiles of B77W departures with varying TOW.

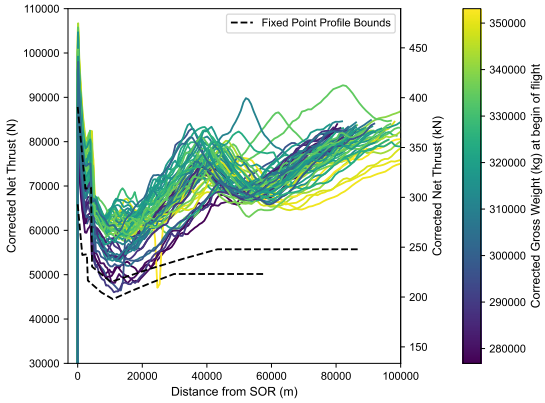

Figure A.8: Filtered thrust profiles of B77W departures with varying TOW compared to the FPP.

The 3 different climb modes for departures significantly decrease the performance of the climb slope and distance method, as can be seen in Figure A.12. However, the specific energy method shows a very good correlation with take-off weight.

The noise contour and delta plots for B77W departures are visualized in Figure A.15, Figure A.16, Figure A.17, Figure A.18, Figure A.19, and Figure A.20. Here, much larger contours are visible for the ACMS and new thrust and weight Doc. 29 models. The main reason for this larger contour is again the use of non matching FPP. The larger engine thrust results in much more noise emissions over the entire visualized area. Also, differences can be observed in the delta plot comparing the new thrust and weight Doc. 29 model with the ACMS Doc. 29 model. For the Boeing 777-300ER the climb mode is selected based on the

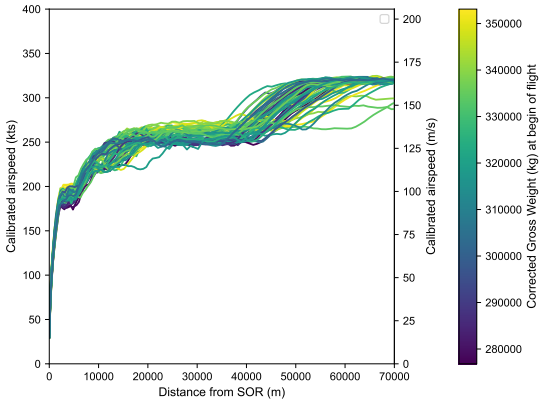

Figure A.9: Filtered CAS profiles of B77W departures with varying TOW.

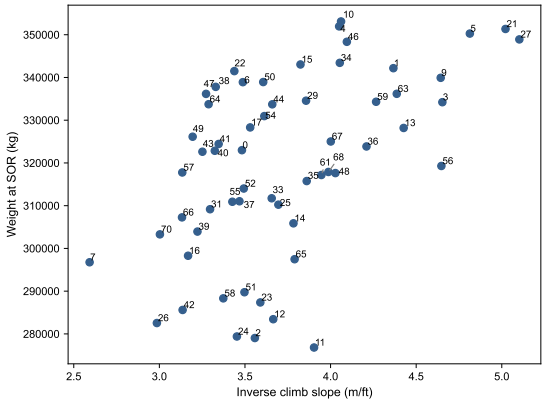

Figure A.10: TOW plotted against the inverse climb slope for B77W departures.

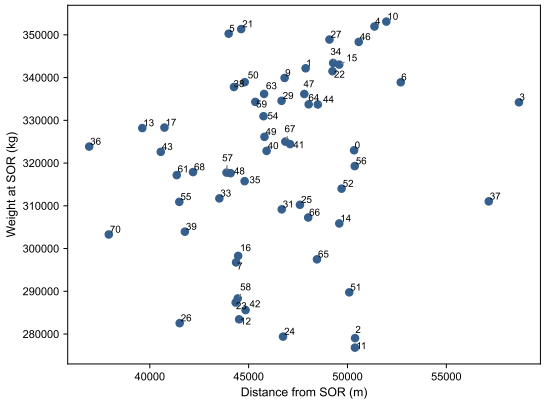

Figure A.11: Weight plotted against the distance from the SOR at which a ground speed of 340 knots is reached for B77W departures.

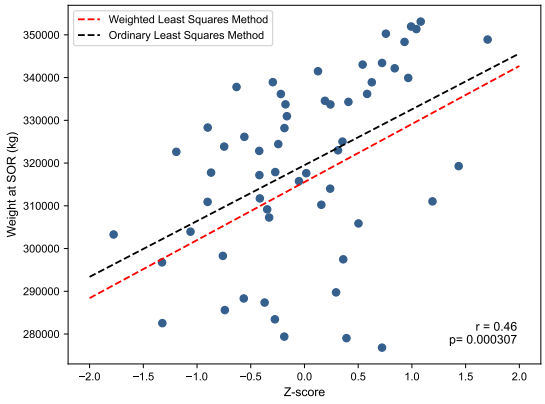

Figure A.12: Aircraft TOW plotted against the combined z-scores fitted with an OLS and a WLS method for B77W departures.

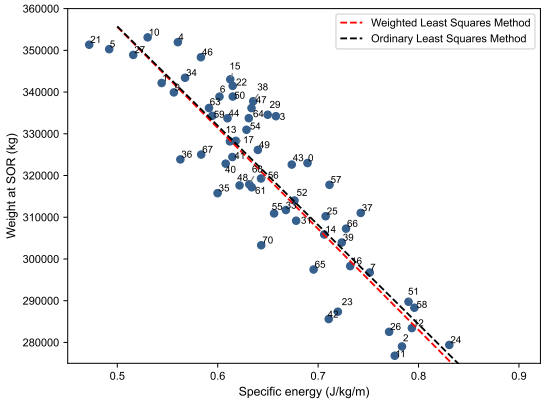

Figure A.13: Specific energy per meter plotted against the weight of the aircraft for B77W departures.

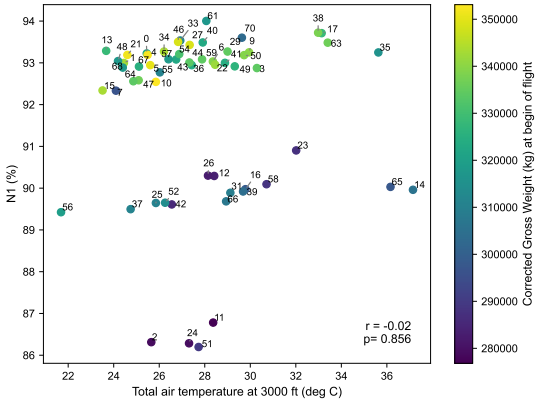

Figure A.14: N1% plotted against total air temperature for B77W departures.

estimated weight of the aircraft. Aircraft below 280,000 kilograms are assigned to the climb mode with the lowest N1% setting, aircraft between 280,000 and 315,000 kilograms to the middle climb mode, and aircraft above 315,000 kilograms to the climb mode with the highest N1% setting. Therefore, the differences in

the noise contour plots of the ACMS Doc. 29 model and the new thrust and weight Doc. 29 model can be explained by misidentifying the climb modes.

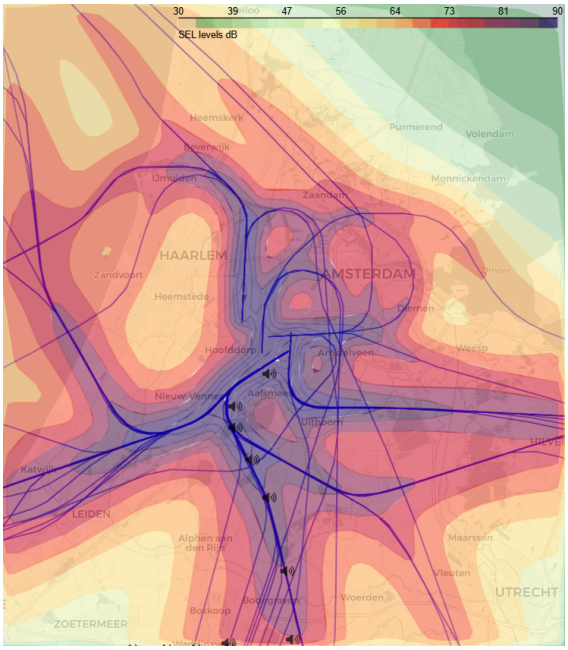

Figure A.15: Noise contour plot of B77W departures using the original Doc. 29 calculation methodology.

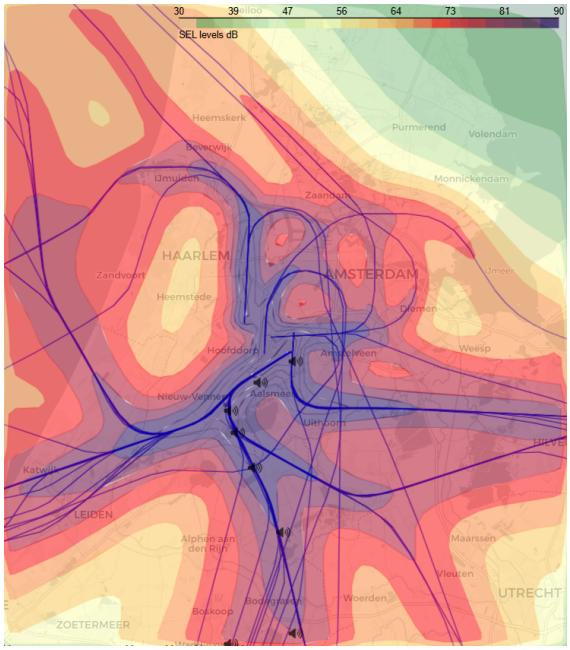

Figure A.16: Noise contour plot of B77W departures using the ACMS Doc. 29 calculation methodology.

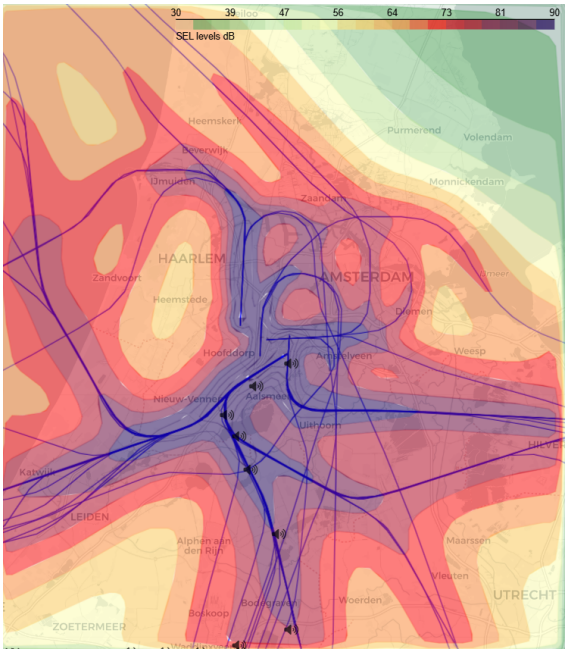

Figure A.17: Noise contour plot of B77W departures using the new thrust and weight Doc. 29 calculation methodology.

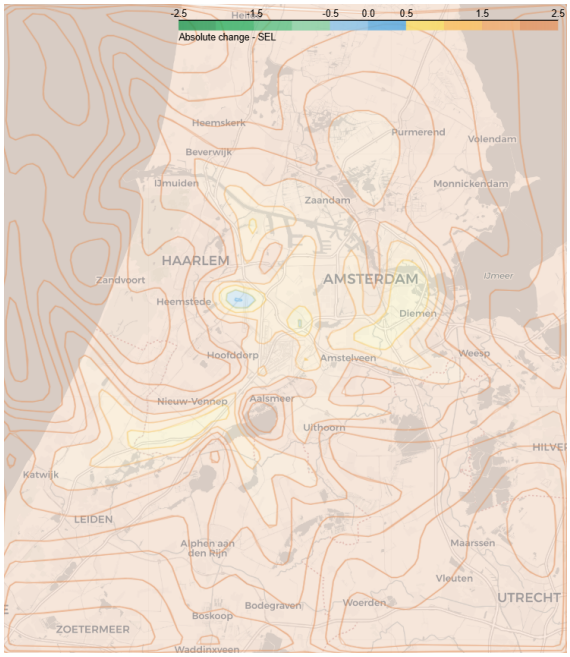

Figure A.18: Noise contour delta plot of B77W departures comparing the ACMS Doc. 29 model with the original Doc. 29 model.

As the thrust model needs to be trained with independent data, only 8 flight remain in the test data set. Noise contours are again visualized in Figure A.21, Figure A.22, and Figure A.23. The delta plots in Figure A.24 and Figure A.25 show differences further from the airport most likely caused by thrust peaks that are not

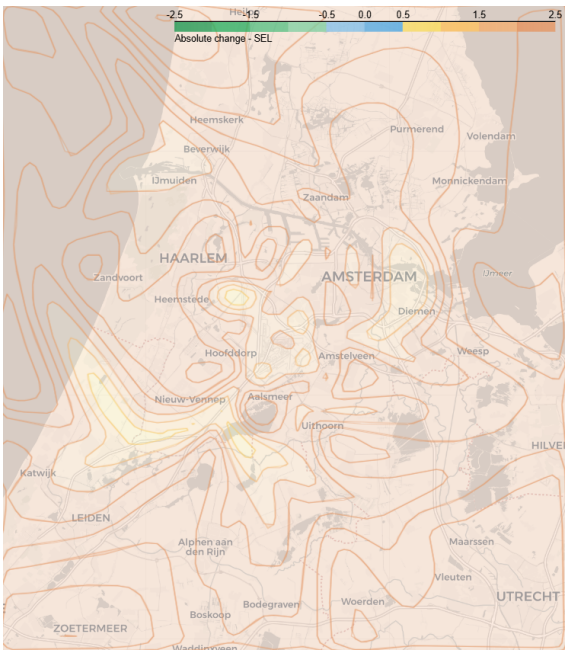

Figure A.19: Noise contour delta plot of B77W departures comparing the new thrust and weight Doc. 29 model with the original Doc. 29 model.

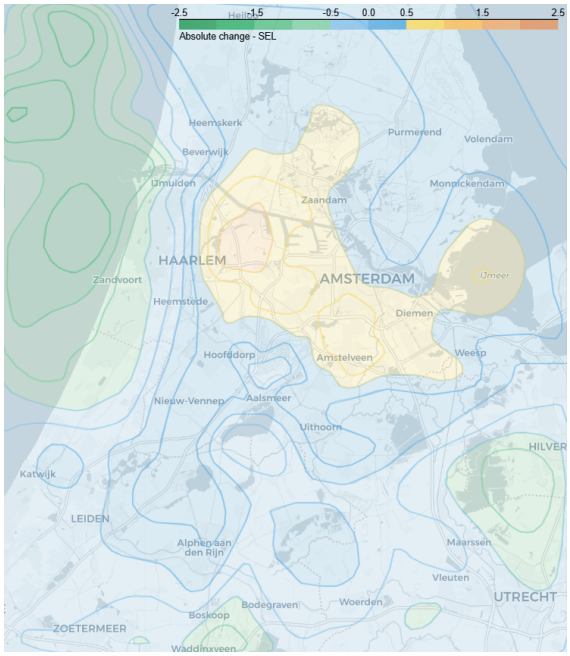

Figure A.20: Noise contour delta plot of B77W departures comparing the new thrust and weight Doc. 29 model with the ACMS Doc. 29 model.

captured by the FPP. The ACMS Doc. 29 model matches accurately with the new thrust Doc. 29 model in Figure A.26.

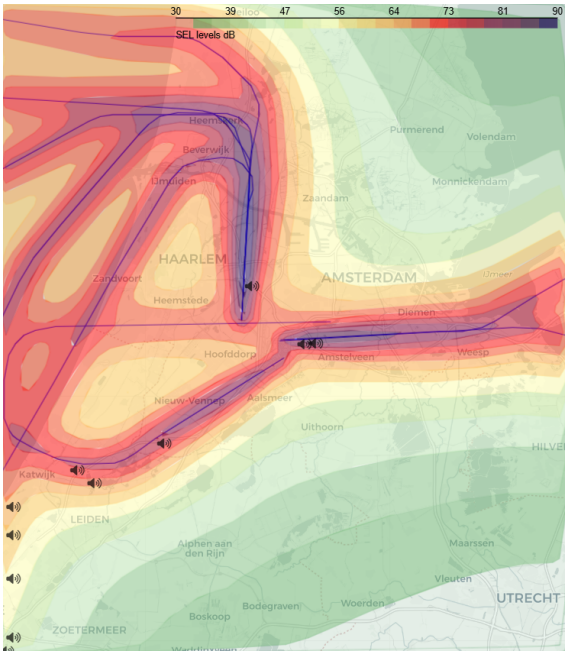

Figure A.21: Noise contour plot of B77W arrivals using the original Doc. 29 calculation methodology.

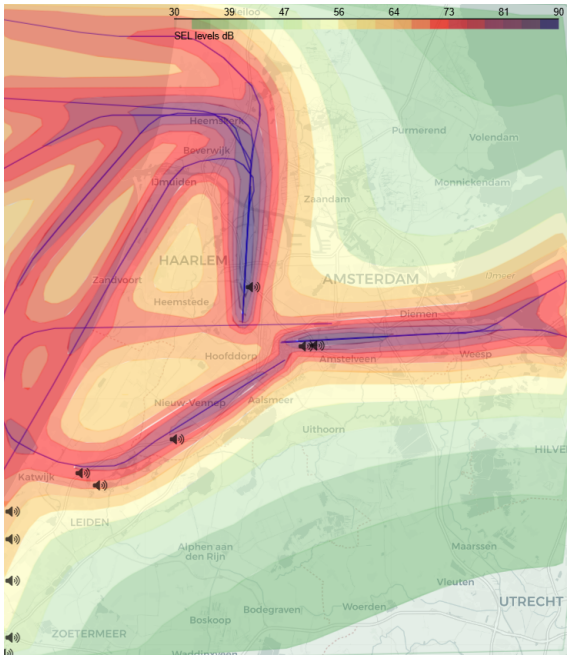

Figure A.22: Noise contour plot of B77W arrivals using the ACMS Doc. 29 calculation methodology.

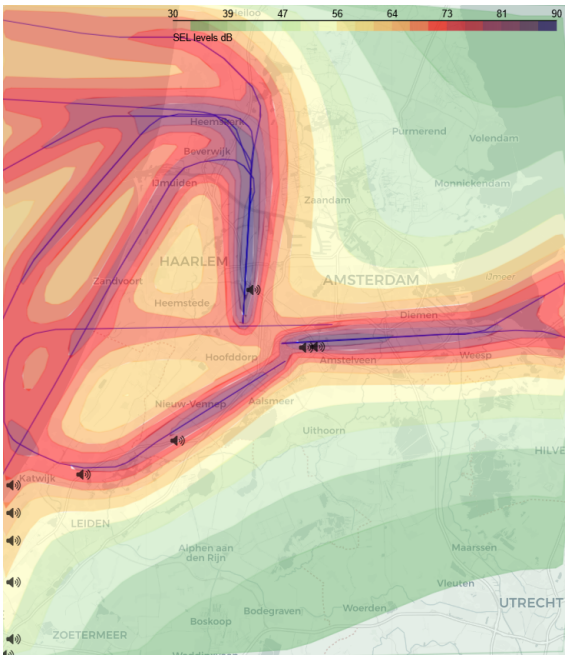

Figure A.23: Noise contour plot of B77W arrivals using the new thrust Doc. 29 calculation methodology.

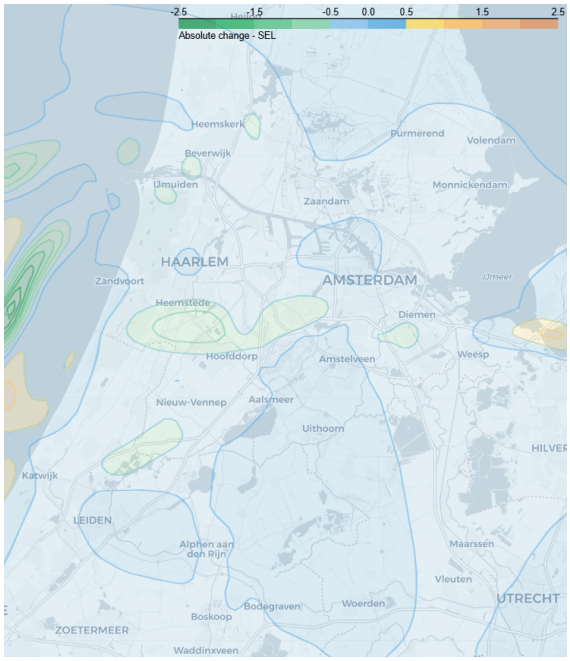

Figure A.24: Noise contour delta plot of B77W arrivals comparing the ACMS Doc. 29 model with the original Doc. 29 model.

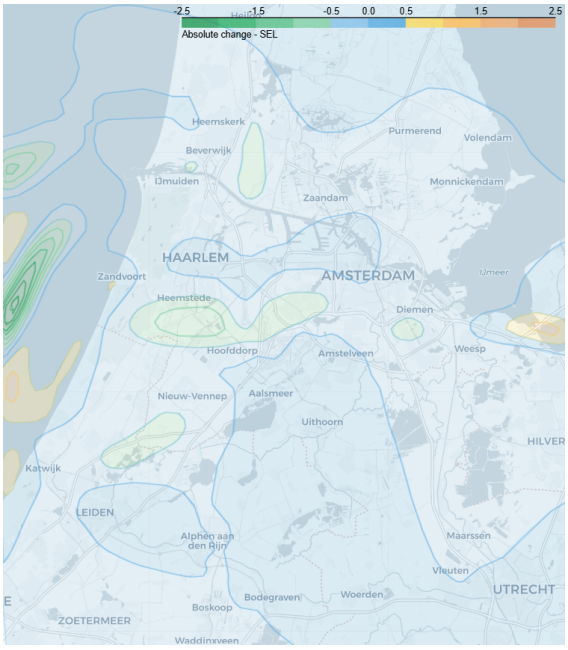

Figure A.25: Noise contour delta plot of B77W arrivals comparing the new thrust Doc. 29 model with the original Doc. 29 model.

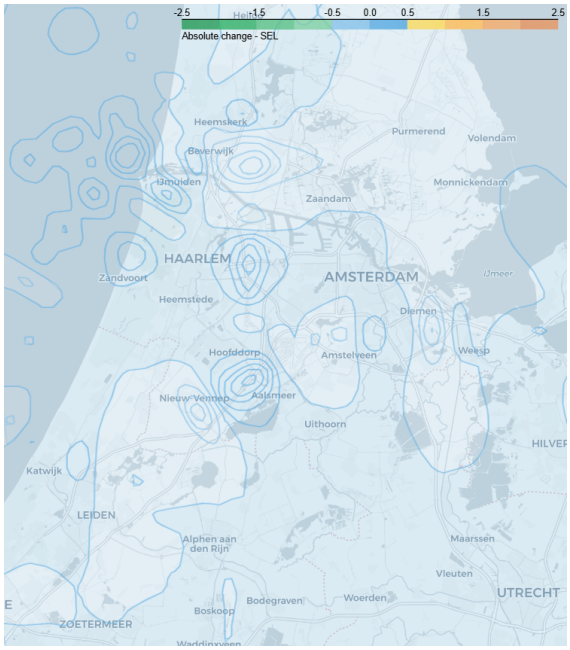

Figure A.26: Noise contour delta plot of B77W arrivals comparing the new thrust Doc. 29 model with the ACMS Doc. 29 model.

A.3. Airbus A321neo

For the Airbus A321neo, the ANP-proxy A321-232 is used. This same proxy is used for the Airbus A321ceo, an older version of the Airbus A321 aircraft. The FPP are therefore designed for the older aircraft and for both types the aircraft performance is modeled equally. The only difference in the computation of the noise levels is the correction factor.

The altitude profiles are steeper than predicted by the FPP, as shown in Figure A.27. Also, Figure A.30 shows higher thrust levels than predicted by the FPP are observed in the data. Partially, this effect can be explained by the steeper altitude profile. The steeper profile leads to a larger correction factor when converting thrust to corrected net thrust, as this correction factor includes the ratio between the pressure at altitude and the pressure at sea level. Again, the comparison with the FPP shows the importance of correctly modeling the flight performance per aircraft type. Therefore, it can be concluded that changes to the aircraft configuration, keeping the maximum take-off weight and thrust roughly the same, can still significantly alter the aircraft performance behavior.

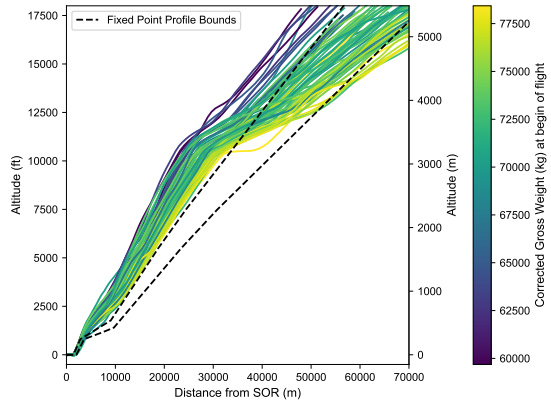

Figure A.27: Filtered altitude profiles of A21N departures with varying TOW compared to the FPP.

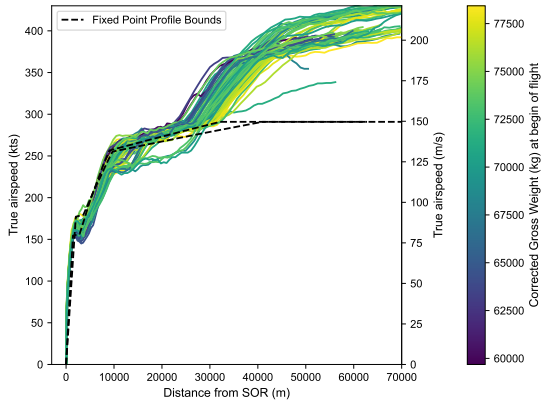

Figure A.28: Filtered TAS profiles of A21N departures with varying TOW compared to the FPP.

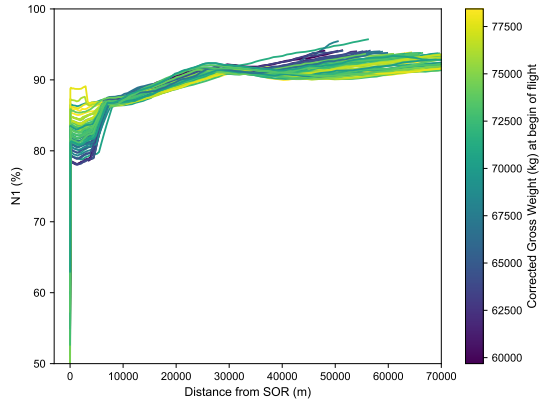

Figure A.29: Filtered N1% profiles of A21N departures with varying TOW.

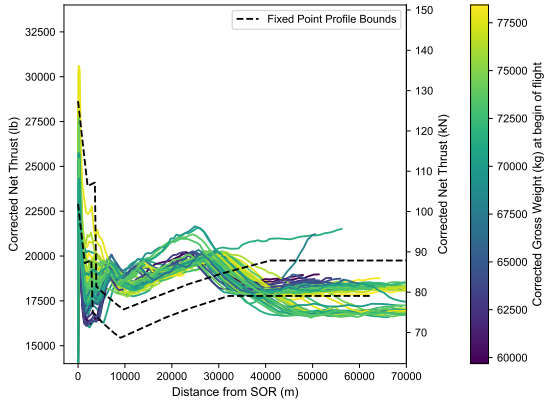

Figure A.30: Filtered thrust profiles of A21N departures with varying TOW compared to the FPP.

Again the noise contour plots for the original, ACMS and new thrust and weight Doc. 29 model for departures are visualized in Figure A.37, Figure A.38, and Figure A.39. The delta plots in Figure A.40 show less noise directly underneath the flight paths for the ACMS model compared to the original Doc. 29 model, while more noise is observed relatively further away. This can be attributed to achieving a higher altitude earlier, meaning the noise travels further. Figure A.41 shows a similar effect. Figure A.42 indicates small differences between the ACMS model and the new thrust and weight model, meaning the new method significantly

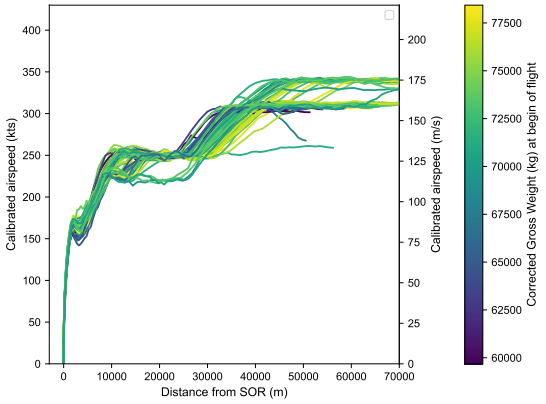

Figure A.31: Filtered CAS profiles of A21N departures with varying TOW.

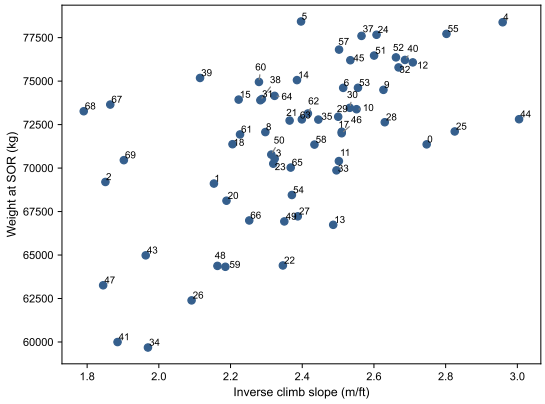

Figure A.32: TOW plotted against the inverse climb slope for A21N departures.

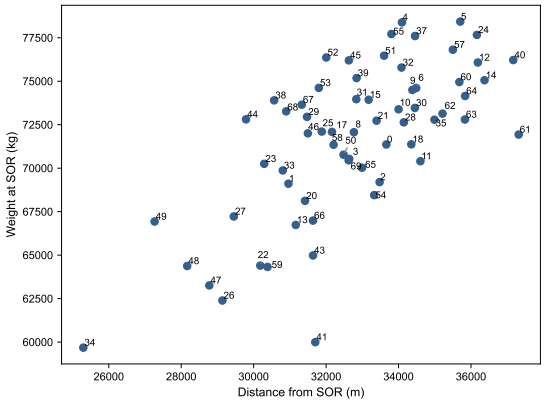

Figure A.33: Weight plotted against the distance from the SOR at which a ground speed of 320 knots is reached for A21N departures.

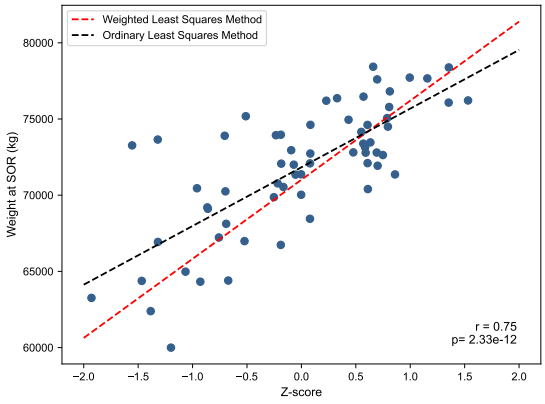

Figure A.34: Aircraft TOW plotted against the combined z-scores fitted with an OLS and a WLS method for A21N departures.

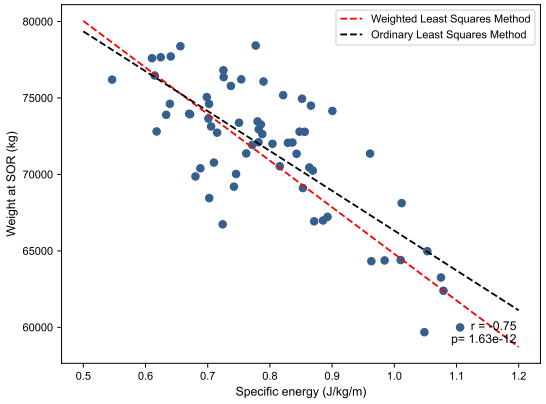

Figure A.35: Specific energy per meter plotted against the weight of the aircraft for A21N departures.

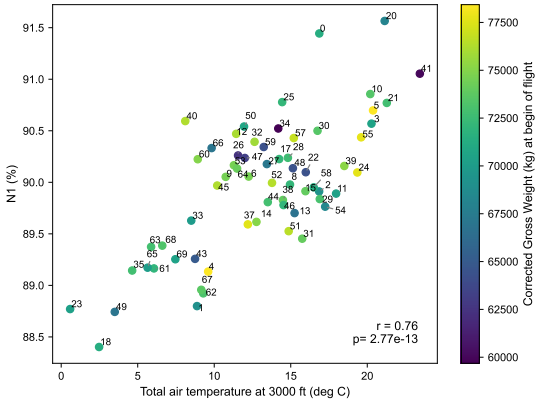

Figure A.36: N1% plotted against total air temperature for A21N departures.

improved the noise modeling. Small differences are still visible near the airport, likely due to errors in the weight estimation propagating to the take-off thrust input parameters.

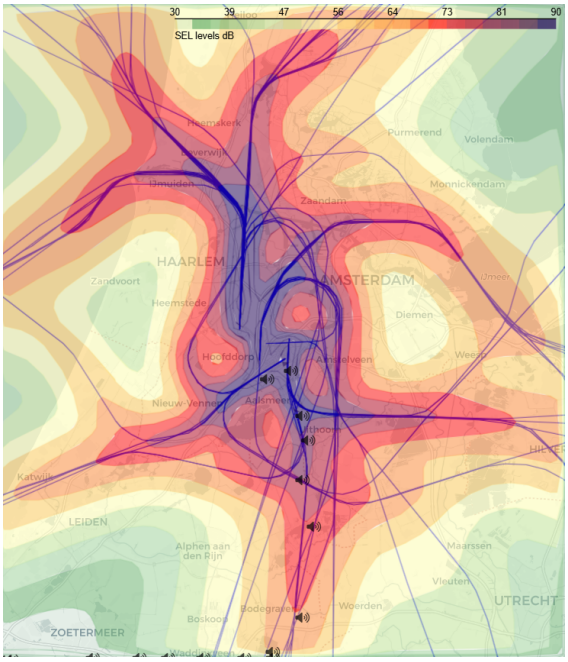

Figure A.37: Noise contour plot of A21N departures using the original Doc. 29 calculation methodology.

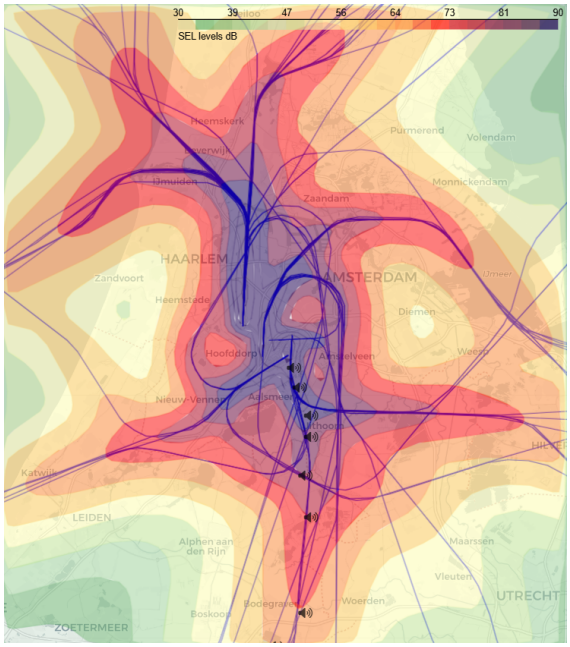

Figure A.38: Noise contour plot of A21N departures using the ACMS Doc. 29 calculation methodology.

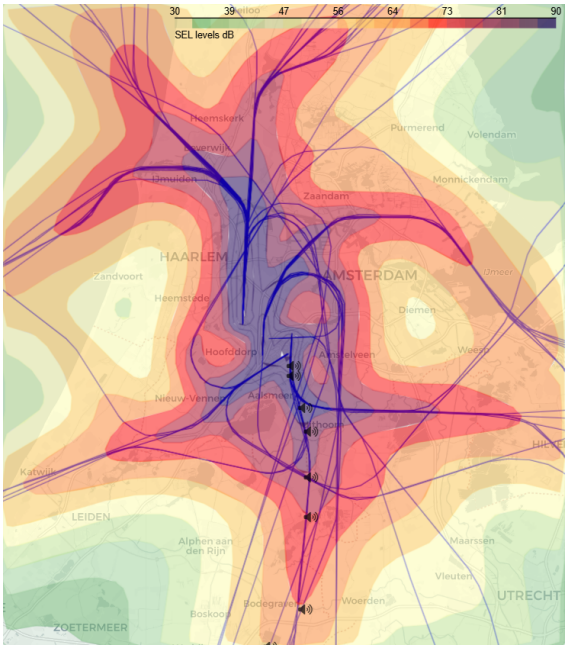

Figure A.39: Noise contour plot of A21N departures using the new thrust and weight Doc. 29 calculation methodology.

Figure A.40: Noise contour delta plot of A21N departures comparing the ACMS Doc. 29 model with the original Doc. 29 model.

Noise contours for arrivals are plotted in Figure A.43, Figure A.44, and Figure A.45. The delta plot in Figure A.46 again shows an increased noise load due to thrust peaks. Figure A.47 seems completely different compared to Figure A.46 , but colors changed due to grid values being close a boundary of the discrete color scale. In Figure A.48 it can be seen that the difference is marginal between the ACMS Doc. 29 model and the new thrust Doc. 29 model.

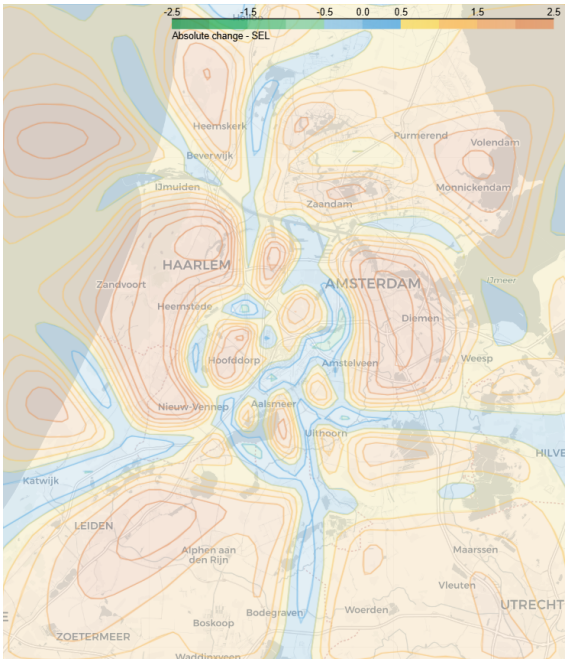

Figure A.41: Noise contour delta plot of A21N departures comparing the new thrust and weight Doc. 29 model with the original Doc. 29 model.

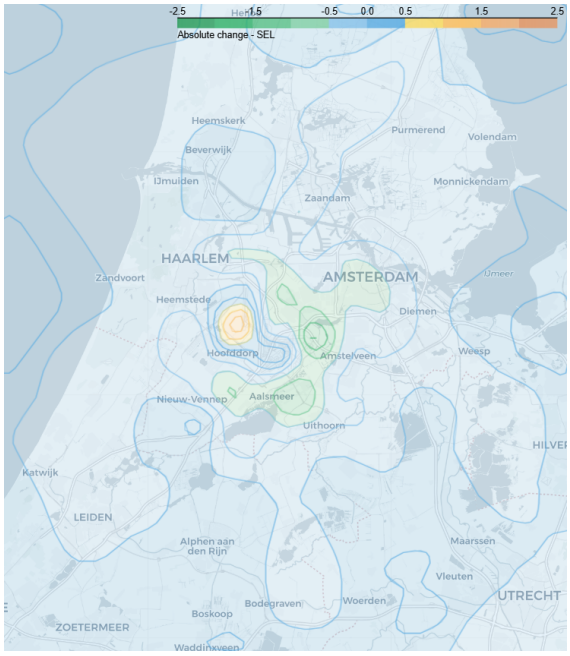

Figure A.42: Noise contour delta plot of A21N departures comparing the new thrust and weight Doc. 29 model with the ACMS Doc. 29 model.

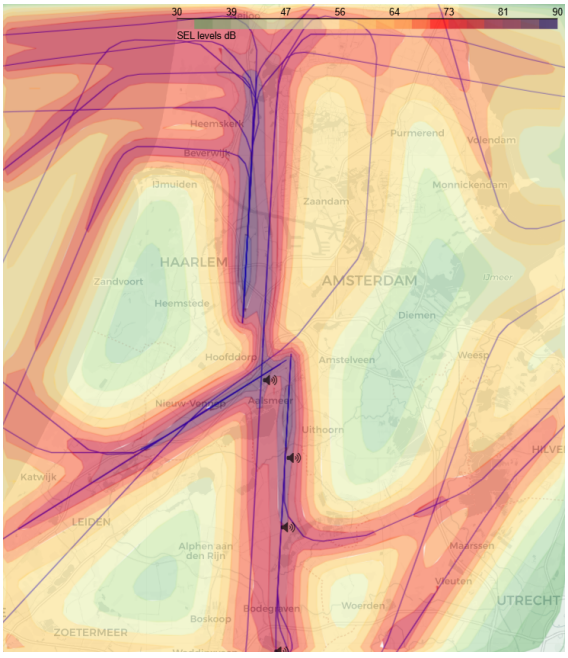

Figure A.43: Noise contour plot of A21N arrivals using the original Doc. 29 calculation methodology.

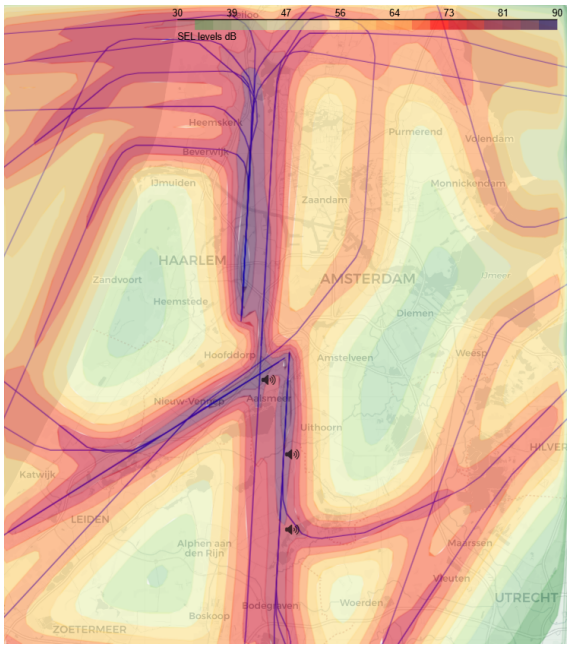

Figure A.44: Noise contour plot of A21N arrivals using the ACMS Doc. 29 calculation methodology.

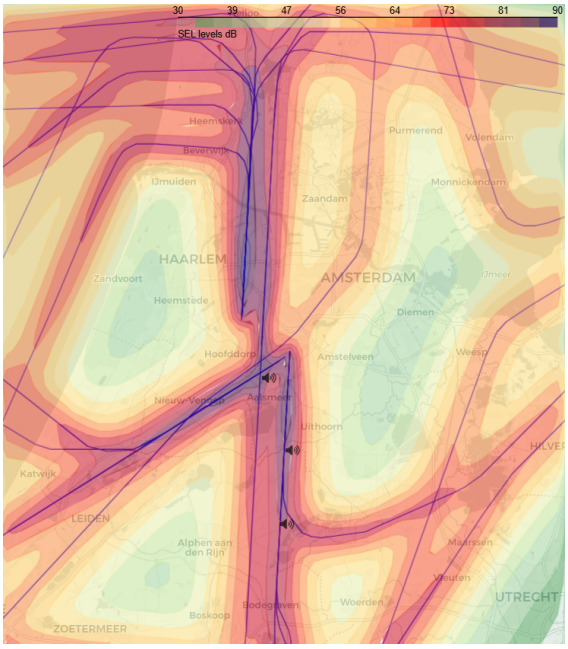

Figure A.45: Noise contour plot of A21N arrivals using the new thrust Doc. 29 calculation methodology.

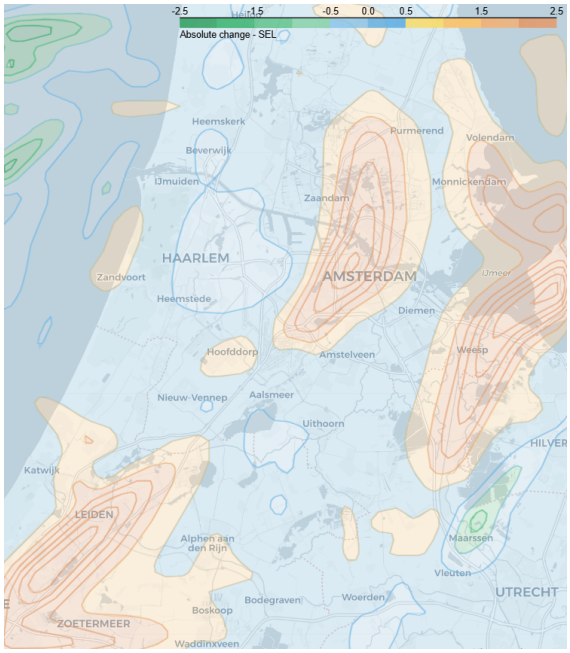

Figure A.46: Noise contour delta plot of A21N arrivals comparing the ACMS Doc. 29 model with the original Doc. 29 model.

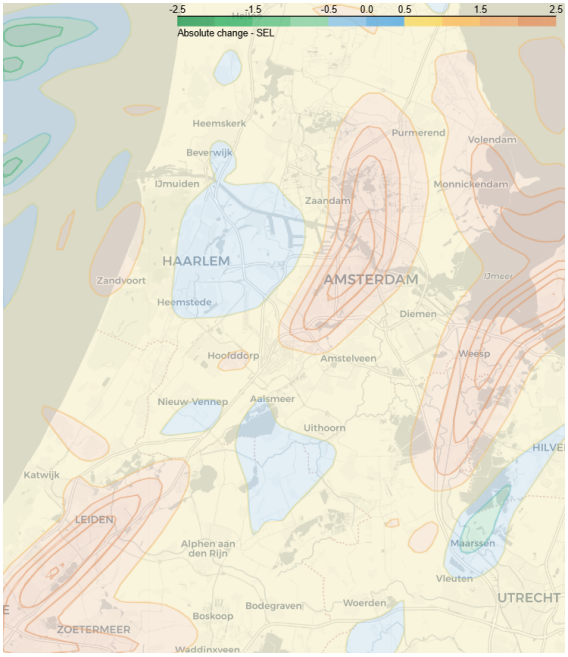

Figure A.47: Noise contour delta plot of A21N arrivals comparing the new thrust Doc. 29 model with the original Doc. 29 model.

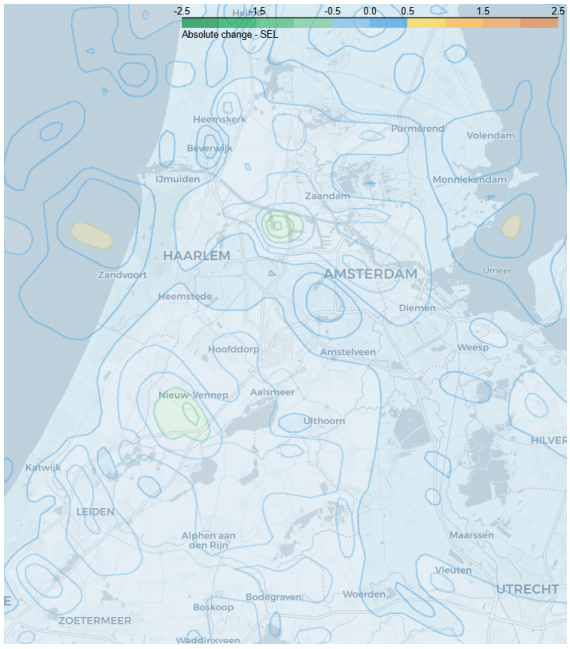

Figure A.48: Noise contour delta plot of A21N arrivals comparing the new thrust Doc. 29 model with the ACMS Doc. 29 model.

A.4. Boeing 737-800

The Boeing 737-800 aircraft type uses the Boeing 737-700 ANP-proxy to model performance behavior via the FPP. In Figure A.49, the bandwidth if the FPP is too small. Furthermore, for many flights, the take-off is performed at a slower speed, as seen in Figure A.50, most likely due to the introduction of the so called opti-climb procedures. Similar results are visible in Figure A.53. Again, multiple climb modes are visible in Figure A.51. The thrust profiles in Figure A.52 have the correct bandwidth, but TOW seems to show less correlation with the profiles. This is also visible in Figure A.56 and Figure A.57, significantly reducing the performance of the weight estimation for this type of aircraft. Due to this, less correlation between the ACMS Doc. 29 noise model and the new thrust and weight Doc. 29 near the airport is expected compared to other aircraft types.

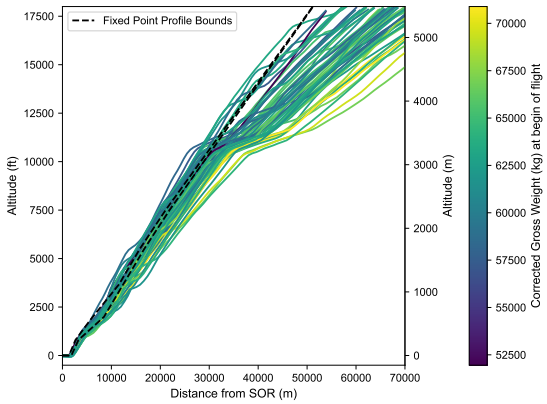

Figure A.49: Filtered altitude profiles of B738 departures with varying TOW compared to the FPP.

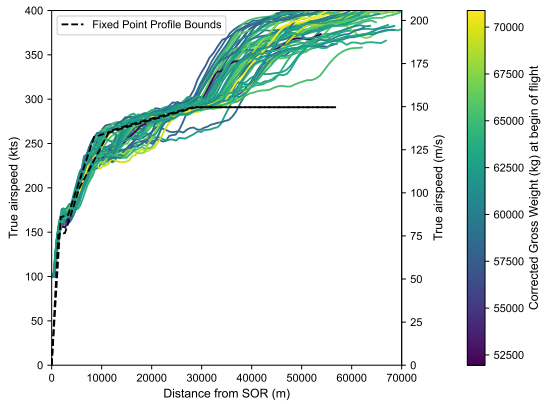

Figure A.50: Filtered TAS profiles of B738 departures with varying TOW compared to the FPP.

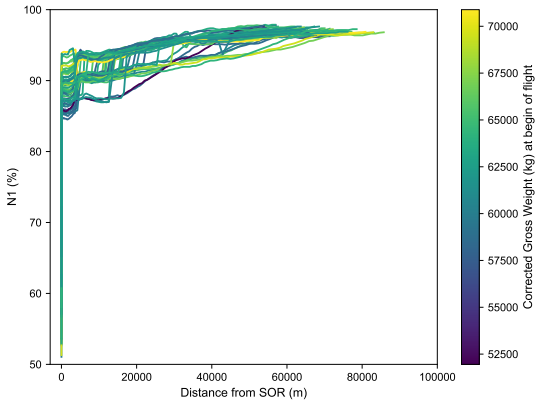

Figure A.51: Filtered N1% profiles of B738 departures with varying TOW.

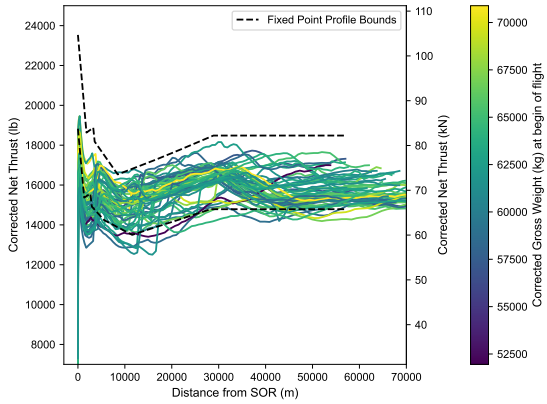

Figure A.52: Filtered thrust profiles of B738 departures with varying TOW compared to the FPP.

The noise contour plots for the original, ACMS and new thrust and weight Doc. 29 model for departures are visualized in Figure A.59, Figure A.60, and Figure A.61 respectively. The delta plots in Figure A.62 and Figure A.63 show similar results. In Figure A.64 there are small differences close to the airport and further away from the airport. Near the airport differences can be attributed to errors in the weight estimation propagating towards the thrust estimation. Further away, the original Doc. 29 model overestimates the noise levels due to aircraft in reality flying at higher altitudes with similar thrust levels.

Figure A.65, Figure A.66, and Figure A.67 show the noise contours for arrivals. In Figure A.68, significant differences are visible, located relatively further away from the airport. Noise at these locations is underestimated, most likely due to errors in the thrust modeling. The new thrust Doc. 29 model seems to

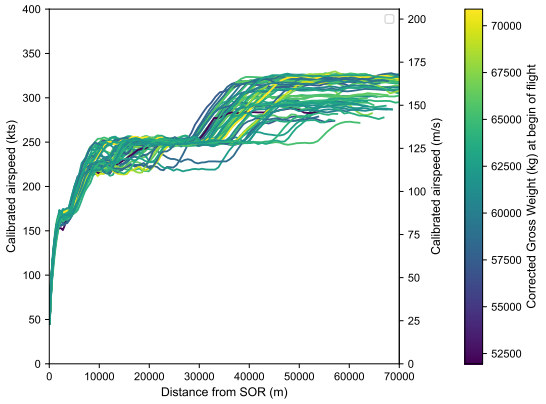

Figure A.53: Filtered CAS profiles of B738 departures with varying TOW.

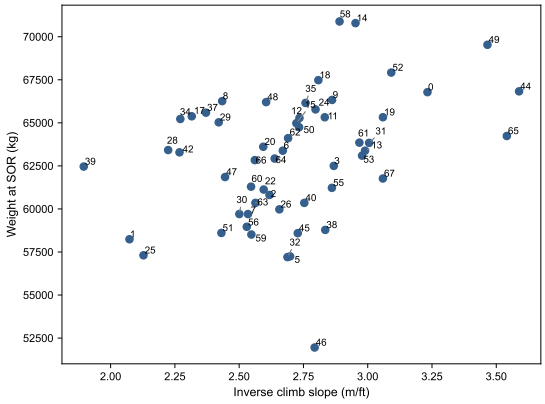

Figure A.54: TOW plotted against the inverse climb slope for B738 departures.

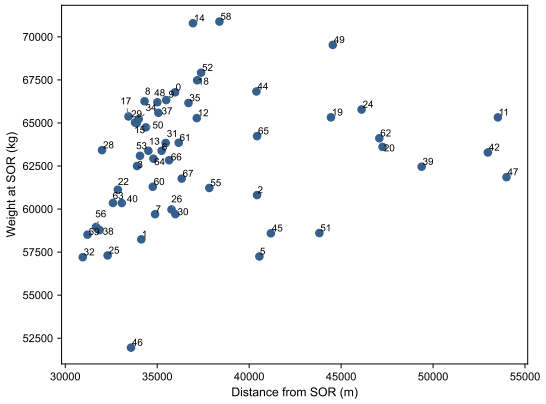

Figure A.55: Weight plotted against the distance from the SOR at which a ground speed of 320 knots is reached for B738 departures.

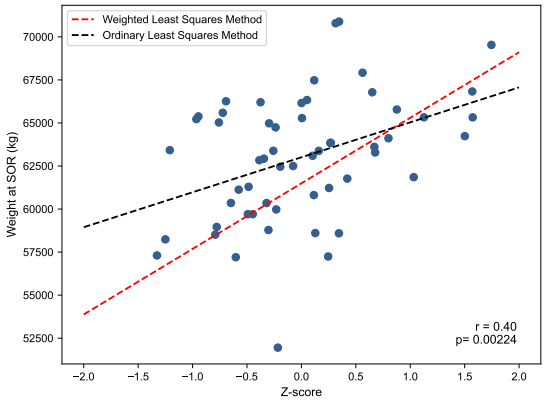

Figure A.56: Aircraft TOW plotted against the combined z-scores fitted with an OLS and a WLS method for B738 departures.

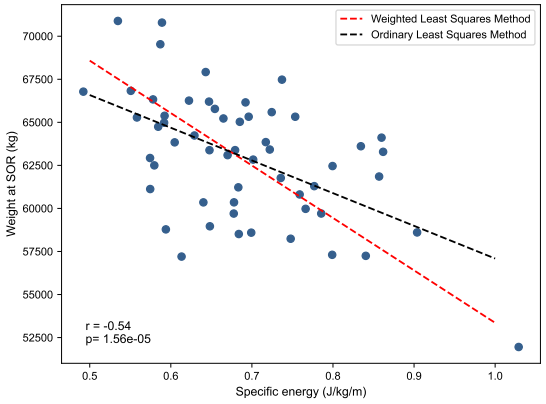

Figure A.57: Specific energy per meter plotted against the weight of the aircraft for B738 departures.

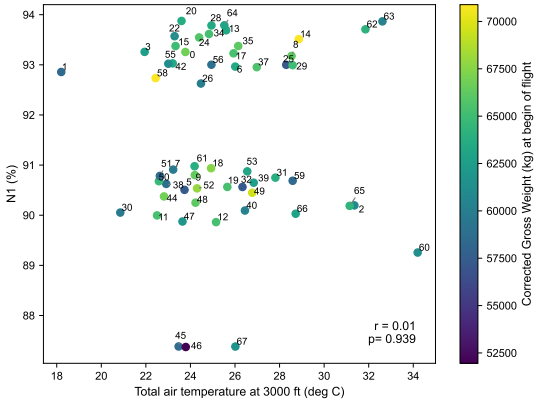

Figure A.58: N1% plotted against total air temperature for B738 departures.

underestimate noise near the airport, as seen in Figure A.69 and Figure A.70, modeling less noise than is produced in reality. As aircraft usually follow the glideslope at this stage of the flight, this result is unexpected and should be investigated further.

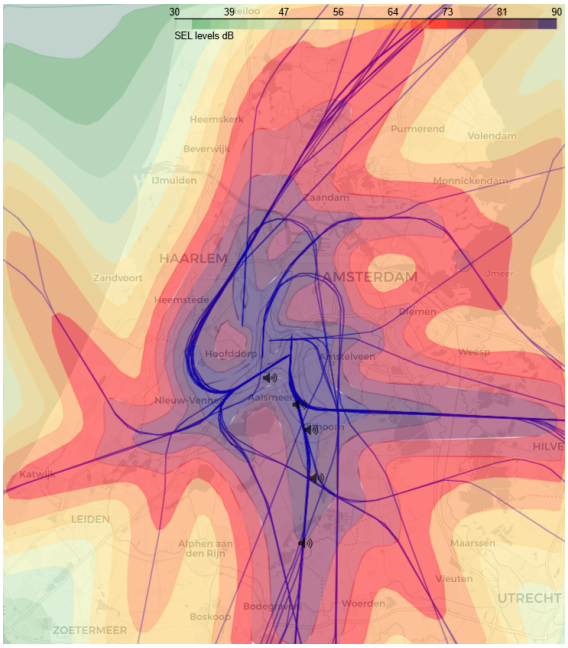

Figure A.59: Noise contour plot of B738 departures using the original Doc. 29 calculation methodology.

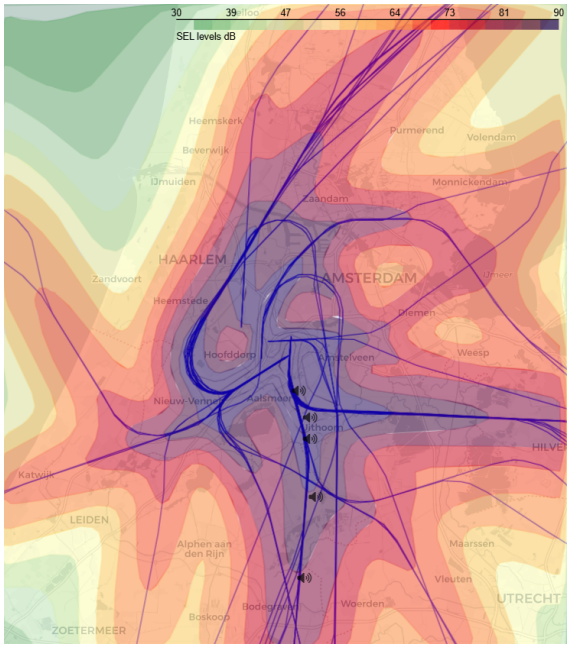

Figure A.60: Noise contour plot of B738 departures using the ACMS Doc. 29 calculation methodology.

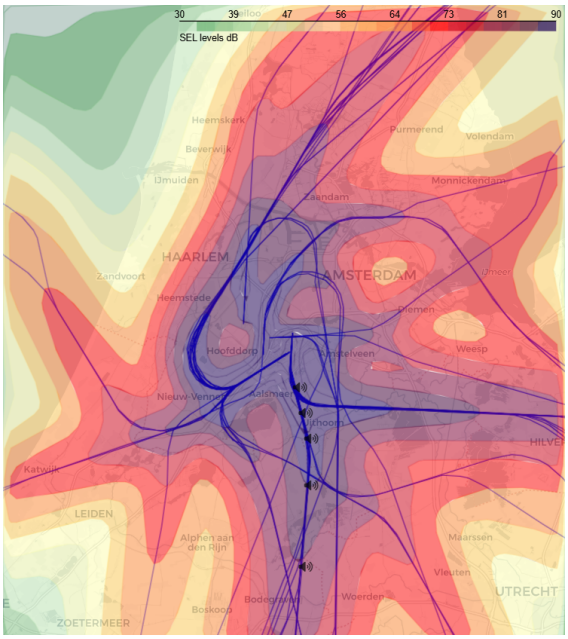

Figure A.61: Noise contour plot of B738 departures using the new thrust and weight Doc. 29 calculation methodology.

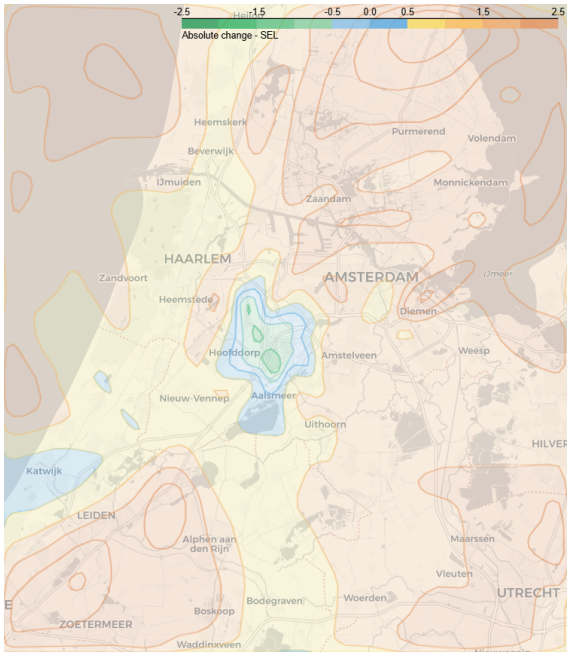

Figure A.62: Noise contour delta plot of B738 departures comparing the ACMS Doc. 29 model with the original Doc. 29 model.

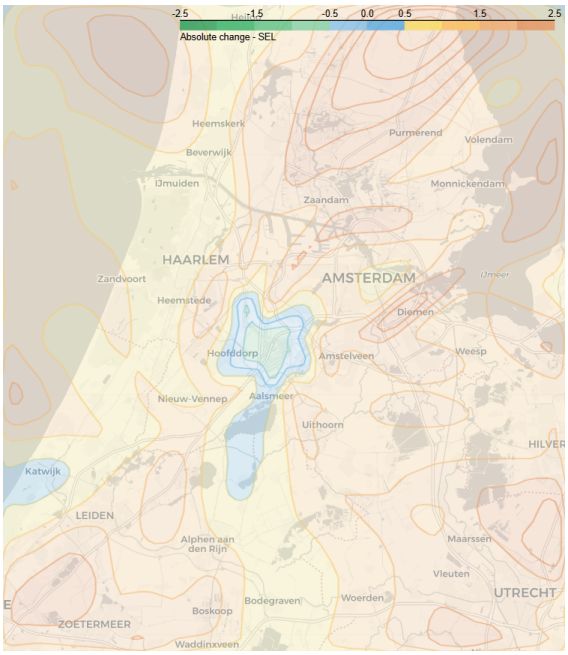

Figure A.63: Noise contour delta plot of B738 departures comparing the new thrust and weight Doc. 29 model with the original Doc. 29 model.

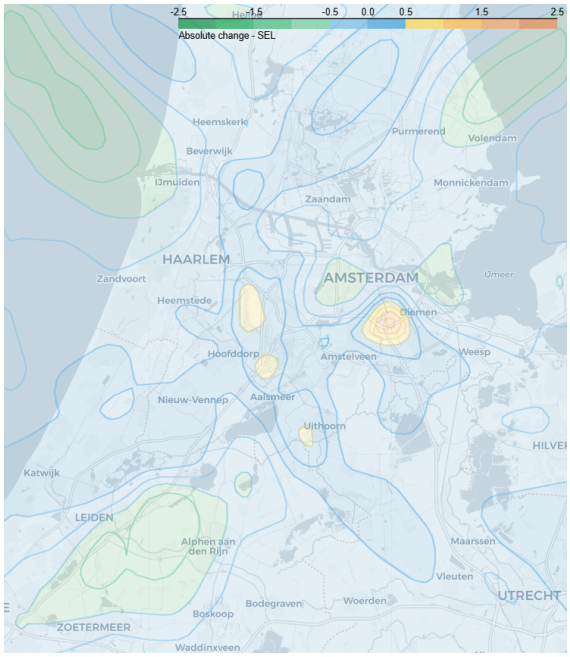

Figure A.64: Noise contour delta plot of B738 departures comparing the new thrust and weight Doc. 29 model with the ACMS Doc. 29 model.

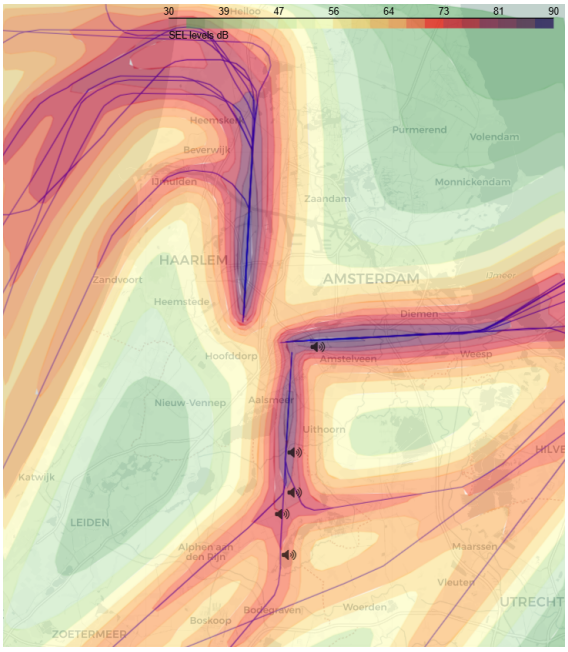

Figure A.65: Noise contour plot of B738 arrivals using the original Doc. 29 calculation methodology.

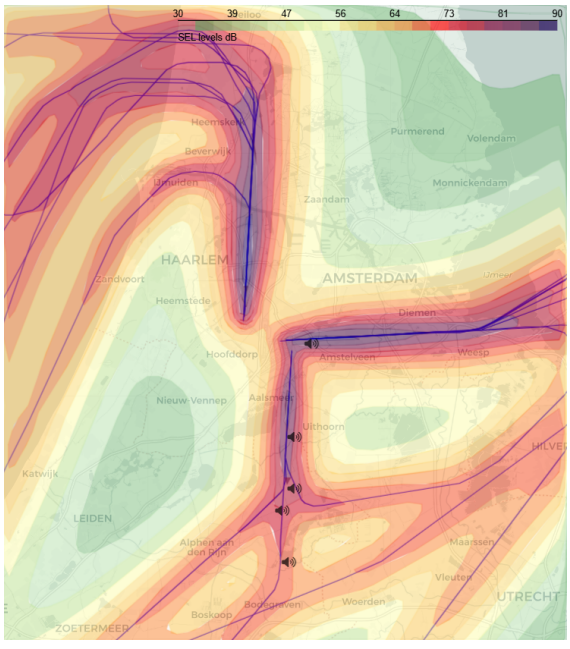

Figure A.66: Noise contour plot of B738 arrivals using the ACMS Doc. 29 calculation methodology.

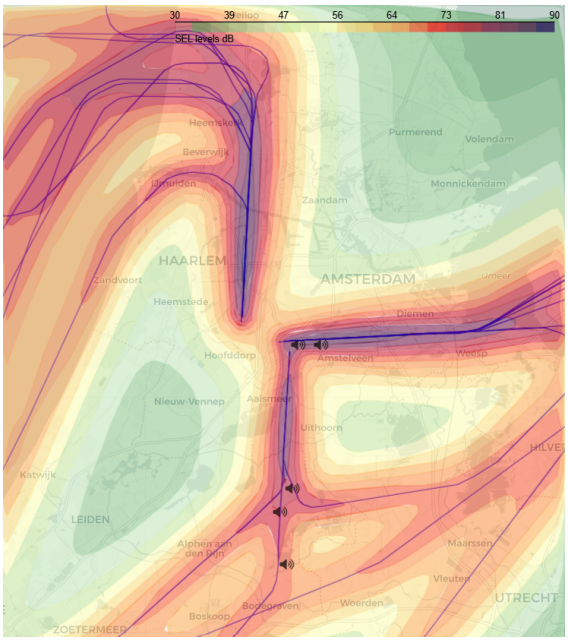

Figure A.67: Noise contour plot of B738 arrivals using the new thrust Doc. 29 calculation methodology.

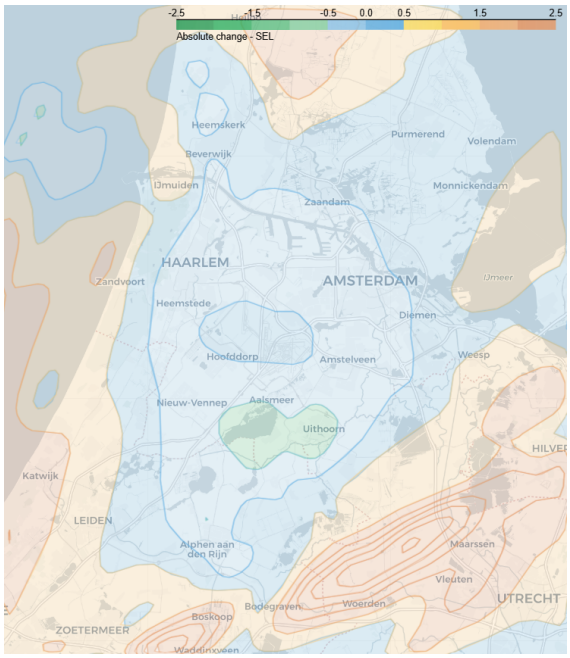

Figure A.68: Noise contour delta plot of B738 arrivals comparing the ACMS Doc. 29 model with the original Doc. 29 model.

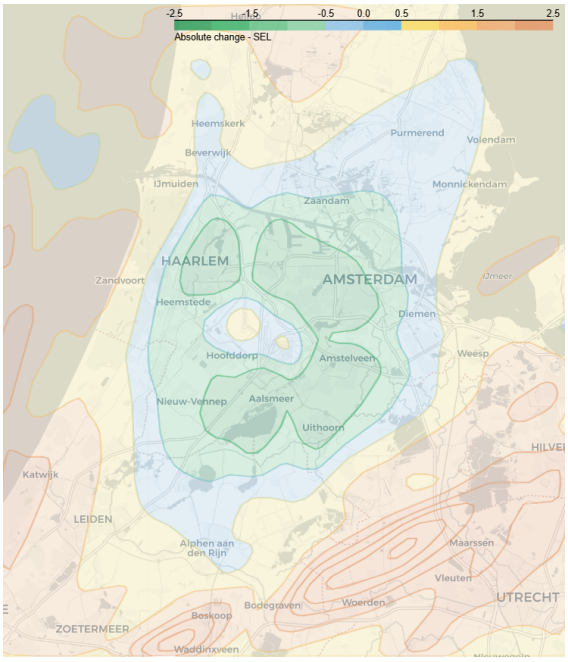

Figure A.69: Noise contour delta plot of B738 arrivals comparing the new thrust Doc. 29 model with the original Doc. 29 model.

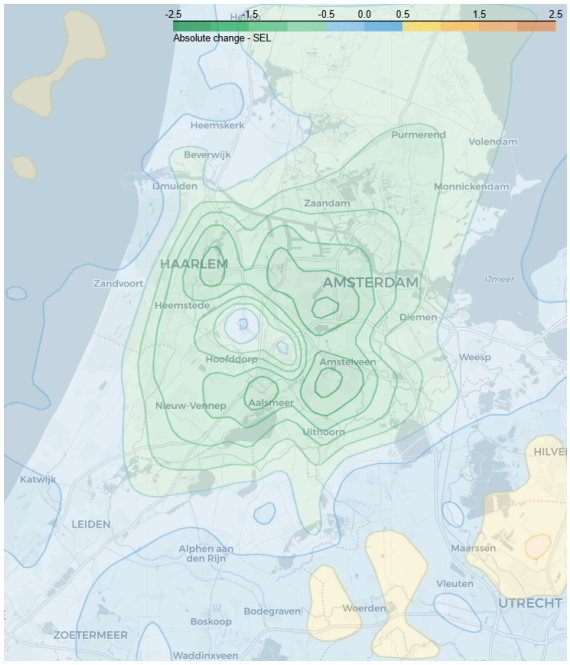

Figure A.70: Noise contour delta plot of B738 arrivals comparing the new thrust Doc. 29 model with the ACMS Doc. 29 model.